Technische Universität München
TUM School of Medicine and Health

The involvement of non-coding RNAs in smooth muscle cell dynamics in atherosclerosis and abdominal aortic aneurysm

Hanna Lydia Winter

Vollständiger Abdruck der von der TUM School of Medicine and Health

der Technischen Universität München zur Erlangung einer

Doktorin der Naturwissenschaften (Dr. rer. nat)

genehmigten Dissertation.

Vorsitz: Prof. Dr. Alessandra Moretti

Prüfer*innen der Dissertation:

1. Prof. Dr. Lars Mägdefessel
2. Prof. Dr. Aphrodite Kapurniotu
3. Prof. Dr. Judith Sluimer

Die Dissertation wurde am 16.05.2023 bei der Technischen Universität München eingereicht und durch die TUM School of Medicine and Health am 08.11.2023 angenommen.

Preface

Parts of the results of this dissertation have been accepted for publication by Cell Molecular Therapy on the 28th of April 2023. Figures, Figure legends, sentences, or passages may be adopted and are cited accordingly.

Winter, H., G. Winski, A. Busch, E. Chernogubova, F. Fasolo, Z. Wu, A. Bäcklund, B. B. Khomtchouk, D. J. Van Booven, N. Sachs, H.-H. Eckstein, I. Wittig, R. A. Boon, H. Jin and L. Maegdefessel (2023). "Targeting long non-coding RNA NUDT6 enhances smooth muscle cell survival and limits vascular disease progression." Molecular Therapy.

Experiments and data which were not performed or acquired by the author are mentioned accordingly, including information on the person who actually executed the work.

Table of Contents

List of Abbreviations

18F-FDG	Fluorodeoxyglucose (18F)
AAA	Abdominal Aortic Aneurysm
ACE	Angiotensin-Converting-Enzyme
AngII	Angiotensin II
ApoE	Apolipoprotein E
ASO	Antisense Oligonucleotide; GapmeRs from Qiagen (Hilden)
BCA	Bicinchoninic Acid Assay
CAD	Carotid Artery Disease
cDNA	complementary DNA
CEA	Carotid Endarterectomy
CT	Computed Tomography
CTA	Computed Tomography Angiography
CVD	Cardiovascular Disease
DEB	Drug Eluting Balloon
DMSO	Dimethyl Sulfoxide
DNA	Desoxyribonucleic Acid
EC	Endothelial Cell
ECL	Enhanced Chemiluminescence
ECM	Extracellular Matrix
EVAR	Endovascular Aortic Repair
FAM	Fluorescein Amidites
FFPE	Formalin Fixed Paraffin Embedded
GFP	Green Fluorescent Protein
hAoSMCs	Human Aortic Smooth Muscle Cells
hCtSMCs	Human Carotid Smooth Muscle Cells
HDL	High-Density Lipoprotein
HE	Hematoxylin and Eosin
EvG	Elastica Van Gieson
IHC	Immunohistochemistry
ISH	*In Situ* Hybridization
kDa	Kilodalton
LB	Lysogeny Broth
LC-MS/MS	Liquid Chromatography-Tandem Mass Spectrometry
LDL/oxLDL	Low-Density Lipoprotein / oxidized LDL
LDLR	Low-Density Lipoprotein Receptor
LNA	Locked Nucleic Acid
lncRNA	Long Non-Coding RNA
miRNA/miR	microRNA
MMP	Matrix Metalloproteinase
mRNA	messenger RNA
NAT	Natural Antisense Transcript
ncRNA	Non-Coding RNA
Nts	Nucleotides
OCT	Optimal Cutting Temperature
PCR	Polymerase Chain Reaction
PPE	Porcine Pancreatic Elastase
PTA	Percutaneous Transluminal Angioplasty
PVDF	Polyvinylidene Fluoride

qRTPCR	quantitative real-time PCR
RIP	RNA Immunoprecipitation
RNA	Ribonucleic Acid
scRNAseq	Single Cell RNA Sequencing
SEM	Standard Error of Means
siRNA	Short Interfering RNA
SMC	Smooth Muscle Cell
TIA	Transient Ischemic Attack
TIMP	Tissue Inhibitor of Metalloproteinase
UTR	Untranslated Region
VLDL	Very Low-Density Lipoprotein
vSMC	Vascular Smooth Muscle Cell

List of Figures

List of Tables

1. Introduction

1.1. Cardiovascular Diseases

Cardiovascular diseases (CVDs) remain the most common cause of death worldwide. They are steadily increasing in high- but also in low-income countries (Forsdahl *et al*. 2009, Virani *et al.* 2021). In Europe, 39 to 45% (of men and women, respectively) account for CVD-related deaths (Timmis *et al.* 2022). The ischemic heart disease and stroke mortality rate of all CVD-related deaths make up 84.9% (Ridker 1999, Forsdahl *et al.* 2009).

CVD risk factors were mainly established in the Framingham Heart Study, which started in the late 40s. This study discovered hypertension, hyperlipidemia (total, High-Density Lipoprotein (HDL), and Low-Density Lipoprotein (LDL) cholesterol), and diabetes mellitus to have an impact on CVDs (Mahmood *et al.* 2014, Libby 2021). For instance, nearly one-third of coronary heart diseases are connected to elevated blood pressure levels (Mahmood *et al.* 2014). Later on, newly identified markers such as lipoprotein (a), fibrinogen, or high-sensitivity C-reactive protein (CRP) further helped with assessing myocardial infarction occurrence (Thomas *et al.* 2018). CVDs reduce economic growth and remain a social challenge, so governments started to focus on preventive measures (Virani *et al.* 2021).

1.1.1. Atherosclerosis – Stroke and Carotid Artery Disease

1.1.1.1. Clinical – Diagnosis and Therapy

Carotid artery disease (CAD) describes the clogging of the carotid artery by lipid deposits, also called plaques, which block the blood supply to the brain. This can lead to an ischemic stroke or a transient ischemic attack (TIA) where infarctions in the spine, the retina, or the focal cerebrum cause a dysfunction over a longer or shorter (2-15min, TIA) time (Sacco *et al.* 2013). CAD rapidly developed into a burden in society. It inclined by 59.13% since the year 2000 in a heterogenous (gender and age) study population (Song *et al.* 2020).

Atherosclerosis is the main underlying cause of the pathologies mentioned above. Therefore, it is crucial to understand this disease's process and cellular contributors to develop suitable preventive or therapeutical measures.

Prevention starts with the change in health behaviors like smoking, physical activity, diet, and body weight (Hong *et al.* 2017, Arnett *et al.* 2019). If primary prevention is unsuccessful, risk factors like hypertension, diabetes, and dyslipidemia arise over time (Hong *et al.* 2017). These might sooner or later lead to cardiovascular or cerebrovascular diseases like CAD or stroke. However, secondary prevention aims to control new and existing CVDs. Measures include antiplatelet-, antithrombotic or antihypertensive therapy, and lipid-lowering therapy (Meschia *et al.* 2017).

Recent advances in CVD treatment poses the CANTOS trial. In this study, patients with high CRP were treated every three months with canakinumab, an anti-inflammatory antibody targeting Interleukin-1b (IL1B). This led to a significantly reduced rate of recurrent cardiovascular events; unfortunately accompanied by a higher risk and occurrence of fatal infections, such as sepsis. (Ridker *et al.* 2017).

Diagnosis of carotid artery stenosis includes duplex ultrasonography, magnetic resonance angiography (MRA), and computed tomographic angiography (CTA) (Meschia *et al.* 2017). If a diagnosis is made upon a recent event, such as a TIA, the patient will be classified as symptomatic. A patient will be seen as asymptomatic if they are diagnosed without a previous event or by chance.

Atherosclerotic plaques cause increasingly narrow carotid arteries over time, which has been connected to a higher risk for ischemic stroke (Barnett *et al.* 1998). To reduce this threat, the plaque can be surgically removed by carotid endarterectomy (CEA), or a stent can be placed in the plaque area. According to the North American Symptomatic Carotid Endarterectomy (NASCET) trial, patients with a high symptomatic stenosis degree (>50%) benefit more from surgery than from medical therapy (Barnett *et al.* 1998, Rerkasem *et al.* 2020). For patients with stenosis lower than 50%, there was no difference (Barnett *et al.* 1998, Rerkasem *et al.* 2020). Other postoperative treatment, such as anti-statin and anti-platelet therapy, is necessary (Naylor 2017). For asymptomatic patients, CEA can reduce the ipsilateral stroke risk by 30% within three years (Chambers and Donnan 2005). However, the authors of this database review also point out that women did not benefit from CEA, but only men did (Chambers and Donnan 2005). Moreover, a recently published meta-analysis highlights a dependency between stenosis degree and stroke risk also for asymptomatic patients (Howard *et al.* 2021). Therefore, it is crucial to evaluate each asymptomatic patient before CEA carefully.

1.1.1.2. Molecular Pathology

In 1858, Rudolf Virchow was the first to regard inflammation as the initiator of atherosclerosis (Virchow 1989). More than a decade later, Russell Ross could verify that atherosclerosis is indeed caused by inflammation rather than accumulated lipids or injury (Ross 1999). Around the same time, the primary classification which defines the plaque development stages based on histological characterizations was published (Stary *et al.* 1994, Stary *et al.* 1995). Stary et al. classified and named six stages in total. Later on, Virmani *et al.* modified the system (Virmani *et al.* 2000).

Atherosclerotic lesion development starts with risk factors (e.g. hypertension, cigarette smoking, or low shear stress) which lead to leaky endothelial cells in the intima, the innermost layer of the vessel wall (Libby *et al.* 2011, Seneviratne *et al.* 2013). These cells usually regulate thrombosis and the vascular tone (Lusis *et al.* 2004). LDL particles from the circulation then migrate into the vessel wall (Skalen *et al.* 2002) and oxidize at their new location, the intima media (Figure 1a).

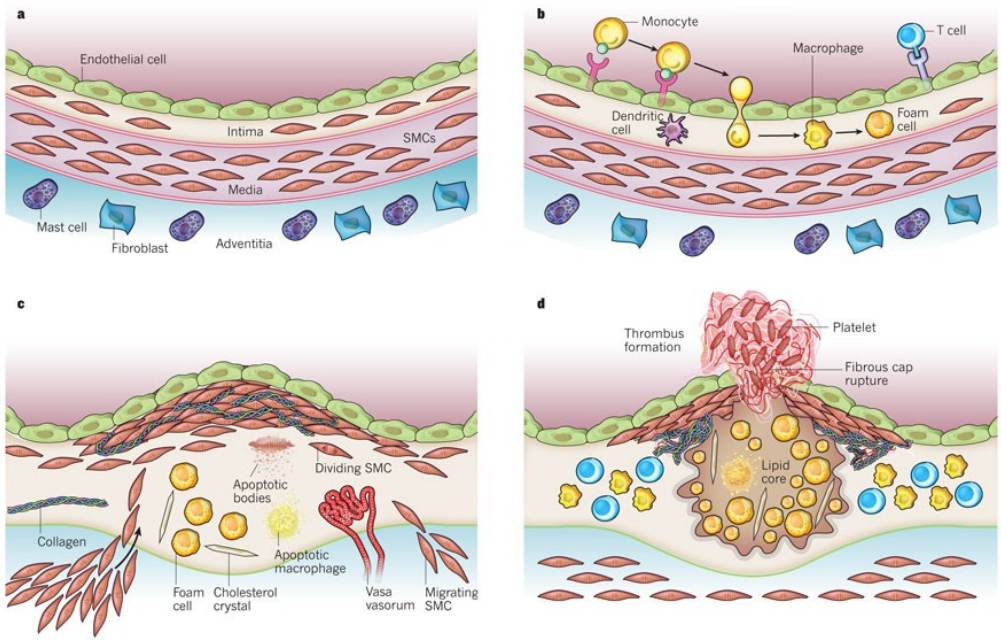

Figure 1 Atherosclerosis Development. (Libby *et al.* 2011), Nature 473, 317–325 (2011)

This activates the receptor molecules on the endothelial cells such as m-CSF, toll-like receptors or ICAM-1 and VCAM-1 (Kita *et al.* 2001, Edfeldt *et al.* 2002), which attract monocytes to transmigrate and differentiate into macrophages (Figure 1b). The oxidized LDL (oxLDL) binds to the macrophage-expressed scavenger receptors such as CD36 or LOX-1 (Endemann *et al.* 1993, Khatana *et al.* 2020) and turns them into lipid-rich foam cells, which further engulf oxLDL (Endemann *et al.* 1993, Kita *et al.*

2001, Berliner *et al.* 2009, Steinberg and Witztum 2010, Hansson and Hermansson 2011).

After a while, these cells undergo apoptosis and are cleared by other macrophages. From there, a pro-inflammatory and apoptotic cascade is initiated. This includes failed macrophage-mediated efferocytosis (Gui *et al.* 2022), and increased matrix metalloproteinase (MMP) (Johnson 2007) expression. The cells produce high amounts of IL-6, IL-18, and MCP-1 (van Tits *et al.* 2011, Colin *et al.* 2014) and can induce apoptosis (Okura *et al.* 2000) or autophagy (Ouimet *et al.* 2011). Since the dead cells cannot be properly cleared, necrotic cores form, which engulf all debris and dead cells, which, due to impaired efferocytosis, cannot be removed.

The produced cytokines (Halvorsen *et al.* 2008) and MMPs (Johnson 2007) trigger vascular smooth muscle cells (vSMCs) from the media layer of the vessel to proliferate and migrate into the intima. Eventually, they form the fibrous cap, which separates the necrotic core from the lumen (Ross 1993). The fibrous cap (FC) components are collagen, elastin, foam cells, and lymphocytes (Figure 1c) (Saba *et al.* 2010). Redgrave *et al*. measured FCs of more than 500 patients and concluded that plaques that ruptured had a thinner, unstable fibrous cap (<200µm) compared to unruptured lesions (Redgrave *et al.* 2008). Thinning can occur through cap-resident SMC apoptosis (Kolodgie *et al.* 2001, Clarke *et al.* 2006) or via macrophages and MMPs (Bentzon *et al.* 2014), which further degrade the matrix (primarily collagen). Several efforts have been made to identify the stability status, for example *via* MRI, where the outcome overlapped nearly 90% with the histological results (Hatsukami *et al.* 2000).

A very rupture-prone region of the fibrous cap is the so-called shoulder region (Falk *et al.* 1995, Barlis *et al.* 2008). If this region or the fibrous cap itself is too thin, a rupture can occur. In that case, the lesions' content (especially procoagulants) is exposed to the blood (Figure 1d). This leads to thrombus formation, eventually vessel occlusion, and an ischemic event such as stroke or TIA (Libby 2008, Bentzon *et al.* 2014). Another event apart from rupture is the superficial erosion of endothelial cells, which also results in a thrombus (Farb *et al.* 1996, Virmani *et al.* 1999, Shah 2003).

There were already several attempts to therapeutically intervene with the lesion's initiation, progression, and rupture: anti-LDL antibodies to decrease oxLDL within the lesions (Hartvigsen *et al.* 2009), PCSK9 and statin inhibitors which have been shown to reduce the plaque volume (Nicholls *et al.* 2007, Nicholls *et al.* 2016),

or a mucosal vaccine against ApoB to induce an anti-inflammatory response via ApoB-specific regulatory T-Cells (Klingenberg *et al.* 2010, Herbin *et al.* 2012) or drug-eluting stents (Jonasson *et al.* 1988, Marx and Marks 2001). However, most of the studies are still in clinical trials and not yet commercially available for patients.

1.1.1.3. Mouse Models

Already in 1908, Alexander Ignatowski realized that rabbits that are fed a fatty diet, develop plaques in the aortic wall (Ignatowski 1909, Lee *et al.* 2017). Later on, Nicolai Anichkov discovered that cholesterol is the leading cause of the developed plaques (1983 (N. Anitschkow 1913)).

Nowadays, these diet-induced mouse models are commonly used in atherosclerosis research. Especially Western-type diets (21% fat and 0.15% cholesterol) (Vesselinovitch *et al.* 1968, Gistera *et al.* 2022) or high-fat diets (40% fat or higher) (Speakman 2019) fed for 12-16 weeks (Golforoush *et al.* 2020) can trigger atherosclerosis, especially in the aortic arch. Another possibility poses transgenic mouse strains such as the Apolipoprotein E knockout (*ApoE*$^{-/-}$) mouse or the Low-density lipoprotein receptor knockout (*Ldlr*$^{-/-}$) mouse, which are the most frequently chosen models (Figure 2).

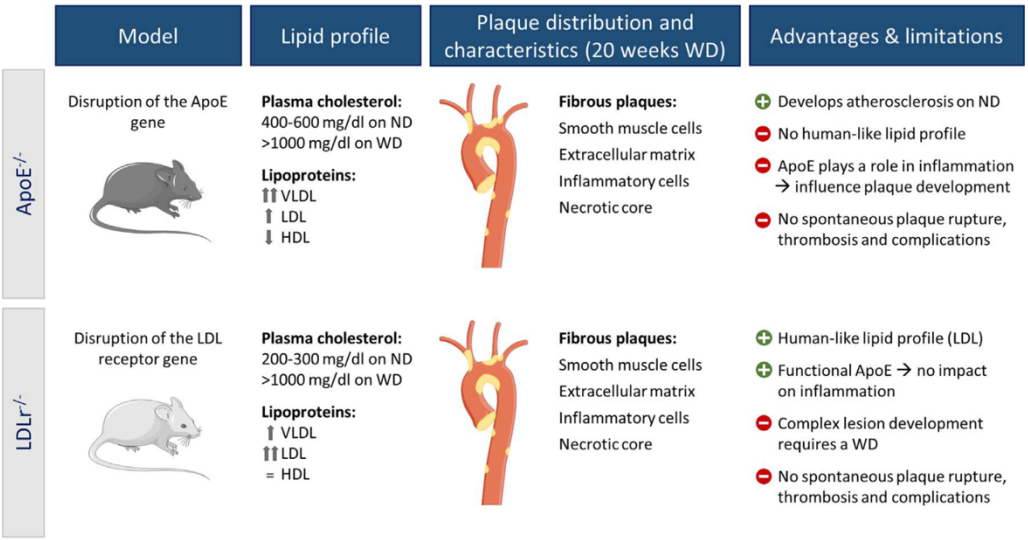

Figure 2 Transgenic Mouse Strains used in Atherosclerosis Research. From (Emini Veseli *et al.* 2017), Eur J Pharmacol 816, 3-13

The ligand ApoE facilitates very low-density lipoprotein (VLDL) and chylomicrons uptake *via* various lipoprotein receptors. Therefore the knockout leads to high VLDL, ApoB-containing lipoproteins, and chylomicrons levels in the blood (Gistera *et al.* 2022). A significant advantage of this model is that it develops

atherosclerosis under a regular chow diet showing an up to 6x increase in plasma cholesterol levels (Nakashima *et al.* 1994, Plump and Breslow 1995, Emini Veseli *et al.* 2017). However, the plaques developed in this model do not naturally rupture (Golforoush *et al.* 2020).

Moreover, the lipid profile does not resemble the human situation, where LDL is especially highly abundant in the circulation (Emini Veseli *et al.* 2017). The *Ldlr* knockout mouse possesses a very similar lipid profile to humans. By knocking out the receptor for Ldl, Ldl plasma levels are highly elevated, accompanied by fully functional ApoE, which also plays a role in other inflammatory processes (Oppi *et al.* 2019).

Neither the diet nor the knockout alone can cause spontaneous plaque rupture in mice (Emini Veseli *et al.* 2017). Therefore, it is necessary to intervene surgically to trigger this – in human disease – important event. The two mainly used models are the tandem ligation by Chen *et al*. (Chen *et al.* 2013) and the inducible plaque rupture model by Sasaki *et al*. (Sasaki *et al.* 2006). For the model by Chen *et al*., a tandem stenosis (with 150µm or 450µm distance) is introduced to the carotid artery of *ApoE* $^{-/-}$ mice fed a high-fat diet (Chen *et al.* 2013). Seven weeks after the surgery, multiple characteristics were observed: ruptured fibrous caps, intraluminal thrombus formation, and intraplaque hemorrhage (Chen *et al.* 2013), showing both stable and unstable segments throughout the tandem stenosis.

The inducible plaque rupture model is performed by ligating the left carotid artery of 9-week-old *ApoE* $^{-/-}$ mice on a chow diet proximally to the bifurcation (Sasaki *et al.* 2006). After four weeks, a polyethylene cuff is placed around the artery, which has a cone-like shape causing disturbed flow patterns that eventually leads to plaque rupture after four days (Sasaki *et al.* 2006).

1.1.2. Abdominal Aortic Aneurysm

1.1.2.1. Clinical (Diagnosis and Therapy)

An aneurysm (from greek, ἀνερυσμα, dilation) is a permanent dilation resulting from a weakened arterial vessel wall with a diameter increase of at least 50% (Wanhainen *et al.* 2020). The classification depends on the site, origin, and histological features (Johnston *et al.* 1991) – the abdominal aortic aneurysm (AAA) is mainly located between the renal branches and the iliac arteries.

Sampson *et al.* combined data from 26 studies and estimated the global incidence per 100.000 in 1990 to range from 0.89 to 176.08 (age group 40-44 and 75-79, respectively) (Sampson *et al.* 2014). The global prevalence reached from 8.43 to 2422.53 respectively – both aspects with a decreasing trend in 2010 (Sampson *et al.* 2014). To elucidate AAA risk factors, the Tromsø study was conducted. In four thousand participants, who were screened over seven years, male sex (2.7x higher risk) and increasing age, as well as smoking (13x higher risk), hypertension, and hypercholesteremia, were identified to trigger disease initiation and progression (Forsdahl *et al.* 2009, Lindholt *et al.* 2012). Still, also genetics seem to play a role (Shibamura *et al.* 2004, Golledge *et al.* 2006). Interestingly, diabetes was identified to be a protective trait in several studies, contrary to atherosclerosis (Blanchard *et al.* 2000, Lederle 2012, Shah *et al.* 2015). Other studies confirmed these results with higher cohorts, such as 3.1 million patients (Kent *et al.* 2010).

Similar to CAD diagnosis, ultrasound during a routine examination, CT but also palpation can aid in diagnosing asymptomatic AAAs (Sakalihasan *et al.* 2005). More advanced, functional imaging techniques such as ^{18}F-FDG (Fluorodeoxyglucose) can also be used (Marini *et al.* 2012, Sakalihasan *et al.* 2018, Arnett *et al.* 2019).

To study AAA prevalence and growth speed, the Glouchester Aneurysm Screening Programme (GASP) was initiated in 1990 and includes data from over 81.000 patients (Earnshaw *et al.* 2004, Oliver-Williams *et al.* 2018). While in 1990, 5% of the study population was diagnosed with AAA (>3cm), in 2015, only 1.3% were diagnosed (Oliver-Williams *et al.* 2018). Growth rates of those diagnosed changed from 0.05 in the first five years of follow-up to 0.36 between 15-19 years, indicating that most aneurysms grow exponentially (Oliver-Williams *et al.* 2018). However, the optimal surveillance interval still has to be determined as AAAs display such variety in appearance, size, and growth rate.

The main, life-threatening complication that can arise from an AAA is aortic rupture, with a reported mortality risk of 76% (Lindholt *et al.* 2012). Around 50% of patients experiencing an aortic rupture die on their way to the hospital (Chaikof *et al.* 2009). Even after surgical treatment, in-hospital mortality remains high (Kuhnl *et al.* 2017). Currently, the only possibility poses surgical intervention. Smaller aneurysms (<5.5cm) are rather surveilled since Lederle *et al.* and the UK Small Aneurysm Trial Participants could show that there is no improvement in survival if surgery is performed on smaller aneurysms (1998, Lederle *et al.* 2002). Fusiform aneurysms of more than

5.5cm (in women 4.5-5cm) are considered for either open or endovascular surgery (Sakalihasan *et al.* 2018). During open aortic repair an arterial prosthesis is inserted to replace the aneurysm (Sakalihasan *et al.* 2018). This is mainly used in young and healthy patients due to its better long-term endurance paired with a lower need for surveillance (Sakalihasan *et al.* 2018). Also ruptured AAAs are treated with open repair.

Juan Carlos Parodi established endovascular Aortic Repair (EVAR) in 1991 (Parodi *et al.* 1991). A bifurcated graft is inserted via the femoral or iliac arteries and fixed to the aortic wall via stents (Parodi *et al.* 1991, Sakalihasan *et al.* 2005, Golledge *et al.* 2006). This method excludes the aneurysm from circulation rather than replacing it. However, so-called endoleaks can occur when blood leaks through untight stents into the aneurysm sac (Parodi *et al.* 1991, Sakalihasan *et al.* 2005, Golledge *et al.* 2006). If a patient is unsuitable for EVAR due to the aortic morphology, open repair is performed (Sakalihasan *et al.* 2018).

The IMPROVE and the DREAM trials aim to compare the clinical outcome between open repair and EVAR (Prinssen *et al.* 2004, Investigators 2017). EVAR-treated patients had lower three-year mortality and risk of complications, while their quality of life was higher (Prinssen *et al.* 2004, Investigators 2017). This trend might further increase due to improved material and deployment mechanisms (Sakalihasan *et al.* 2018).

Up to today, the field is in desperate need of adequate and effective pharmacological intervention. Challenges for discovery and clinical studies include the heterogenous growth rate and each aneurysm's anatomy, the drop-out due to vascular repair, and frequent comorbidities (Golledge *et al.* 2017). Previous clinical trials involve doxycycline to inhibit MMP production and inflammation (Meijer *et al.* 2013) or pemiroplast, a mast cell inhibitor (Sillesen *et al.* 2015), but neither did result in a beneficial outcome.

1.1.2.2. Molecular Pathology

Even though the attempts to treat AAAs date back to the roman empire, the underlying molecular mechanisms started to unravel only in the late 20th century and are still ongoing.

Risk factors such as age, smoking status, or sex can initiate an aneurysm and, combined with hemodynamics and the failure to withstand these forces, alter the aortic wall (Curci and Thompson 2004, Michel *et al.* 2011, Back *et al.* 2013). Especially the

infrarenal part of the aorta is prone to AAA development due to the different embryonic origins of SMCs (Tromp *et al.* 2010). Also, the higher susceptibility to longitudinal stress and wall tension have an impact (Moore *et al.* 1992). Vollmar *et al*. showed that AAAs were more common in men with an amputated leg due to the altered flow pattern (Vollmar *et al.* 1989).

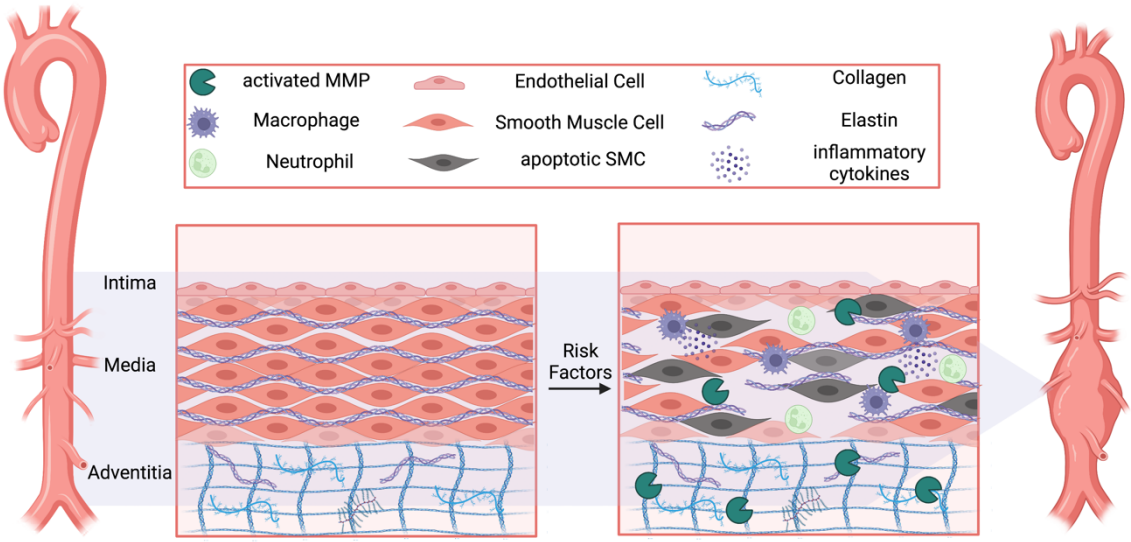

Figure 3 Molecular Mechanisms in AAA. adapted from (Rastogi *et al*. 2022), Front Med 9, 814123; created with BioRender.

The resulting injury recruits immune cells such as macrophages or T-Lymphocytes, but also others (Koch *et al.* 1990), into the media. There, the cells will produce proinflammatory cytokines and pro-enzymatic forms of matrix metalloproteinases (MMPs) (Figure 3) (Newman *et al.* 1994, Curci *et al.* 1998, Ailawadi *et al.* 2003, Raffort *et al.* 2017). These MMPs are activated by cleavage and – over several years – degrade important structural matrix components such as elastin and collagens (Newman *et al.* 1994, Curci *et al.* 1998, Ailawadi *et al.* 2003, Raffort *et al.* 2017). Increased MMP levels were observed in human aneurysm samples (Freestone *et al.* 1995, Thompson *et al.* 1995) and correlated with increasing size (McMillan *et al.* 1997). An MMP-9 and MMP-2 knockdown in mice does not generate AAA after ten weeks of $CaCl_2$ or PPE induction (Pyo *et al.* 2000, Longo *et al.* 2002). Similar results were achieved using doxycycline, an MMP inhibitor (Pyo *et al.* 2000). An MMP-caused decrease in collagen leads more likely to an aortic rupture, whereas a loss of elastin can cause a dilated aorta (Dobrin *et al.* 1984). These molecules' turnover is very slow and even slower in AAA (Satta *et al.* 1995). So, a disrupted balance between newly generated ECM and the destruction thereof has serious consequences (Daugherty and Cassis 2002, Sakalihasan *et al.* 2005, Golledge *et al.* 2006).

As a final step, smooth muscle cells undergo apoptosis and can no longer supply a contractile, intact vessel wall (Figure 3) (Lopez-Candales *et al.* 1997). Overall, the milieu within AAAs is very hypoxic – superoxide (O_2^-) content in aneurysmal tissue is up to 10x higher than in healthy aortic tissue (Miller 2002, Miller *et al.* 2002), which can also further trigger structural cell apoptosis (Li *et al.* 1997).

1.1.2.3. Animal Models

Parallel to unraveling molecular mechanisms involved in AAA, in late 1990/early 2000, experimental models were developed. This section will focus on the Angiotensin II (AngII)-induced mouse model and the porcine pancreatic elastase (PPE) induced model used in this thesis.

The AngII model was discovered by accident when Daugherty and colleagues treated *ApoE* deficient mice with AngII to elucidate its relationship with atherogenesis - "Unexpectedly, pronounced abdominal aortic aneurysms were present in *ApoE*$^{-/-}$ mice infused with AngII." (Daugherty *et al.* 2000). AngII is implicated in cardiovascular diseases (Alderman *et al.* 1991) and accumulates in atherosclerotic lesions (Potter *et al.* 1998). Moreover, Angiotensin-Converting-Enzyme (ACE) inhibitors benefit cardiovascular morbidity and mortality (Pfeffer *et al.* 1992). Osmotic minipumps implanted into the mice's back area provide a continuous AngII delivery over four weeks. This model was also established in *Ldlr*$^{-/-}$ mice (Daugherty and Cassis 1999) and remains the most used in AAA research (Lysgaard Poulsen *et al.* 2016). It induces a non-fusiform suprarenal or thoracic aneurysm (Krishna *et al.* 2020) accompanied by dissection, remodeling, leukocyte infiltration, and neovascularization (Saraff *et al.* 2003) and eventually an intramural rupture (Lysgaard Poulsen *et al.* 2016, Senemaud *et al.* 2017).

The model is relatively simple to perform (Senemaud *et al.* 2017, Golledge *et al.* 2022) and has been further modified (using a lysyl oxidase (LOX) inhibitor (Bhamidipati *et al.* 2014) or a TGFβ antibody (Wang *et al.* 2010)) to reach a higher AAA incidence. However, the main difference to human AAA is its location (infrarenal *vs*. suprarenal) and shape (fusiform *vs*. non-fusiform) (Ruddy *et al.* 2008, Daugherty *et al.* 2011, Busch *et al.* 2021).

The porcine pancreatic elastase (PPE) induced AAA model was established first in rats (Anidjar *et al.* 1990) before it was translated into mice (Pyo *et al.* 2000). The enzyme is known to degrade elastin, one main medial component in the aorta (Busch *et al.* 2021). After identifying and isolating the infrarenal abdominal aorta *in*

vivo, ligatures are placed around the proximal and distal aorta (Pyo *et al.* 2000). At the bifurcation, a needle filled with PPE in saline is inserted and perfuses for 5min to dilate the aorta by 50-70% which leads to the AAA formation. The catheter is removed, and the aorta is closed. After seven days, the changes are not clearly visible as typically the aneurysm starts developing by day 14 with at least 100% increased aortic diameter (Thompson *et al.* 2006). However, ruptures rarely occur in this model (Krishna *et al.* 2020). Microscopically, an increased inflammatory cells presence, MMPs, and cathepsins are visible (Busch *et al.* 2021). Technically, this model requires a high skill level in microsurgery (Lysgaard Poulsen *et al.* 2016) and highly depends on the PPE batches (Senemaud *et al.* 2017). Also, this model has been modified over the years (Busch *et al.* 2018).

A third model, which was not used in this thesis, is the $CaCl_2$-induced AAA model, which was first published in mice by Chiou *et al*. (Chiou *et al.* 2001). Calcium ions accumulate along the elastic layers (Yu and Blumenthal 1965). However, the detailed pathological mechanism remains elusive (Senemaud *et al.* 2017). Calcium chloride is applied peri-arterially to the infrarenal aorta, leading to a 100% increase in abdominal aortic diameter (Chiou *et al.* 2001). If PBS is added, the $CaPO_4$ crystals, necessary for an induced AAA, are formed easier and faster (Yamanouchi *et al.* 2012). On a cellular level, the MMP- and phagocytotic activity increase (Senemaud *et al.* 2017).

Large animal models for AAA include PPE-induced AAA in landrace pigs (Kloster *et al.* 2015) and PPE-induced AAA in *LDLR*$^{-/-}$ Yucatan mini pigs, as previously reported by our group (Li *et al.* 2018), translating the procedure from mice into genetically modified pigs.

However, there is still an unanswered need for a model mimicking the human disease more accurately (fusiform infrarenal location, rupture). Also, more focus must be put on the disease's early stages, which still need to be fully understood.

1.2. Smooth muscle cells

1.2.1. Function in health

Vascular smooth muscle cells (vSMCs) are the main cellular component of an arterial media layer. They are mainly responsible for the vessel's contractility (Bochaton-Piallat and Back 2018) and can respond to altered hemodynamics (Basatemur *et al.*

2019), or they can also regulate blood pressure (Michel *et al.* 2012). vSMCs are also the main producer of ECM proteins such as collagen, elastin, or proteoglycans (Chamley et al. 1977, Basatemur *et al.* 2019). Attention must be paid to the different cellular embryonic origins depending on their location in the arterial tree. Thoracic-resident SMCs have a neural crest origin, whereas SMCs in the abdominal aorta derive from somite precursors (Bennett *et al.* 2016) - or in various organs such as kidney, heart, etc. (Michel *et al.* 2012).

vSMCs express many contractile proteins such as αSMA (Gabbiani *et al.* 1981), Calponin (Duband *et al.* 1993), Smoothelin (van der Loop *et al.* 1996) or Myosin Heavy Chains (Babij *et al.* 1991). These genes are activated by serum response factor (SRF) and its cell-specific co-activator myocardin binding to the CC(A/T-rich)6GG (CArG) element proximally to the respective promoters (Wang *et al.* 2001, Li *et al.* 2003, Yoshida *et al.* 2003). Especially in vascular pathologies, they exert many functions, which will be explained in the following chapters.

1.2.2. Role in CAD

Mature vSMCs are highly plastic and not fully differentiated, enabling a fast response to injury and repair mechanisms, growth factors, extracellular lipids and lipoproteins, and more (Owens *et al.* 2004, Allahverdian *et al.* 2018). This process is called phenotypic switching and describes losing contractile marker genes (Regan *et al.* 2000), while the migrative and proliferative capacity increases (Ross 1993, Ross 1999, Gomez and Owens 2012). Phenotypic switching can also be induced by Krüppel-like Factor 4 (KLF4). Shankman and colleagues could show that the most cells with an SMC origin do no longer express SMC genes but rather genes related to macrophages (Shankman *et al.* 2015) but also mesenchymal stem cells, characterized by Sca1 expression (Majesky *et al.* 2017). KLF4 can bind to the G/C repressor, leading to contractile gene repression (Figure 4) (Yoshida *et al.* 2012). This KLF-mediated induction is considered disadvantageous in a forming and progressing lesion as it increases SMC-derived foam cells (Shankman *et al.* 2015). Contrary to that is the OCT4-mediated phenotypic switch, which has been shown to result in an SMC-rich, thick fibrous cap (Cherepanova *et al.* 2016).

KLF4 can be inhibited by miR-143/145 or TGFβ, which prevents this process (Figure 4) (Xu *et al*. 2009, Davis-Dusenbery *et al*. 2011, Vacante *et al*. 2019). However, phenotypic switching is – usually – a reversible process, but in an

atherosclerosic context, vSMCs are constantly exposed to stimuli that induce phenotypic switching (Pan *et al.* 2020).

The observed adapted phenotypes come in a wide variety. Mesenchymal-like vSMCs are characterized by low contractile marker expression while they can self-renew which is accompanied by multipotency marker expression (Stem cell antigen 1, Sca1^{+}). Thus, these cells can give rise to cells in the plaque as a first response to injury by facilitating tissue repair (Bennett *et al.* 2016, Dobnikar *et al.* 2018, Tang *et al.* 2020). This and the following phenotype are triggered by KLF4 expression (Liu *et al.* 2005).

vSMCs can also acquire a macrophage or foam cell-like phenotype, exerting phagocytotic functions (Bennett *et al.* 2016). A prominent marker for these modulated vSMCs is LGALS3 but also more typical macrophage markers like CD11b, CD45, and F4/80 (Wolf and Hunziker 2020), which are replacing contractile gene expression such as MYOCD (Ackers-Johnson *et al.* 2015, Bennett *et al.* 2016). This phenotype has been observed in human and murine atherosclerosis (Alencar *et al.* 2020, Depuydt *et al.* 2020, Pan *et al.* 2020). Especially this phenotype poses a problem – the markers which have been used to identify vSMCs (ACTA2^{+}) and macrophages (CD68^{+}) have to be used with caution as some CD68 positive cells might have a vSMC background without expressing ACTA2 (Gomez *et al.* 2018).

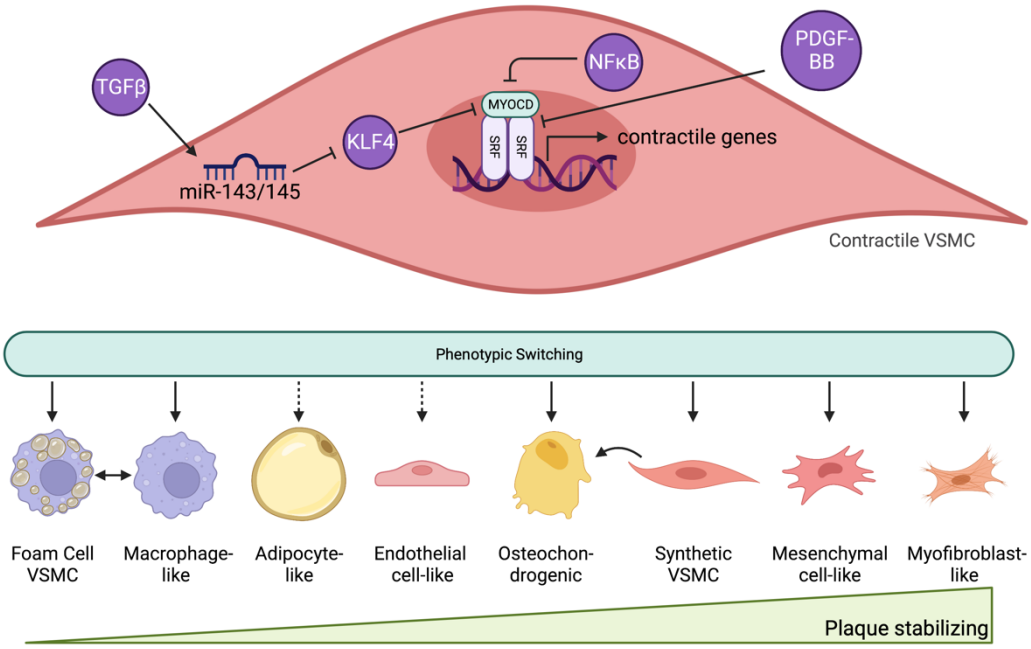

Figure 4 Regulation of SMC contractility and phenotypic switching. Adapted from (Grootaert and Bennett 2021), Cardiovasc Res 11, 2326-2339

Further, nearly three-quarters of all foam cells within a murine *ApoE*$^{-/-}$ plaque derive from vSMCs (Wang 2019). Half of all foam cells in human lesions express vSMC markers rather than leukocyte marker CD45 (Allahverdian *et al.* 2014). These cells have also been shown to engulf oxLDL actively (Feil et al. 2014).

A lineage-tracing experiment has shown that nearly all chondrocyte-like cells and 80% of osteochondrogenic-like cells are of vSMC origin (Naik *et al.* 2012). These cells have elevated runt-related transcription factor (RUNX2), SRY-related HMG-Box (SOX9), and Osteopontin (Durham *et al.* 2018) levels. Depending on their location, they secrete calcifying vesicles and contribute to plaque rupture or vessel stiffening (Durham *et al.* 2018).

Adipocyte-like vSMCs have been described in one scRNAseq study (Long *et al.* 2014, Chen *et al.* 2020). They further show increased lipogenesis genes in human atherosclerosis (Davies *et al.* 2005).

Fibromyocytes, also called fibroblast-like vSMCs, have been discovered recently by Wirka and colleagues and are observed to appear after vascular injury and during aortic aneurysm as well as atherosclerosis progression (Wirka *et al.* 2019).

All the phenotypes mentioned above (Figure 4) were discovered recently due to the advanced methodology in the field. Especially combining single-cell RNA sequencing and lineage tracing enabled the majority of the findings (Wirka *et al.* 2019, Depuydt *et al.* 2020, Pan *et al.* 2020). Lineage tracing is achieved by crossing a mouse with a fluorescent tracking marker with a mouse containing a cell-specific promoter gene – in the case of vSMCs Myh11 – linked to a drug-inducible recombinase (Bennett *et al.* 2016, Liu and Gomez 2019). Gomez and colleagues used such a system (crossing Myh11-CreERt2 mice with R26R-YFP reporter mice) in advanced atherosclerosis to determine the cellular origin within the lesion (Gomez *et al.* 2013). Several groups have shown that vSMCs in the lesion derive from only a few clones and expand from there (Feil *et al.* 2014, Chappell *et al.* 2016, Misra *et al.* 2018). The clones show a high proliferative capacity and are the primary source for a forming fibrous cap (Misra *et al.* 2018). However, these cells also undergo senescence, typical in advanced atherosclerotic lesions (Bennett *et al.* 2016).

Senescence is characterized by a low proliferation rate and expression of retinoblastoma protein (RB) which induces senescence (Bennett *et al.* 1998) and telomere shortening (Matthews *et al.* 2006), caused mainly by oxidative stress (Finkel and Holbrook 2000). The consequences for lesions are not beneficial – senescent

cells produce less collagen but more inflammasome components which contribute to the plaque's vulnerability (Gardner *et al.* 2015) and progression in general (Grootaert *et al.* 2018).

1.2.3. Role in AAA

As mentioned before, vSMCs can undergo phenotypic switching (Shankman *et al.* 2015) in response to mechanical injury, hypertension, and aneurysm formation (Ailawadi *et al.* 2009). Their resulting phenotype is characterized by low contractile gene expression but high expression of migrative, fibrotic, and proliferative genes (Owens *et al.* 2004). Also, these so-called synthetic SMCs can produce IL1a, IL1b, and IL-6 – all inflammatory cytokines which are increased in AAA (Boyle *et al.* 2001, Middleton *et al.* 2007, Akerman *et al.* 2018), which hints towards an autocrine mechanism (Beasley *et al.* 1995, Jovinge *et al.* 1997, Wang *et al.* 2001).

Using a particular Myh11-CreERt2/Rosa26 Confetti mouse model, M. Clement et al. found that vSMCs in aortic aneurysms expand clonally and express phagocytotic markers (Clement *et al.* 2019). Similar observations were made by G.Zhao et al. using scRNAseq on PPE-induced aorta: four vSMC subpopulations were identified, out of which three decreased with AAA progression but only one, expressing low contractile markers, increased (Zhao *et al.* 2021).

vSMCs also play a crucial role in ECM regeneration and integrity. If these mechanisms are impaired, vSMCs can detach, which results in migration but also apoptosis (Nordon *et al.* 2011, Rombouts *et al.* 2022). However, also vSMCs can activate MMPs, which degrade structural ECM components to enable migration or apoptosis (Nordon *et al.* 2011, Qian *et al.* 2022, Rombouts *et al.* 2022). This shift towards a proteolytic environment is further enhanced by vSMC-mediated leads to inactivated tissue inhibitors of metalloproteinases (TIMPs) (Raffetto and Khalil 2008, Wang and Khalil 2018).

But vSMC apoptosis – one major critical event in AAA progression – can also be triggered by inflammatory infiltrates, oxidative stress, modified lipoproteins, or a disintegrated ECM (Hsieh *et al.* 2001, Quintana and Taylor 2019, Lu *et al.* 2021). Seeding rat vSMCs into a rat/guinea pig xenograft model (decellularized aorta) could not induce AAA (Allaire *et al.* 2002), which exemplifies a paracrine effect of VSMCs. Therefore, inhibiting vSMCs apoptosis in advanced disease stages poses an effective strategy (Lu *et al.* 2021), keeping in mind their crucial homeostatic function.

1.2.4. FGF2 in SMCs

Fibroblast growth factor 2 (FGF2), also known as basic fibroblast growth factor (bFGF), belongs to the FGF family and plays crucial roles during mesodermal and neuroectodermal development (Burgess and Maciag 1989) but also in injury response or repair (Fox and Shanley 1996). In a cardiovascular disease context, FGF2 and the FGF2 receptor (FGF2R1) are expressed by vSMCs and induce migration and proliferation (Lindner and Reidy 1991, Sato *et al.* 1991). Inhibited receptor or underlying pathway members like MEK, MAP, Ras, or Raf showed their essential contribution to vSMC survival (Miyamoto *et al.* 1998).

FGF2 also regulates vSMCs differentiation into a synthetic phenotype (Kato *et al.* 1998) and functions as a survival factor in quiescent/differentiated cells (Fox and Shanley 1996). Recent results show that only FGF2 can induce proliferation in quiescent cells (Tsuji-Tamura and Tamura 2022). Inhibited or low FGF2 in vSMCs leads to apoptosis (Miyamoto *et al.* 1998), the main event in both CAD and AAA, as mentioned earlier. However, bFGF applied exogenously was an effective measure against vSMC apoptosis in AAA: Using a biodegradable hydrogen sheet loaded with bFGF, Kawai and colleagues reported less expanded aortas accompanied by improved contractile capabilities (Kawai *et al.* 2018). Hoshina and colleagues obtained similar results (Hoshina *et al.* 2004). These features and preclinical applications of bFGF make it a desirable target in late-stage atherosclerosis or AAA.

1.3. Long non-coding RNAs

1.3.1. General function/biogenesis

In 1968, Britten and colleagues discovered that many regions in the genome do not code for proteins but were thought to be non-functional junk (Britten and Kohne 1968). However, in 1991, the long non-coding RNA (lncRNA) *XIST* was found to regulate X-chromosome inactivation (Brown *et al.* 1991). Later, the FANTOM and the ENCODE consortia unraveled that 70-80% of the genome is transcribed while only 2% of mRNA is translated (Carninci *et al.* 2005, Consortium 2012, Djebali *et al.* 2012). This, in turn, means that a large amount of the genome consists of ncRNAs. The NONCODEV5, released in 2018, includes nearly 550.000 lncRNAs, a class of ncRNAs longer than 200nt (Kapranov *et al.* 2007, Fang *et al.* 2018).

lncRNAs are similarly processed to mRNA; they are transcribed by RNA polymerase II, are capped at the 5' end, spliced and polyadenylated (Chen 2016). But lncRNAs are not as abundant and less conserved than mRNAs (Cabili *et al.* 2011, Derrien *et al.* 2012). Their localization within the cell mainly determines a lncRNA's function– most lncRNAs are found in the nucleus, where they tend to regulate transcriptional processes and chromatin remodeling (Geisler and Coller 2013, Hartford and Lal 2020). lncRNAs found in the cytoplasm can associate with RNA-binding proteins, mediate mRNA and protein stability, or even code for a micropeptide (Ji *et al.* 2015, Hartford and Lal 2020, Statello *et al.* 2021).

Many noncoding RNAs have been wrongly annotated as they contain a promoter/open reading frame (ORF) smaller than a particular cutoff (Galindo *et al.* 2007, Cai *et al.* 2017). Thresholds were adjusted due to more advanced and modern techniques like ribosome profiling. This led to the discovery of micropeptides encoded by presumably non-coding RNAs (ncRNAs), which can be highly tissue and cell-type-specific (Lee *et al.* 2012, Ingolia *et al.* 2014).

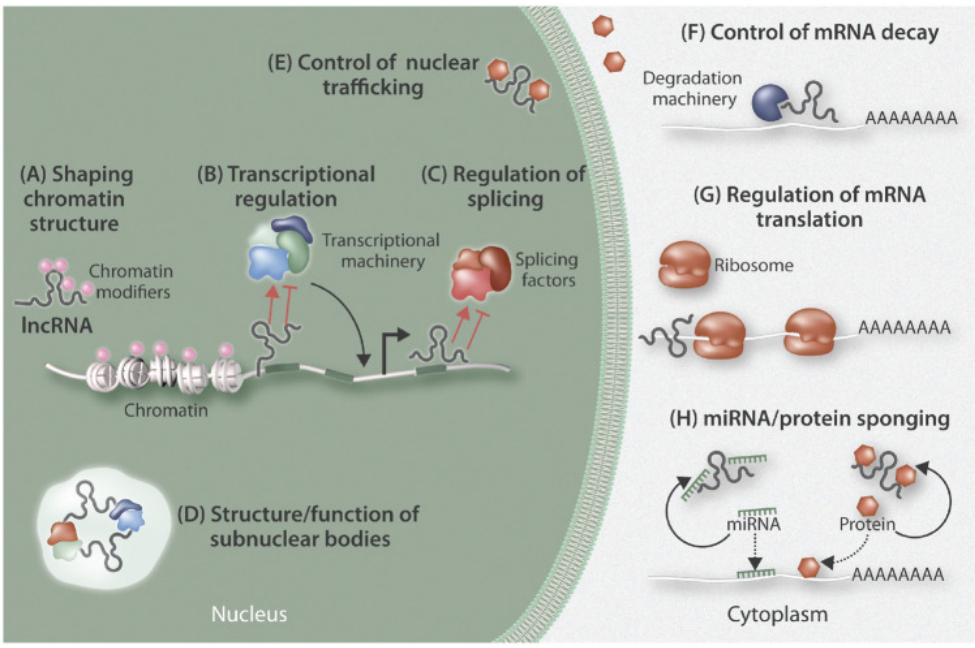

Figure 5 lncRNA functions in- and outside of the nucleus. From (Fasolo *et al*. 2019), Cardiovasc Res 115, 1732-1756.

In general, lncRNAs can interact with DNA, RNA, and protein, displaying a significant potential for regulatory functions (Figure 5) (Schmitz *et al.* 2016). For example, lncRNAs can recruit or act as a decoy for chromatin modifiers, thus regulating the chromatin accessibility (Schmitz *et al.* 2010, Grote and Herrmann 2013). lncRNAs can interact with mRNA or protein, which results in changes in turnover,

stability, or even localization (Kim *et al.* 2005, Gong and Maquat 2011, Guttman and Rinn 2012, Rinn and Chang 2012). But also microRNAs can be regulated by lncRNA *via* microRNA sponging and other competitive mechanisms (Figure 5) (Salmena *et al.* 2011, Statello *et al.* 2021).

1.3.2. role in cardiovascular disease

lncRNAs are essential regulators orchestrating gene expression. However, in a disease-related context, lncRNA expression levels can both increase or decrease, which has detrimental effects on disease progression. A few examples will follow, mainly focusing on lncRNAs in different AAA and CAD crucial cell types.

Genome-wide association studies (GWAS) discovered the first risk locus (INK4) for a plethora of cardiovascular diseases such as coronary artery disease, atherosclerosis, and ischemic stroke on chromosome 9p21.3 (Samani *et al.* 2007, Helgadottir *et al.* 2008, Gschwendtner *et al.* 2009, Jarinova *et al.* 2009). The lncRNA *ANRIL* (antisense ncRNA in the INK4 locus) was found in the antisense direction within the locus (Jarinova *et al.* 2009). Further, single-nucleotide polymorphisms (SNPs) are rather detected in the lncRNAs' locus than in the protein-coding locations (Harismendy *et al.* 2011). It is expressed by various plaque-resident cells such as ECs, SMCs, and macrophages(Broadbent *et al.* 2008). The mechanism of action by *ANRIL* is affecting its target genes in *trans* and inducing proliferation while reducing apoptotic pathways (Holdt *et al.* 2013).

Another lncRNA that our laboratory has recently discovered to regulate advanced atherosclerotic lesions and further destabilized plaques is *MIAT* (Myocardial Infarction Associated Transcript) (Fasolo *et al.* 2021). Symptomatic patients show an increased *MIAT* expression compared to asymptomatic or healthy subjects (Ye *et al.* 2019). *MIAT* knockdown in carotid SMCs led to low proliferation and migration rates while apoptotic events increased (Fasolo *et al.* 2021). *MIAT* can bind the KLF4 promoter region, thus regulating phenotypic switching directly and promoting proinflammatory macrophage-like SMCs (Fasolo *et al.* 2021). Also, *in vivo* experiments in *ApoE*$^{-/-}$ *MIAT* $^{-/-}$ mice and in *LDLR*$^{-/-}$ pigs confirmed the role of *MIAT* in SMC trans-differentiation (Fasolo *et al.* 2021).

H19 was among the first ncRNAs described in the '90s (Brannan *et al.* 1990) and since then, it has been reported to regulate p53 (Raveh *et al.* 2015) but also to play a role in the cardiovascular context (Li *et al.* 2018, Lv *et al.* 2018, Zhang *et al.* 2018). In atherosclerosis, *H19* levels are reduced in lesional endothelial/intimal cells

(Hofmann *et al.* 2019), while in the AAA context, *H19* levels in aortic aneurysm but also in calcific aortic valves are strongly upregulated (Hadji *et al.* 2016, Li *et al.* 2018). Also, in the AngII and the PPE model, *H19* was highly increased (Li *et al.* 2018). *H19* knockdown in these two models repressed dilated aneurysms (Li *et al.* 2018). The same group showed that *H19* induces apoptosis *via* HIF1alpha promoter region binding and Sp1 (a transcription factor) recruitment (Li *et al.* 2018).

These studies exemplify the various effects lncRNAs can have on vascular diseases. Further lncRNAs which have been examined in the context of cardiovascular diseases are *MEG3* (Boon *et al.* 2016, Sun *et al.* 2017, Bai *et al.* 2019), *GAS5* (Meng *et al.* 2020), *SENCR* (Bell *et al.* 2014), *MYOSLID* (Zhao *et al.* 2016), *HOTAIR* (Carrion *et al.* 2014), *HIF1alpha-AS1* (Zhao *et al.* 2014), and *lincRNA-p21* (Wu *et al.* 2014) to name a few.

1.3.3. Natural Antisense Transcripts: FGF2 and *NUDT6*

Natural antisense transcripts (NATs) are oppositely oriented to a protein-coding gene. They are also fully processed (polyadenylation, capping) and (partly) overlap complementarily with their sense transcript's exon (Werner 2013). In 2015, it was reported that at least 38% of the annotated transcriptome also expressed a NAT after performing strand-specific RNA sequencing (ssRNA-seq) on nine different specimen types of cancer from close to 400 patients (Balbin *et al.* 2015). NATs can be further separated into *cis* and *trans,* where NATs are expressed from the same genetic locus or separately, respectively (Pelechano and Steinmetz 2013). *Cis*-NATs usually have a perfect complementarity with their sense transcript in the untranslated region (UTR). Using that, NATs regulate their sense transcript by repressing (*via* promoter competition/binding site occlusion) or activating gene expression. Still, NATs also exert their functions in processes like mRNA stability, where they mask degradation sites, splice, or contribute to cellular transport (Pelechano and Steinmetz 2013).

In general, NATs can – due to their spatial proximity and organization – react more rapidly than transcription factors, allowing cells to adapt faster to changing conditions (Shimoni *et al.* 2007), even though they are usually relatively lowly expressed – up to 10x less than their sense target (Ozsolak *et al.* 2010).

The attempt in the field to elucidate the mechanism of action and kinetics led to two significant hypotheses: (1) Upon a certain level of transcribed sense transcript, antisense transcription is initiated, which leads to delayed repression of the sense gene. (2) The NAT can remove "transcriptional noise" until the moment when the

sense transcript surpasses the threshold of expressed NAT (Koshland *et al.* 1982, Xu *et al.* 2011, Pelechano and Steinmetz 2013).

One example of a sense-antisense pair is *NUDT6* and its sense gene, *FGF2*. *NUDT6* was discovered in 1989 in Xenopus oocytes by Kimelman and colleagues (Kimelman and Kirschner 1989). Its exons 4 (56nts) and 5 (583nts) share complementarity with the third *FGF2* exon in a total length of 637nts, with the longer overlap being critical for the *FGF2* regulation by *NUDT6* (Figure 6) (MacFarlane *et al*. 2010). The complementary locus is highly conserved between species like *Mus musculus, Rattus norvegicus, Bos taurus, Sus scrofa,* and *Homo sapiens* (Murphy and Knee 1994, Knee *et al.* 1997).

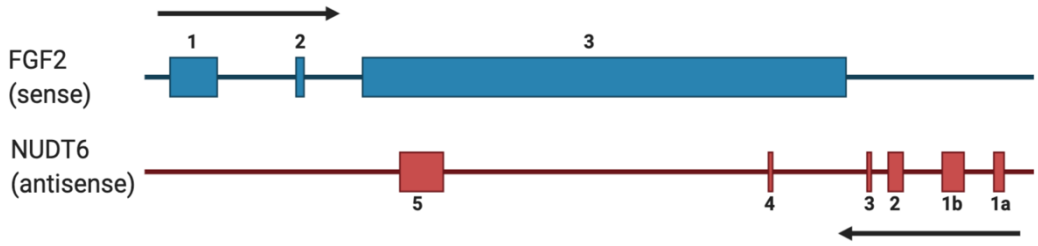

Figure 6 FGF2 and *NUDT6* sense-antisense pair. Adapted from (McEachern and Murphy 2014), Mol Endocrinol 28, 477-89

Its name, Nudix Hydrolase 6 (*NUDT6*), comes from its coding potential for a 25kDa Nudix motif polypeptide, which was also first described by Kimelman *et al*. (Kimelman and Kirschner 1989). He further hypothesized that the regulation is facilitated post-transcriptionally *via* adenine-to-inosine conversion caused by *NUDT6,* which is only exerted on dsRNA, a *NUDT6* – *FGF2* hybrid (Kimelman and Kirschner 1989).

1.4. Gaps in knowledge and Aim of the Thesis

Both carotid artery disease and abdominal aortic aneurysm remain significant mortality risks within society. Especially in a late disease stage, they both pose an increased risk for patients with events like carotid plaque rupture leading to an ischemic stroke or an aortic rupture with a mortality rate of up to 80% (Lindholt *et al.* 2012). There is no pharmaceutical treatment available (Golledge 2019). Many efforts are made in researching the genesis of both diseases: Many aspects that are thought to be harmful in the early stages might be beneficial in an advanced stage of the respective disease.

Performing a transcriptomic array of stable and unstable carotid plaques revealed several upregulated ncRNAs in unstable lesions. One of them was *NUDT6* which caught our attention due to its natural antisense inhibition activity towards *FGF2,*

a gene that is downregulated in unstable lesions. FGF2 is known to be a potent mitogen for SMC proliferation and migration (Lindner and Reidy 1991, Fox and Shanley 1996, Miyamoto *et al.* 1998, Tsuji-Tamura and Tamura 2022), an impaired process in advanced-stage vascular diseases which paves the ground for plaque- or aortic rupture. However, the role of *NUDT6* in cardiovascular diseases is unknown.

Therefore, this thesis aims to investigate the involvement of *NUDT6* in vascular disease progression, if inhibition of this ncRNA benefits FGF2 expression and SMC survival, and if it would reduce the rupture rate or halt the aortic growth respectively *in vivo*. Further, it will be elucidated if *NUDT6* interacts with other partners apart from *FGF2* in the context of vascular diseases, especially smooth muscle cells. Thus, new therapeutic paths can be unraveled using target regulation via inhibition of a NAT.

2. Materials

2.1. Chemicals

Name	Cat #	Manufacturer
Acetic Acid	33209-1L-M	Sigma (Steinheim, GER)
Agarose SERVA	11404.04	Serva (Heidelberg, GER)
Ampicillin Sodium Salt	A0166-5G	Sigma (Steinheim, GER)
Angiotensin II human	A9525-5mg	Sigma (Steinheim, GER)
Bovine Serum Albumine	A9576-50ml	Sigma (Steinheim, GER)
Bovine Serum Albumine	A7030-50g	Sigma (Steinheim, GER)
Chloroform	32211-1L-M	Sigma (Steinheim, GER)
Citric Acid monohydrate	1.00244.1000	Merck (Darmstadt, GER)
Collagenase A	11088793001	Roche (Mannheim, GER)
Diethyl pyrocarbonate	D5758	Sigma (Steinheim, GER)
Dimethyl solfoxide	D8418-250ml	Sigma (Steinheim, GER)
DPBS without CaCl and MgCl	D8537-500ml	Sigma (Steinheim, GER)
DTT 100mM	P117C	Promega (Madison, WI, USA)
EDTA powder	324503	Merck (Darmstadt, GER)
EDTA, 0.5M	E522-100ML	VWR (Darmstadt, GER)
Eosin	11503.01	Morphisto (Frankfurt am Main, GER)
Ethanol 70%	T913.3	Carl Roth (Karlsruhe, GER)
Ethanol 96%	T171.4	Carl Roth (Karlsruhe, GER)
Ethanol 99%	5054.1	Carl Roth (Karlsruhe, GER)
Formaldehyde solution 16%, Methanol-free	28908	Life Technologies (Bleiswijk, NL)
GelRed Dye	41002	Biotium (Fremont, CA, USA)
Glycerol	G5516-500ml	Sigma (Steinheim, GER)
H2O2	1.08597.1000	Merck (Darmstadt, GER)
Hämalaunlösung sauer nach Mayer	T865.2	Carl Roth (Karlsruhe, GER)
HCl 2N	T134.1	Carl Roth (Karlsruhe, GER)
Hematoxylin STO	VEH-3404-100	Vector Laboraroties (Burlingame, CA, USA)
Isopropanol	6752.5	Carl Roth (Karlsruhe, GER)
Kanamycin Sulfate	11815-024	Gibco (Darmstadt, GER)
KCl	6781.3	Carl Roth (Karlsruhe, GER)
LB Broth Base	12780/052	Life Technologies (Bleiswijk, NL)
Lipopolysaccharides	L2360-10MG	Sigma Aldrich (Steinheim, GER)
MgCl2	M8266-100g	Sigma (Steinheim, GER)
Milk Powder blotting grade	T175.2	Carl Roth (Karlsruhe, GER)
NaCl	9265.1	Carl Roth (Karlsruhe, GER)

NaOH 2N	T135.1	Carl Roth (Karlsruhe, GER)
NP-40 IGEPAL	I8896-50ML	Sigma (Steinheim, GER)
oxLDL	Gift	gifted by Ewa Ehrenborg Group, Karolinska Institutet, SE
Paraformaldehyde, 4%	HL96753.1000	Histolab (Askim, SE)
PBS tablets	18912-014	Gibco (Paisley, UK)
Pikrofuchsinlösung		Hospital Pharmacy (Klinikum rechts der Isar)
Resorcinfuchsin nach Weigert		Hospital Pharmacy (Klinikum rechts der Isar)
Sodium Deoxycholate	D6750-25g	Sigma (Steinheim, GER)
TRIS Base	A411.2	Carl Roth (Karlsruhe, GER)
Tris HCl	T3253-500g	Sigma (Steinheim, GER)
Triton x-100	x100-500ml	Sigma (Steinheim, GER)
Tween 20	P9416-50ml	Sigma (Steinheim, GER)
Tween 40	p1504-100ml	Sigma (Steinheim, GER)
Weigert'sche lösung i		Hospital Pharmacy (Klinikum rechts der Isar)
Weigert'sche lösung ii		Hospital Pharmacy (Klinikum rechts der Isar)
Xylol	9713.5	Carl Roth (Karlsruhe, GER)

2.2. Buffers

2.2.1. Bacterial Culture

Kanamycin Stock

50mg	Kanamycin
1ml	ddH_2O

Ampicillin Stock

100mg	Ampicillin
1ml	ddH_2O

LB Broth

25g	LB Broth Base
1L	ddH_2O

Autoclave before use.

1x TBE Buffer for Agarose Gel Electrophoresis

20ml	50x TAE Buffer
980ml	ddH_2O

1.5% Agarose Gel for Gel Electrophoresis

1.5g	Agarose
100ml	ddH_2O

Boil in the microwave until dissolved. Add 10µl of 10000X GelRed and cast the gel. Allow the gel to set for 1h at RT.

2.2.2. RNA Pulldown

RNA Folding Buffer

20mM	Tris-HCl pH 7.5
100mM	KCl
10mM	$MgCl_2$
20 U	RNaseOUT

in RNase-free H_2O

Lysis Buffer

50mM	Tris HCl pH 8
150mM	NaCl
0.5% (v/v)	NP-40 IGEPAL
1x	cOmplete Protease Inhibitor

in RNase-free H_2O

For 5ml Lysis Buffer, add ½ tablet of cOmplete Protease Inhibitor and 10µl RNaseOUT.

Dilution Buffer

20mM	Tris-HCl pH 7.4
150mM	NaCl
2mM	EDTA pH 8
0.5%	Triton X-100
1x	cOmplete Protease Inhibitor
	RNaseOUT

in RNase-free H_2O.

Prepare Dilution Buffer with 200mM NaCl the same way. Add an adequate amount of RNaseOUT as suggested by the manufacturer.

Protease and RNA Inhibitors were added freshly in each aliquot of the buffer used for the experiment.

Mass-Spectrometry Washing Buffer

10mM	Tris-HCl pH 7.4
150mM	NaCl

2.2.3. SDS-PAGE and Western Blotting

Complete RIPA

2880µl	RIPA Buffer
30µl	Protease Cocktail
30µl	Phosphatase Cocktail II
30µl	Phosphatase Cocktail III

30µl	EDTA

1x MES Running Buffer

50ml	20x Bolt MES Running Buffer
950ml	ddH_2O

10x TBS

24g	Tris Base
88g	NaCl
900ml	ddH_2O

Adjust pH to 7.6 and fill up to 1L with ddH_2O.

1x TBS-T

100ml	10X TBS
1ml	Tween-20
900ml	ddH_2O

5% BSA or 5% milk in TBS-T

100ml	TBS-T
5g	BSA or milk

2.2.4. Cell Culture

Freezing Medium

70%	FBS
20%	Smooth Muscle Cell Growth Medium
10%	DMSO

RSB

500µl	1M Tris pH7.4
1000µl	0.5M NaCl
500µl	0.3M $MgCl_2$
48ml	ddH_2O

RSBG40

500µl	1M Tris pH7.4
1000µl	0.5M NaCl
500µl	0.3M $MgCl_2$
5ml	19% Glycerol
43ml	ddH_2O

Before use, add 0.5% NP-40 IGEPAL (50µl in 10ml) and 0.5mM DTT (50µl in 10ml from 0.1M Stock).

Detergent

0.3g	Sodium Deoxycholate
660µl	Tween-40
to 10ml	H_2O

2.2.5. Staining

10X TRIS Buffer

60.5g	Tris Base
90g	NaCl
900ml	ddH_2O

adjust pH to 7.6 and fill up to 1L with ddH_2O.

Citric Acid Buffer for Antigen Retrieval

4.2g	Citric Acid Monohydrate
1.7L	ddH_2O

adjust pH to 6 and fill up to 2L with ddH_2O.

Proteinase K Buffer

5ml	1M Tris-HCL pH7.4
2ml	0.5M EDTA
0.2ml	5M NaCl
to 1L	RNase-free H_2O

Autoclave.

SSC Solutions

5x SSC	250ml 20x SSC	750ml RNase-free H_2O
1x SSC	50ml 20x SSC	950ml RNase-free H_2O
0.2x SSC	10ml 20x SSC	990ml RNase-free H_2O

Autoclave.

PBS

2	PBS Tablets
1l	RNase-free H_2O

Autoclave.

PBS-T pH 7.4

1ml	Tween-20
1l	autoclaved PBS in RNase-free H_2O

KTBT

7.9g	Tris-HCl
8.7g	NaCl
0.75g	KCl
1l	RNase-free H_2O

Autoclave.

RNase-free Water

1ml	Diethyl pyrocarbonate
1l	ddH_2O

Shake well and let evaporate for 30min under a chemical hood.

Autoclave.

2.3. Ready-to-use Reagents and Solutions

2.3.1. PCR

Name	Cat #	Manufacturer
High-Capacity RNA-to-cDNA Kit	4387406	Applied Biosystems (Vilnius, LT)
High-Capacity cDNA Reverse Transcription Kit with RNase Inhibitor	437966	Applied Biosystems (Vilnius, LT)
miRNeasy Micro Kit	1071023	Qiagen (Hilden, GER)
miRNeasy Mini Kit	217004	Qiagen (Hilden, GER)
QIAzol Lysis Reagent	79306	Qiagen (Hilden, GER)
TaqMan Fast Advanced Master Mix	4444557	Applied Biosystems (Vilnius, LT)
TaqMan Gene Expression Master Mix	4369016	Applied Biosystems (Vilnius, LT)
TaqMan Universal Master Mix II, no UNG	4440040	Applied Biosystems (Vilnius, LT)

2.3.2. Bacterial Culture

Name	Cat #	Manufacturer
Biotin RNA Labeling Mix 10x conc.	11685597910	Roche (Mannheim, GER)
CutSmart buffer	B6004S	New England Biolabs (Ipswich, MA, USA)
GelPilot DNA Loading Dye	239901	Qiagen (Hilden, GER)
GeneRuler Low Range DNA Ladder	SM0323	Thermo Fisher Scientific (Darmstadt, GER)
imMedia Agar with Ampicillin	Q60120	Thermo Fisher Scientific (Darmstadt, GER)
imMedia Agar with Kanamycin	Q61120	Thermo Fisher Scientific (Darmstadt, GER)
LB Broth Base	12780052	Thermo Fisher Scientific (Darmstadt, GER)
QIAprep Spin Miniprep Kit	27104	Qiagen (Hilden, GER)
S.O.C. Medium	15544034	Thermo Fisher Scientific (Darmstadt, GER)

2.3.3. RNA Pulldown and RNA Immunoprecipitation

Name	Cat #	Manufacturer
Magna RIP RNA-Binding Protein Immuniprecipitation Kit	17-700	Merck (Darmstadt, GER)
MyOne Streptavidin C1 Beads	65002	Thermo Fisher Scientific (Darmstadt, GER)
Pierce Silver Stain for Mass Spectrometry	24600	Thermo Fisher Scientific (Darmstadt, GER)
QIAquick PCR Purification Kit	28106	Qiagen (Hilden, GER)
Quick Spin Columns for radiolabeled RNA purification	11 274 015 001	Roche (Mannheim, GER)
RiboRuler RNA Marker	SM1833	Thermo Fisher Scientific (Darmstadt, GER)
Rneasy MinElute Cleanup Kit	74204	Qiagen (Hilden, GER)
SYBR™ Green II RNA Gel Stain	S7564	Thermo Fisher Scientific (Darmstadt, GER)
TBE Urea Gels 6%	EC6865BOX	Thermo Fisher Scientific (Darmstadt, GER)
TBE Urea Sample Buffer 2X	LC6876	Thermo Fisher Scientific (Darmstadt, GER)

2.3.4. Western Blot

Name	Cat #	Manufacturer
10X Bolt Sample Reducing Agent	B0009	Thermo Fisher Scientific (Darmstadt, GER)
10x TBE Electrophoresis Buffer	B52	Thermo Fisher Scientific (Darmstadt, GER)
20x Bolt MES Buffer	B0002	Thermo Fisher Scientific (Vilnius, LIT)
50X TAE Electrophoresis Buffer	B49	Thermo Fisher Scientific (Darmstadt, GER)
Bolt 4-12% Bis Tris Plus 10 well	NW04120BOX	Thermo Fisher Scientific (Darmstadt, GER)
Bolt 4-12% Bis Tris Plus 15 well	NW04125BOX	Thermo Fisher Scientific (Darmstadt, GER)
ECL Prime Western Blotting Detection Reagent	RPN2236	Cytiva (Marlborough, MA, USA)
NuPAGE LDS Sample Buffer	NP0007	Thermo Fisher Scientific (Darmstadt, GER)
PageRuler Prestained Protein Ladder	26616	Thermo Fisher Scientific (Darmstadt, GER)
Pierce BCA Protein Assay Kit	23227	Thermo Fisher Scientific (Rockford, IL, USA)
Pierce Fast Western Blot Kit ECL Substrate	35050	Thermo Fisher Scientific (Darmstadt, GER)

Restore PLUS Stripping Buffer	46430	Thermo Fisher Scientific (Darmstadt, GER)
RIPA Buffer 1X	89901	Thermo Fisher Scientific (Darmstadt, GER)
Trans-blot turbo transfer pack, 0.2µm pvdf	1704156	Bio Rad (Hercules, CA, USA)
VeriBlot for IP Detection Reagent (HRP)	ab131366	abcam (Cambridge, UK)

2.3.5. Cell Culture

Name	Cat #	Manufacturer
DMEM-F12	D0697-500ML	Sigma Aldrich (St.Louis, MO, USA)
Caspase 3/7 Green Apoptosis Reagent	4440	Essen BioScience (Herfordshire, UK)
Dulbecco's PBS	D8537	Sigma Aldrich (St.Louis, MO, USA)
FBS	10270106	Thermo Fisher Scientific (Darmstadt, GER)
Lipofectamine 3000	L3000001	Thermo Fisher Scientific (Darmstadt, GER)
Lipofectamine RNAiMAX	13778150	Thermo Fisher Scientific (Darmstadt, GER)
Opti-MEM	31985070	Thermo Fisher Scientific (Darmstadt, GER)
Opti-MEM, no phenol red	11058021	Thermo Fisher Scientific (Darmstadt, GER)
SMC Growth Medium	311-500	Cell Applications (San Diego, CA, USA)
SMC Growth Medium	PB-311K-500	PELO Biotech (Planegg, GER)

2.3.6. Staining

Name	Cat #	Manufacturer
AEC Solution	415182F	Nichirei (Chuo, Tokyo, JPN)
CC/Mount	C9368	Sigma Aldrich (St.Louis, MO, USA)
Dako REAL Antibody Diluent	S2022	DAKO (Glostrup, DK)
Dako REAL Detection System Peroxidase/DAB Rabbit/Mouse	K5001	DAKO (Glostrup, DK)
Eukitt mounting medium	03989-100ml	Sigma Aldrich (St.Louis, MO, USA)
Immedge Pen	VECTH-4000	VWR (Darmstadt, GER)
miRCURY LNA miRNA ISH Buffer Set (FFPE)	339450	Qiagen (Hilden, GER)

Normal Goat Serum	G6767-100ML	Sigma Aldrich (St.Louis, MO, USA)
Normal Sheep Serum	013-000-121	Jackson ImmunoResearch (West Grove, PA, US)
Sakura O.C.T. Compound	12351753	Fisher Scientific (Waltham, MA, USA)
UltraPure SSC, 20X	15557036	Thermo Fisher Scientific (Darmstadt, GER)
Vectastain ABC-HRP-Kit	PK-6100	Vector Laboraroties (Burlingame, CA, USA)

2.3.7. Antibodies

Antigen	Species & Clonality	Dilution	Purpose	Cat #	Distributor
αSMA	Ms, mono	1:250	IHC	M0635	DAKO (Glostrup, DK)
αSMA	Rb poly	1:250	IHC	ab5694	abcam (Cambridge, UK)
βActin	Ms, mono	1:1000	WB	A1978	Sigma (St.Louis, USA)
βTubulin	Rb, poly	1:500	WB	ab6046	abcam (Cambridge, UK)
CSRP1	Rb, poly	1:100	IHC	ab70010	abcam (Cambridge, UK)
		1:500	WB		
CRP1	Rb, poly	5µg	IP	PA5-86703	Invitrogen (Carlsbad, CA,USA)
CDC42	Rb, poly	1:250	IHC	ab187643	abcam (Cambridge, UK)
		1:20000	WB		
DIG	Sh, Fab-fragments	1:800	ISH	11093274910	Roche (Basel, CH)
FGF2	Rb, poly	1:500	IHC	ab8880	abcam (Cambridge, UK)
FGF2	Rb, mono	1:1000	WB	ab215373	abcam (Cambridge, UK)
IgG H&L	Gt anti-rabbit	1:10000	WB	ab205719	abcam (Cambridge, UK)
IgG H&L	Gt anti-mouse	1:10000	WB	ab205718	abcam (Cambridge, UK)

2.3.8. Nucleic Acids

Name	Cat #	Manufacturer
CDC42 siRNA	s2765	Thermo Fisher Scientific (Darmstadt, GER)
CEBPB siRNA	s2892	Thermo Fisher Scientific (Darmstadt, GER)
CSRP1 siRNA	s3654	Thermo Fisher Scientific (Darmstadt, GER)
EV plasmid	PS100001	Origene (Rockville, MD, USA)
GFP plasmid	gifted	Dr. Francesca Fasolo
DH5a competent cells	18263-012	Sigma Aldrich (St.Louis, MO, USA)
NUDT6 plasmid	RC203470	Origene (Rockville, MD, USA)
NUDT6 sirna	122202	Thermo Fisher Scientific (Darmstadt, GER)
Silencer Negative Control siRNA1	AM4611	Thermo Fisher Scientific (Darmstadt, GER)

2.3.9. *NUDT6* Detection Probes ISH

Sequence	species	RNA Tm
/5DigN/GGCAATGAAGTGGCTCTGCA/3Dig_N/	mouse	75°C
/5DigN/TCGCACGCTCCAACTGGCGGAT/3Dig_N	human	85°C

2.3.10. *in vivo* GapmeRs ("*Nudt6*-ASO" or "*NUDT6*-ASO")

Mouse GapmeR

Sequence	Target
GGACCTGAATTCTGA	*Nudt6*
/5TYE563/AACACGTCTATACGC	SCR

Porcine GapmeR

Sequence	Target
GGCAATAAATCGGCTT	*NUDT6*

2.3.11. TaqMan Primers

Gene	Species	Cat#
ACTA	pig	HS00426835_G1
ACTB	mouse	MM02619580_G1
ACTB	pig	SS03376081_u1
αSMA	mouse	MM00725412_s1
CDC42	human	HS00918044_g1
CSRP1	human	HS00187916_m1
FGF2	human	HS00266645_m1
FGF2	mouse	MM01285715_m1
FGF2	pig	SS03375809_U1

GAPDH	human	HS03929097_gH
MYHC	pig	SS03373508_M1
NUDT6	human	HS00246601_M1
NUDT6	mouse	MM01285702_g1
RPLPO	human	HS00420895_gH
UBC	human	HS00824723_m1

2.4. Enzymes and Enzyme Inhibitors

Name	Cat #	Manufacturer
DNase I Amplification Grade	18068-015	Invitrogen (Carlsbad, CA, USA)
cOmplete Protease Inhibitor Tablets	11697498001	Roche (Mannheim, GER)
Halt Protease Inhibitor Cocktail	78429	Thermo Fisher Scientific (Darmstadt, GER)
HindIII	R0104S	New England Biolabs (Ipswich, MA, USA)
Phosphatase Inhibitor Cocktail II	P5726	Sigma Aldrich (St.Louis, MO, USA)
Phosphatase Inhibitor Cocktail III	P0044	Sigma Aldrich (St.Louis, MO, USA)
RNase-free Dnase Set	79254	Qiagen (Hilden, GER)
RNaseOUT	10777-019	Thermo Fisher Scientific (Darmstadt, GER)
T7 RNA Polymerase	P2077	Promega (Madison, WI, USA)
Trypsin-EDTA	25200056	Thermo Fisher Scientific
TURBO Dnase	AM2238	Invitrogen (Carlsbad, CA, USA)
Xho1	R0146S	New England Biolabs (Ipswich, MA, USA)

2.5. Experimental Animals and Primary Cells

Background	Genotype	Experiments	Provider
C57BL/6J	*ApoE* $^{-/-}$	AngII + CAR	Taconic Bioscience (Silkeborg, DK)
C57BL/6N	n/a	PPE	Jackson Laboraroties (Bar Harbor, ME, USA)
Yucatan mini pig	*LDLR*$^{-/-}$	PPE	Exemplar Genetics (Coralville, IA, USA)

Name	Cat #	Manufacturer
hAoSMCs	354p-05a	Cell Applications (San Diego, CA, USA)
hCtSMCs	3514-05a	Cell Applications (San Diego, CA, USA)
Yucatan Pig Fibroblasts	n/a	Gift from Prof. Yonglun Luo, Aarhus University, Denmark

2.6. Material for *in vivo* studies

Name	Cat #	Manufacturer
10-12x20mm PTA balloon	SBI120020080	Medtronic (Dublin, IRE)
5.0 Vicryl	J500G	Ethicon (Sollentuna, Sweden)
9-11x20mm PTA balloon	SBI100040080	Medtronic (Dublin, IRE)
High Fat Diet for Pigs	C1090	Altromin (Lage, GER)
Isoflurane	sc-470926	Santa Cruz Biotechnologies (Dallas, TX, USA)
Mouse Microbubble Kit	31S1052S	Xceltis (Mannheim, GER)
Osmotic Minipumps	2001	Alzet (Cupertino, CA, USA)
plastic cast	1.570.001	Promolding (Den Haag, NL)
Porcine Pancreatic Elastase	E7885-20MG	Sigma Aldrich (Darmstadt, GER)

2.7. Consumables

Name	Cat #	Manufacturer
25cm2 c/n Flask	3289	Corning (Corning, NY, USA)
75cm2 c/n Flask	3290	Corning (Corning, NY, USA)
Amplitube PCR Reaction Strips	T320-2N	Simport (Saint-Mathieu-de-Beloeil, CAN)
Cell Culture Flask, 175cm2	660 175	Greiner (Melsungen, GER)
CultureSlides	354104	Falcon (Corning, NY, USA)
EASYstrainer	542 070	Greiner (Frickenhausen, GER)
FastGene Fast 96 well pcr plate	FG-03890	Nippon Genetics (Düren, GER)
Imagelock Plates	4379	Sartorius (Ann Arbor, MI, USA)
Injekt 20ml luer solo	4606205V	Braun (Melsungen, GER)
Millex GP 0.22µm	SLGP033RS	Merck (Cork, IRE)
Omnifix-f	9161406V	Braun (Puchheim, GER)
PCR Clear Seal	FG-93AC	Nippon Genetics (Düren, GER)

2.8. Equipment

Name	Manufacturer
ABJ 220-4M Scale	KERN (Balingen-Frommern, GER)
Analog vortex mixer	VWR (Darmstadt, GER)
Olympus Slideview VS200	Olympus (Shinjuku, Tokyo, JPN)
Binder C 150 Incubator	Binder (Tuttlingen, GER)
BioGen Series PRO 200 Ruptor	PRO Scientific (Oxford, CT, USA)
Centrifuge 5415 D	Eppendorf (Hamburg, GER)
Certomat R Bacterial Shaker	B.Braun (Melsungen, GER)
Certomat HK Bacterial Shaker	B.Braun (Melsungen, GER)
Cold Plate EG1150C	Leica (Wetzlar, GER)
Cryo 1°C Freezing Container	Nalgene (Rochester, NY, USA)
DM 4000 B Microscope	Leica (Wetzlar, GER)

Dynamag 2 Magnet	Thermo Fisher Scientific (Darmstadt, GER)
Epoch Plate Reader	BioTek (Winooski, VT, USA)
GelDoc XR+ Imaging System	BioRad (Hercules, CA, USA)
GTS Sonoporation System	Sonitron (Sint-Niklaas, BEL)
Heat Plate	Medax (Neumünster, GER)
HERA Cell 240i Incubator	Thermo Fisher Scientific (Darmstadt, GER)
HERA Safe KS Sterile Benches	Thermo Fisher Scientific (Darmstadt, GER)
HERA Therm Oven	Thermo Fisher Scientific (Darmstadt, GER)
Heraeus Fresco 21 Centrifuge	Thermo Fisher Scientific (Darmstadt, GER)
Hula Mixer	Invitrogen (Carlsbad, CA, USA)
Incucyte ZOOM S2	Essen BioScience (Herfordshire, UK)
InoLab pH7110 pH-Meter	WTW (Weilheim, GER)
InSlide Out Oven Model 241000	Boekel Scientific (Feasterville, PA, USA)
Logiq S7 System	GE (Frankfurt am Main, GER)
MasterCycler nexus gradient	Eppendorf (Hamburg, GER)
MCO-230AICUV-PE	PHC (Etten-Leur, NL)
Mictorome RM2552	Leica (Wetzlar, GER)
Mini Plate Centrifuge	Nippon Genetics (Düren, GER)
Mini Star Centrifuge	VWR (Darmstadt, GER)
NanoDrop 2000C	Thermo Fisher Scientific (Darmstadt, GER)
Pellet Mixer	VWR (Darmstadt, GER)
PowerPac Electrophoresis Unit	BioRad (Hercules, CA, USA)
PrimoVert Microscope	Zeiss (Oberkochen, GER)
QuantStudio 3	Applied Biosystems (Darmstadt, GER)
Sicomatic Pressure Cooker	WMF (Geislingen a.d.Steige, GER)
Sub-Cell GT Agarose Gel Unit	BioRad (Hercules, CA, USA)
Thermal Shake Lite	VWR (Darmstadt, GER)
Thunder Imager	Leica (Wetzlar, GER)
Trans-Blot Turbo	BioRad (Hercules, CA, USA)
TS-100 Thermal Shaker	Biosan (Riga, LV)
VacuPump	Integra (Zizers, CH)
VariMax Platform Rocker	Thermo Fisher Scientific (Darmstadt, GER)
Veriti Cycler	Applied Biosystems (Darmstadt, GER)
Vevo 2100 Imaging System	VisualSonics (Toronto, CAN)
VMS-A Magnetic Stirrer	VWR (Darmstadt, GER)
Water Bath WNB14	Memmert (Schwabach, GER)
Water Bath GFL 1052	GFL (Burgwedel, GER)
Western Blot Imaging System c600	Azure Biosystems (Dublin, CA, USA)
WoundMaker 96	Essen BioScience (Herfordshire, UK)
Xcell SureLock for Electrophoresis	Thermo Fisher Scientific (Darmstadt, GER)

2.9. Software

Software	Manufacturer
Image Lab V4.1 Build 16	Bio Rad (Hercules, CA, USA)
Gel Analyzer v19	Istvan Lazar, PhD

Incucyte Base Analysis Software and Migration Module	Essen Bioscience (Herfordshire, UK)
Leica Application Suite X (LAS X)	Leica (Wetzlar, GER)
Microsoft Office for Mac v16.59	Microsoft (Redmond, WA, USA)
NDP Viewer 2	Hamamatsu Photonics (Hamamatsu, JP)
Prism for Mac OS X v8, v9	GraphPad Software (La Jolla, CA, USA)
QuantStudio Design & Analysis Software v1.4.3	Thermo Fisher (Darmstadt, GER)
cSeries Capture Software	Azure Biosystems (Dublin, CA, USA)

3. Methods

3.1. Molecular Biology – Nucleic Acid

RNA isolation from cells, human tissue and murine samples

To isolate RNA, cells were washed once with PBS. Then, Qiazol (Qiagen) was added – 700µl (6 well plate), 500µl (12 well plate), or 350µl (24 well plate) per well. Cells were scraped off the surface with a cell scraper (Sigma) and transferred to a microcentrifuge tube after flushing the well twice. Then, the RNeasy mini kit (Qiagen) was used according to the manufacturer's instructions. If the estimated yield was expected to be very little, the RNeasy micro kit (Qiagen) was used. If DNA templates (from plasmids) have to be removed, the additional DNase step, which can be found in the supplement of the manufacturer's protocol, was performed. Briefly, 140µl (6 well) or 70µl (12/24 well) of chloroform (Merck) was added to each sample, vortexed for 20s, and incubated for 2min before centrifuging at 12000g for 15min at 4°C. The transparent phase on top was transferred to a new tube and mixed with 1.5 volume of 100% Ethanol (Carl Roth). The mix was pipetted on the corresponding spin column (depending on the kit). After one wash step with RWT buffer, two RPE buffer washes (or one RPE wash step and one 80% Ethanol (Carl Roth) wash step for miRneasy micro kit) were performed before the RNA was eluted. Depending on the expected yield, the volume of eluting agent (RNase-free water) was adapted. In most cases, 30µl or 14µl was used for elution. After the last centrifugation, samples were put on ice.

For the RNA pulldown analysis, 15µl elution volume and DNase digest (Qiagen) with the miRneasy micro kit were performed.

For RNA isolation from tissue, a tissue ruptor (PRO scientific) was used. A 20-30µg piece was cut from the tissue sample on ice and immediately transferred to a Qiazol-containing microcentrifuge tube. Since human tissue is calcified, the samples were snap-frozen in liquid nitrogen to make homogenization easier. Each sample was homogenized for 30s. Then, the sample was cooled down on dry ice. In between samples, the blade was washed in Ethanol and water. After 3-5 rounds, most of the tissue is homogenized. For mouse tissue like the aorta, the tissue was directly homogenized without the use of liquid nitrogen. Around 3-4 rounds of 30s each were needed. The protocol was then followed as described above. For mouse tissue, the miRneasy micro kit was used due to low yield.

cDNA synthesis

To generate a more stable intermediate product, RNA was reverse transcribed to cDNA using the High-Capacity RNA-to-cDNA Kit (Applied Biosystems) or the High-Capacity cDNA Reverse Transcription Kit with RNase Inhibitor (Applied Biosystems). **Table 1** shows the setup for a cDNA reaction using each of the two kits. Reverse transcription was performed in a thermocycler (Eppendorf and Thermo Fisher). The programs are shown in **Table 2**. Prior to usage, RNA was diluted accordingly to 100-400ng, depending on availability and concentration. For RNA pulldown eluate analysis, all RNA (15µl) was used for cDNA synthesis, except for Input Controls (1.5µl). cDNA was stored at 4°C short term and -20°C long term.

Components	Kit # 4387406	Kit # 4374966
2x RT Buffer Mix	10µl	-
20x RT Enzyme Mix	1µl	-
10x RT Buffer		2.0µl
25x dNTP Mix (100mM)		0.8µl
MultiScribe RT		1.0µl
10x RT Random Primers		2.0µl
RNase Inhibitor		1.0µl
RNA	100-400ng	100-400ng
Nuclease-free Water	To 20.0µl	To 10µl

Table 1 *Reaction setup for cDNA generation.*

Kit #		Step 1	Step 2	Step 3	Step 4
4387406	Temperature	37°C	95°C	4°C	
	Time	60min	5min	infinite	
4374966	Temperature	25°C	37°C	85°C	4°C
	Time	10min	120min	5min	infinite

Table 2 *Thermocycling profile for cDNA generation.*

Both adapted from High-Capacity cDNA Reverse Transcription Kit with RNase Inhibitor Cat#4374966 from Thermo Fisher.

Quantitative Real-Time PCR

This method enables the quantification of a given cDNA generated in the previously described step. Here, TaqMan reagents (Applied Biosystems) have been used, which

are labeled with a FAM reporter dye. Before using the cDNA in this assay, it has to be diluted to 100ng. Then, a TaqMan reaction is prepared using either the Gene Expression Master Mix (Applied Biosystems) or the Fast Advanced Master Mix (Applied Biosystems), according to **Table 3**. A full list of used TaqMan assays can be found in the material section 2.3.11. The PCR is performed in a QuantStudio 3 machine (Applied Biosystems) with settings recommended by the manufacturer (**Table 4**). The cycle number was set to 40. In order to analyze the quantified cDNA, the $\Delta\Delta$-C_t method was used to finally calculate the fold change.

Components	
TaqMan Master Mix (2X)	10µl
TaqMan Assay (10X)	1µl
Nuclease-free Water	6µl
cDNA Template	2µl [100ng]

Table 3 *Reaction setup for qRT-PCR. Adapted from Gene Expression Master Mix Cat#4369016 from Thermo Fisher.*

	UNG incubation	Polymerase Activation	PCR - Denature	PCR - Anneal
Temperature	**50°C**	**95°C**	**95°C**	**60°C**
Time	**2min**	**10min**	**15sec**	**60sec**

Table 4 *Thermocycling profile for qRT-PCR. Adapted from Gene Expression Master Mix Cat#4369016 from Thermo Fisher.*

Quantitation of DNA and RNA

To be able to use an equal amount of RNA for cDNA generation and to receive information on nucleic acid purity, RNA was quantified using the NanoDrop 2000 Spectrophotometer (Thermo Fisher). After blanking and measuring 2µl of water to ensure proper blanking, 2µl of each undiluted RNA sample was measured. The absorbance ratio of 260nm and 280nm was used to define the purity of the sample – RNA samples with a ratio of 1.8 to 2.1 and DNA samples with a ratio of 1.7 to 1.9 were regarded as pure.

Transformation of competent bacteria

Transformation is the process of bacteria taking up extracellular genetic material from their surroundings. Utilizing this mechanism leads to the expression of a large amount of DNA which normally exceeds the capacity of *E.coli* bacteria. However, bacteria used for transformation are made competent to take up free DNA from the environment. This can be done by chemicals or electroporation. Here, chemically

competent Library Efficiency DH5α cells (Invitrogen) were used. 50µl cells per reaction were thawed on ice, then 0.5µl of plasmid DNA and 0.5µl of DNase-free water were added to the cells which were then stirred carefully with the pipette tip. Cells were incubated on ice for 10 min. Then, cells were placed into a 42°C Thermo Cycler (VWR) without shaking to open up the pores of the membrane, allowing the plasmid DNA to be taken up by the cells. The mix was incubated on ice for 2-5min min before adding 100µl of S.O.C medium (Thermo Fisher) and shaking for 1h at 225rpm at 37°C. 80µl were spread on an LB agar plate containing the respective antibiotic (*NUDT6* and Empty Vector: Kanamycin; *GFP*: Ampicillin; 1:1000) close to a Bunsen burner flame. The plates were incubated at 37°C overnight.

Overnight Culture Inoculation

After letting the plates incubate at 37°C overnight, a single colony was picked with a clean pipette tip and ejected into 5ml of LB medium in a 50ml Falcon containing the respective antibiotic in a 1:1000 dilution. In addition, one blank 5ml LB medium with a pipette tip serves as a control. Cultures were incubated overnight at 37°C and 225rpm in a bacteria shaker (B.Braun Biotech). If there is no growth (milky LB) in the blank control on the next day, the cultures can be further processed.

DNA isolation from competent *E.coli* bacteria

To isolate the DNA from the competent *E.coli*, the QIAprep Spin Miniprep Kit (Qiagen) was used following the manufacturer's instructions. Briefly, 2x 2ml of overnight culture was pelleted at 8000rpm in a tabletop centrifuge (Thermo Fisher) for 3min at RT. Then, cells were resuspended in buffer P1 before buffer P2 was added. The tube was inverted until the suspension became clear. For better lysis control, LyseBlue reagent was added to buffer P2. After no longer than 5min, Buffer N3 was added and the tube was inverted again 4-6 times and centrifuged for 10min at 13000rpm. The supernatant was added to a spin column and centrifuged, washed once with buffer PB and once with buffer PE, with centrifugation in between. To remove any leftover wash buffer, the column was once more centrifuged for 1min. Then, the column was placed on a 1.5ml Eppendorf tube, and 30µl DNase-free water was added. After letting the column stand for 1min, the sample was centrifuged for 1min. DNA purity and concentration were determined afterward and stored at -20°C.

Enzymatic Digestion

To produce a template for the *in vitro* transcribed biotinylated RNA, which was used in the RNA pulldown, the respective plasmid had to be linearized. The prerequisite for this procedure was a T7 promoter proximal to the MCS/the inserted DNA sequence. This was the case for both, the *GFP* (pcDNA3.1(-) backbone) and the *NUDT6* (pCMV6-Entry backbone) vector. Enzymes were used according to **Table 5**. 5µg of each plasmid was used together with 10x reaction buffer (New England Biolabs), 50U of the respective enzyme (New England Biolabs), and water to a reaction volume of 100µl. The reaction was incubated at 37°C on a Thermo Cycler (VWR) for 60min at 350rpm. Then, an inactivation step followed depending on the enzyme used (see **Table 5**). The reaction was stored at -20°C for long time or 4°C for short time.

Vector	Restriction Enzyme	Inactivation
GFP	HindIII	80°C for 20min
NUDT6	XhoI	65°C for 20min

Table 5 *Restriction Enzymes used for respective vector linearization.*

PCR purification

In order to remove any leftover enzyme and undigested template DNA, the samples underwent PCR purification after the enzymatic digestion. Here, the QIAquick PCR purification kit (Qiagen) was used according to the manufacturer's instructions. In summary, the sample was mixed with buffer PB, placed into a QIAquick column, and centrifuged to bind DNA to the column. Then, a wash step with PE buffer with centrifugation followed. To elute the DNA, 30-50µl of water was added to the column. After 1min, the purified DNA was eluted *via* centrifugation into a sterile Eppendorf tube.

Agarose gel electrophoresis

To ensure complete linearization, 100ng of digested and therefore linearized plasmid and 100ng of undigested, circular plasmid were loaded on a 1.5% agarose gel. Samples were diluted with DNase-free water and 5x loading dye (Qiagen). The gel ran for 1.5h at 140V. DNA ladder (Thermo Fisher) with a range from 2000 bp to 100 bp was used to check for length. Gels were imaged using the GelDoc system (BioRad) under UV light. Circular DNA runs slightly slower through the agarose gel compared to linearized DNA, so by comparing digested to undigested samples, it was ensured that the enzyme completely linearized the DNA.

In vitro transcription and biotinylation

After linearization, the DNA needs to be transcribed into RNA to incorporate biotinylated oligos. For that, 1µg of the plasmid DNA was used as a template for *in vitro* transcription using the T7 RNA Polymerase (Promega) according to **Table 6**. The reaction was incubated for 2h at 37°C at 300rpm. To remove any DNA template, the reaction was incubated with 1µl of TURBO DNase (Thermo Fisher) followed by quenching with 0.4µl 0.5M EDTA.

Components	
Plasmid	1µg
5x Transcription Optimized Buffer	4µl
10x Biotinylated Oligos	2µl
DTT, 100mM	2µl
RNase OUT	0.24µl
Nuclease-free Water	To 18µl
T7 RNA Polymerase	2µl

Table 6 *Reaction setup used for* in vitro *transcription of* NUDT6 *and* GFP *plasmids.*

Sephadex Columns

In order to do a clean-up and concentrate of the *in vitro* transcribed RNA, Sephadex Quick Spin Columns (Roche) were used according to the manufacturer's instructions, In brief, columns were inverted a few times, the buffer was drained, and they were inserted into a collection tube. Then, the RNA was pipetted on top, and the column was centrifuged for 4min at 1100g. RNA was measured using the NanoDrop Spectrophotometer (Thermo Fisher) and stored at -80°C.

RNA gel electrophoresis and -staining

To determine the correct size of the RNA as well as its purity in form of the absence of a smear, RNA gel electrophoresis was performed. 500ng or 1µg of RNA was mixed with 2x TBE Urea Sample Buffer (Thermo Fisher) and water to 15µl followed by a 5min incubation at 70°C with 300rpm. Then, RNA was separated on a 6% TBE-Urea Gel (Thermo Fisher) at 150V for around 90min. To check for fragment size, RiboRuler RNA ladder (Thermo Fisher) was loaded in addition to the sample RNA. To visualize the RNA bands, the gel was stained with SYBR Green II RNA Gel Stain (Thermo Fisher) according to the manufacturer's instructions. Briefly, the stock was diluted

1:10000 in TBE buffer, and the pH was adjusted to 8. While protecting it from light, the gel was stained in the prepared dilution for 30min while agitating gently. The gel was imaged using the GelDoc System (BioRad). If there was more than one band of the designated size or if there was any form of smear in the gel, the samples were excluded for RNA pulldown.

RNA Folding

Immediately before or during an incubation time of the pulldown, the RNA needs to fold into its natural secondary structure. To do that, 250ng of biotinylated RNA is mixed with 75µl folding buffer and is incubated for 2min at 90°C followed by 3min on ice and 25min at room temperature. The folded RNA is stored on ice until usage. The RNA cannot be frozen again once folded and has to be used on the same day.

RNA Pulldown

First, the cells had to be prepared for the experiment (see “Cell Culture – Sample Preparation for RNA Pulldown”). Then, 150µl of freshly prepared complete lysis buffer was added to the pellets followed by a 30min incubation on ice flicking the tubes occasionally 1-2 times during the lysis. The sample was pelleted at 17000g for 30min at 4°C, and the cell lysate supernatant was transferred into a new tube. 3x of the initial volume of dilution buffer was added.

Either during lysis or centrifugation, 20µl of MyC1 Streptavidin beads (Thermo Fisher) were washed three times with dilution buffer using a magnetic rack (Thermo Fisher) and finally resuspended in 100µl complete dilution buffer.

Then, the beads were added to the cell lysate and incubated head over tail at 4°C for 30min. The supernatant was then transferred into a new tube while taking a 5% input sample. 100µl of the folded RNA was added into the cell lysate and incubated head over tail at 4°C overnight.

On the next day, dilution buffer and 200mM NaCl dilution buffer were prepared by adding the appropriate amounts of inhibitors. Then, 80µl of Streptavidin beads per reaction were washed 3x in dilution buffer, resuspended in 100µl dilution buffer, and added to the samples. The mix was incubated head over tail at 4°C for 3 hours. Finally, 3 washing steps using the dilution buffer and the magnetic rack followed by a head-over-tail incubation at 4°C for 10min and 1 wash step as described but with 150mM NaCl dilution buffer was performed. Then, samples were washed 2x briefly in MS

buffer before resuspending in 50µl M/S buffer of which 40µl were sent for LC-MS/MS analysis. For RNA analysis, 6µl of the sample was mixed with 100µl of QIAzol (Qiagen). The remaining 4µl were mixed with 1µl of 4x LD buffer (Thermo Fisher) for gel electrophoresis and silver staining.

RNA Immunoprecipitation

To verify the identified interaction partners from the RNA pulldown, we used RNA-IP or RIP where a similar approach is used. The experiment was performed with the MagnaRIP Kit (Merck) according to the manufacturer's instructions. Briefly, cells of one T125 flask (Corning) were washed in PBS twice and scraped. After a brief centrifugation to pellet the cells, RIP Lysis buffer (included in the kit) was added and the lysate was incubated for 5min on ice before it was used or stored at -80°C. 300µl of cell lysate was needed for one run. Two runs were always performed in parallel in order to analyze both, RNA and protein. Provided magnetic beads were washed and preincubated for 30min with provided 5µg IgG Control (provided) or CRP-1 antibody (Invitrogen), respectively. Beads were then transferred to the provided IP buffer. The cell lysate was centrifuged, and the supernatant was distributed accordingly – 125µl for IgG, 125µl for CRP-1, and 50µl for Input. The input was frozen immediately at -80°C. Lysate-Antibody-Bead complexes were incubated overnight at 4°C. On the next day, complexes were washed 6x at 4°C using the magnetic separator. For RNA, 700µl Qiazol (Qiagen) was added to the beads. Isolation was performed using the miRneasy microKit (as described earlier). RNA was eluted in 13µl which was all used for cDNA generation, adjusting the volumes of buffer and enzyme accordingly. qRTPCR was performed as described using four housekeeping TaqMan assays and *NUDT6* assay. The experiment was analyzed according to Chen-Plotkin *et al*. by normalizing to housekeeping genes and IgG (Chen-Plotkin *et al.* 2006). The experiment was defined as successful once enrichment was >1.6x.

Protein was analyzed by replacing the buffers with 4xLD and 10x Reducing agent (both from Thermo Fisher) as described in "Western Blot" chapter. Input, IgG, CRP-1 fractions as well as the first wash supernatant and the beads were loaded onto the gel. For further methodological information, please refer to chapter "3.2, subchapter Western Blot". The secondary antibody used was VeriBlot antibody (abcam, Cambridge, UK) in a 1:1000 dilution. This antibody allows for detection without

interfering with denatured IgG, only recognizing native antibodies (which have not been subjected to boiling).

3.2. Molecular Biology – Protein

Bicinchoninic Acid Assay

The concentration of a given protein lysate of sources such as tissue or cells was determined using a bicinchoninic acid (BCA) protein assay.

For cellular protein lysate, cells are washed once with PBS before adding complete RIPA buffer (Thermo Fisher) to the flask (700µl) or well (70µl) and scraping the adherent cells. After transferring the cells to an Eppendorf tube on ice, the sample is homogenized using an electric pestle (VWR) for 30s on ice. Between the different samples, the pestle is washed in Ethanol and distilled water. Samples incubate on ice for 30min before centrifuging at 14000rpm for 15min at 4°C. The supernatant was transferred into a new tube on ice and is ready to be used for protein concentration.

To determine the amount of protein in the samples, the Pierce BCA Protein Assay Kit (Thermo Fisher) was used according to the protocol provided by the manufacturer. Briefly, standard and working solutions were prepared, and the according volume of either standard or sample was pipetted in duplicates. The plate was incubated for 30min in the dark at 37°C. Then, the plate was shaken briefly to evenly distribute the developed color. The plate was put into a plate reader (BioTek). Analysis was also performed according to the manufacturer's instructions by generating a standard curve.

Western Blot

To separate the proteins according to their size, 10-15µg of protein lysate was mixed with 4x Loading Dye (Thermo Fisher) and 10x Reducing Agent (Thermo Fisher) and filled with RIPA buffer to either 30µl (15 well gel) or 40µl. Then, samples are boiled for 10min at 70°C before loading them on a 4-12% Tris-Glycine gel (Thermo Fisher) in a BOLT gel station (Thermo Fisher). The tank was filled with 1x Running Buffer and 5µl of PreStained Protein Marker (Thermo Fisher) was added to at least one well. The gel station was then connected to a power source (BioRad) where 80-100V was applied until the samples reached the lower, separating part of the gel. Then, the voltage was increased to 120V until the samples reached the lower edge of the gel. The gel was removed from its cast by carefully opening it with a Spatula.

For membrane transfer, ready-to-use PVDF membranes with stacks of soaked filter paper (BioRad) were put into one cassette of the Turbo Transfer Machine (BioRad). The gel was placed carefully on top of the PVDF membrane and covered with the intended stack of filter paper (both from BioRad). To ensure complete transfer without air bubbles, a roller was applied. Then, the lid of the chamber was closed, and the 30min program was selected.

After completion, the membrane was transferred into a plastic container filled with 1x TBS-T and placed on the shaker for 5min. Meanwhile, 5%milk (Carl Roth) in TBS-T was prepared and subsequently applied for 1h to block unspecific binding. The primary antibody was prepared in the blocking buffer according to section 2.3.7. and incubated overnight at 4°C on a shaker. On the next day, the antibody was poured into a falcon and stored at -20°C for multiple uses. After 3x5min TBS-T wash, a secondary antibody in blocking buffer was applied according to section 2.3.7. for 1h. Afterward, the membrane was washed for 3x5min with TBS-T. To develop the protein bands, ECL substrate (Cytivia) was used according to the manufacturer's instructions. After a 5min incubation, the membrane was imaged using a Western Blot Imager (Azure Biotech). To be able to quantify the result, was cut to incubate the target antibody and control antibody in parallel. If this was not possible, 3x10min TBS-T wash followed by stripping solution (Thermo Fisher) was used to remove the bound antibody. Signal quantification was performed using GelAnalyzer (www.gelanalyzer.com) software by normalizing to βActin or βTubulin signal.

Silver Staining

To check for differential protein content in the different eluates of the RNA pulldown experiment, the Pierce Silver Stain for Mass Spectrometry (Thermo Fisher) was used according to the manufacturer's instructions. Afterward, a picture was taken to confirm the differential protein content of the two eluates. Once a candidate was identified via LC-MS/MS, the silver staining can identify potential enrichments at the given kDa in either of the two fractions.

Liquid Chromatography with tandem mass spectrometry (LC-MS/MS)

After performing the pulldown experiment, the 6 replicates of each condition (*NUDT6* and *GFP* biotinylated RNA) were sent to Dr. Ilka Wittig, Functional Proteomics Unit at Goethe-University in Frankfurt am Main, Germany for further processing, LC-MS/MS

as well as data analysis. Methods were provided with the analysis sheet and are described here briefly.

Sample Preparation The beads were supplemented with 6M Guanidine hydrochloride and 50mM Tris/HCl as well as 10mM Tris (2-carboxyethyl)phosphine and incubated for 5min at 95°C. Thiol alkylation was performed using 40mM chloroacetamide, and the sample was diluted with 25mM Tris/HCl and 10% acetonitrile to lower Guanidine hydrochloride concentration to 0.6M. Protein digestion was performed using 1µg trypsin overnight at 37°C. The process was stopped with trifluoroacetic acid to a concentration of 0.5%. Then, the peptides were loaded on a multi-stop-and-go tip (StageTip), and purification and elution were performed. Peptides were dried and resolved in 1% acetonitrile and 0.1% formic acid.

HLPC Methods LC/MS was performed on a Q Exactive Plus (Thermo Scientific) which is equipped with an ultra-high performance liquid chromatography unit and a Nanospray Flex Ion-Source. Peptides were loaded on a C18 reversed-phase pre-column (Thermo Scientific) and separated with an emitter tip.

MS The scan rage of the MS reached from 300 to 2000 m/z with a resolution of 70.000 and an automatic gain control value of $3*10^6$ total ion counts combined with a maximal ion injection time of 160ms. Higher charged (2x) ions were chosen for MS/MS scans with a resolution of 17500 and an automatic gain control value set to 10^5 ions with a maximal ion injection time of 150ms.

Data Analysis MaxQuant 2.0.1.0 (Cox and Mann 2008), Perseus 1.6.1.3 (Tyanova *et al.* 2016), and Excel (Microsoft Office 2016) were used. As a fixed modification, carbamidomethylation (+57.02) on cysteines, and as variable modifications, N-terminal acetylation (+42.01) and methionine oxidation (+15.99) were applied. Peptides and proteins with a false discovery rate (FDR) or less than 1% were identified in the human reference proteome set (Uniprot, September 2021, 78120 entries). If a protein was identified 4 or more times in one experimental group, it was included in the analysis. Any lacking values could be replaced by background values from a normally distributed dataset. The significance of potential interactors was calculated using student’s t-test.

3.3. Cell culture

Cultivation of Cells

All work described in this paragraph was performed under sterile conditions under a laminar flow hood (Thermo Fisher) to prevent contamination.

Thawing and Maintaining Cells: One vial of human aortic smooth muscle cells (hAoSMCs) (Lonza or PELO Biotech, Planegg, Germany) or human carotid smooth muscle cells (hCtSMCs) (Lonza or PELO Biotech) were taken from the liquid nitrogen tank where the cells are stored for longer terms. Then, cells were thawed in a 37°C water bath for 1-2min before transferring them into a falcon tube with 5ml of complete smooth muscle cell growth medium (PELO Biotech). After rinsing the vial again 1-2 times, the cells were centrifuged at 500rpm for 5min. If cells were not centrifuged and plated directly, the medium was changed the following day to remove leftover DMSO from the freezing medium (described in “Freezing Cells”). The pellet was resuspended in 5ml (T25), 12ml (T75), or 24ml (T175) of complete smooth muscle cell growth medium and, transferred to the respective flask (all sizes Corning) and stored in an incubator (Binder or Thermo Fisher) at 37°C with 5% CO_2. The medium was changed every 2-3 days with pre-warmed medium.

Passaging Cells: Once cells were confluent, they were washed once in sterile PBS (Sigma Aldrich) before Trypsin-EDTA (Thermo Fisher) was added so that all cells were covered. The flask was placed back into the incubator for 3-5min for the cells to detach. The detachment was confirmed under the microscope (Zeiss). Trypsin was inactivated by adding 10ml of complete culture medium to the cells which were rinsed and collected in a 15ml tube and centrifuged for 5min at 400rpm. For simple passaging and depending on the confluency of the cells and the pellet size, a respective amount of medium was added to the pellet and distributed into the needed amount of flasks (e.g. very confluent cells or big pellet: resuspend in 3-4ml, take each 1ml of cell suspension and add to a new T75 cell culture flask). Then, the medium was added to 12ml, and cells were placed back into the incubator. Flasks were labeled with the respective passage number of cells. In general, the shape and looks of the cells were assessed to decide if they are still usable since after p8-10, cells usually change shape and behavior and become more synthetic.

Counting and seeding cells: If the cells were supposed to be seeded at a certain density for an experiment after trypsinization and centrifuging (described in

“Passaging cells”), cells had to be counted. For that, the pellet was resuspended in 2-4ml (depending on pellet size) and mixed well. 10µl of cell suspension was added to a Neubauer Improved single-use counting chamber (Carl Roth) and placed under the microscope. Cells were counted, and the amount per ml was determined. Then, the number of cells per well was calculated and multiplied by the number of wells. Also, the amount of required medium was calculated. The cells and medium were mixed well by pipetting up and down several times before distributing the cells into their respective wells.

Freezing Cells: Once an experiment is finished, any leftover cells in a flask are grown to confluency and are then frozen down. For that, cells were trypsinized as described above. Then, cells were resuspended in a freezing medium and aliquoted – depending on pellet size – in several CryoTubes (Thermo Fisher). Tubes were labeled with the new passage number and put into a freezing container which was stored at -80°C. After complete freezing of the cells, they were transferred to liquid nitrogen.

Isolating Cells: Since we have a close collaboration with the Vascular Surgery Unit of Klinikum Rechts der Isar, we were able to receive biopsies from AAA repair or carotid endarterectomy for cell isolation from patient samples. The cells were isolated by Dr. Valentina Paloschi, Jessica Pauli, or Dr. Zhiyuan Wu from the same laboratory group. In brief, 1.4mg/ml Collagenase A (Roche) was dissolved in DMEM-F-12 (Sigma-Aldrich) and filtered using a syringe (Braun) and a suitable filter (Merck Millipore). The solution can be aliquoted and stored at -20°C. The biopsy (carotid artery plaque or AAA) was transported to the lab in DMEM/F-12 medium or PBS, transferred to a tissue culture dish, and washed with PBS. Calcifications (and the adventitia in the case of aortic biopsies) were removed using a sterile scalpel and forceps. Then, the biopsy was transferred to a new culture dish filled with 2ml pre-warmed Collagenase A and was then cut into small pieces to help digestion. The rest of the Collagenase A (approx. 8-10ml) was added, and the dish was placed for 4-6h in the incubator while moving it once or twice every hour. To remove any debris, cells were strained after incubation with a 100µm cell strainer (Merck Millipore). The cells were centrifuged at 400g for 5 min and washed twice with 15 ml of DMEM/F-12. Finally, 7ml of DMEM/F-12 was used to resuspend the cell pellet and was then transferred to a T25 flask labeled with a unique identifier in which the cells were incubated for 72h before changing the medium every 2-3 days.

Transfection

The process of transfection describes the introduction of exogenous RNA or DNA into eukaryotic cells. Here, siRNA (Ambion) or GapmeR ASOs (Qiagen) were introduced to silence specific genes. Overexpression was achieved using a *NUDT6* containing plasmid vector (Origene) that was shuttled into the cells.

Transfection using RNAiMAX: For siRNA introduction, Lipofectamine RNAiMax (Invitrogen) was used. The transfection was performed in Opti-MEM reduced serum medium (Gibco). The afternoon before transfection, the cell medium was changed to 2% FBS (Gibco) in Opti-MEM without antibiotics. Immediately before transfection, the medium was changed to 5% FBS in Opti-MEM without antibiotics. siRNA stock of 50µM was diluted 1000x so that the final concentration was 50nM if not indicated otherwise. Experiments were conducted in at least triplicates and included a scrambled negative control transfection reaction as well as a group that only received RNAiMAX. Reagents were mixed according to **Table 7** and incubated for 5min at room temperature before the respective amount was added to the cells. After 24-48h, the medium was removed, and cells were washed once with PBS before the RNA isolation protocol (See “Molecular Biology – Nucleic Acid, RNA isolation”).

Components	6 well	12 well
Opti-MEM	125µl	65µl
RNAiMAX	3µl	1.5µl
Opti-MEM	125µl	65µl
siRNA	2.5µl	1.25µl
per Well	250µl in 2.5ml	125µl in 1.25ml

Table 7 *Transfection reaction for 6 well plates and 12 well plates for siRNAs and RNAiMAX.*

Transfection using Lipofectamine 3000: For overexpressing *NUDT6* in eukaryotic cells, Lipofectamine3000 (Invitrogen, Thermo Fisher) was used. Medium conditions were used as described in “Transfection using RNAiMAX”, so 2% FBS in Opti-MEM overnight followed by 5% FBS in Opti-MEM for the transfection. If not stated otherwise, 100ng of the plasmid vector was used. Reagents were mixed according to **Table 8** and incubated for 5min at room temperature. Then, the respective amount was pipetted into the wells, and the cells were incubated for 48h before RNA isolation according to “Molecular Biology – Nucleic Acid, RNA isolation”.

Components	6 well	12 well
Opti-MEM	125µl	65µl
Lipofectamine	3.5µl	1.875µl
Opti-MEM	125µl	65µl
P3000	1.0µl	0.5µl
Plasmid	100-250ng	250ng
per Well	250µl in 2.5ml	125µl in 1.25ml

Table 8 *Transfection reaction for 6 well plates and 12 well plates for plasmids and Lipofectamine 3000.*

Sample preparation for pulldown or protein

Two T175 flasks of hAoSMCs were washed once with ice-cold PBS and scraped in 5 ml of ice-cold PBS. Cells were spun down at 400g for 5min at 4°C. Then, the pellets were washed twice in ice-cold PBS. After the first wash, 10µl were taken for counting. Then, cells were split into fractions of 1.5M. Cells were finally resuspended in 1ml ice-cold PBS and spun down at 400g for 5min at 4°C.

Cell Stimulation

Angiotensin II Stimulation: To mimic an environment seen in the AngII mouse model and which is known to induce cellular responses and pathogenic features mirroring AAA, hAoSMCs were stimulated with AngII (Sigma Aldrich). Cells were stimulated with 0.5µM AngII. Before, the cell medium was changed to Opti-MEM supplemented with 2.5% FBS. After 24 hours, the cells were harvested, and RNA was isolated as described in “Molecular Biology – Nucleic Acid, RNA isolation”.

Oxidized Low-Density Lipoprotein Stimulation: The equivalent stimulation that leads to the induction of pathogenic changes in hCtSMCs is oxidized low-density lipoprotein (oxLDL) which was kindly gifted to us by the Ehrenborg group from the cardiovascular unit of the Karolinska Institute in Stockholm, Sweden. Cells were stimulated with 2µg/ml oxLDL in Opti-MEM supplemented with 10% FBS. Then, cells were subjected to RNA isolation.

Porcine *in vivo* inhibitor testing

Two vials of primary porcine fibroblast cells were used which were kindly gifted to us by Assoc. Professor Yonglun Luo from Aarhus University, Denmark. Cells were grown in DMEM GlutaMAX (Gibco) supplemented with 15% FBS and 1%

Penicillin/Streptomycin (both from Gibco). Before transfection, cells were cultivated in 2% FBS in DMEM for 16-20h. Once confluent, they were split into 6 well plates and transfected with 50nM per well of *in vivo NUDT6* ASO using RNAiMAX for 48hrs. Then, cells were subjected to RNA isolation.

Nuclear-Cytoplasmic Fractionation

All buffers for this experiment were stored at 4°C, and the experiment itself was performed on ice and at a centrifuge set to 4°C. Cells were washed 1x with cold PBS, scraped, and centrifuged at 4000rpm for 3min. After 2x wash in cold PBS followed by spinning down at 4000rpm for 3min, cells were transferred to an Eppendorf tube. 100µl were taken after the first round of washing for the fraction 'Total'. Then, the pellet was resuspended in 1ml of RSB and incubated on ice for 3min. After another centrifugation step as described above, the cells were carefully resuspended with a 1000µl pipette in 4x pellet volume of RSBG40 (around 200µl) and centrifuged at 7000rpm for 3min. The supernatant was added to a new Eppendorf and labeled 'Cytoplasmic Fraction'. Next, the pellet was resuspended in a 9:1 mixture of RSBG40 and detergent (e.g., 180µl RSBG40 and 20µl detergent), incubated for 5min on ice, and centrifuged at 7000rpm for 3min. The resulting supernatant is pooled with 'Cytoplasmic Fraction'. After 2x wash with 1ml RSBG40 (first time at 7000rpm for 3min, second time 10.000rpm for 5min), the obtained pellet will be labeled 'Nuclear Fraction'. To all samples, 700µl of QIAzol is added. The nucleic fraction is subjected to homogenization as described in "Molecular Biology – Nucleic Acids, RNA isolation". For analysis of qRT-PCR, the average CT of duplicates was taken, and deltaCT was determined by subtracting 'Total' from 'Cytoplasmic Fraction' or 'Nuclear Fraction". The resulting value was subjected to fold change calculation (=2^-(deltaCT)). Both, Cytoplasmic Fraction and Nuclear Fraction were added together which resulted in '100%', and then, both fractions were each subtracted from the '100%' value to see how much percent of total RNA was found either in the cytoplasm or the nucleus.

Live Cell Imaging

The live-cell imaging system Incucyte (Essen Bioscience, now Sartorius) opens up a new way for a more dynamic approach to the surveillance of fast-occurring processes and changes such as proliferation, apoptosis, and migration.

The system is equipped with a 4x, 10x, and 20x objective which take images of pre-defined areas of the well plates at desired time intervals (e.g. every 15min 9 images of a 6 well plate, or every hour, 4 images of a 12 well plate etc.. In that way, one can observe dynamic processes within a set time frame in a defined area.

In the post-analysis pipeline, the cell shape can be defined, confluence areas can be determined, and growth curves can be plotted. In that way, the potential effects of inhibitors/overexpression plasmids are revealed and quantifiable.

To ensure even seeding which is crucial for all experiments conducted in the Incucyte, the plates were all placed on the sterile bench for 15min to 30min after seeding to ensure homogenous cell distribution. Also, no wells were left empty when performing an assay to allow equal temperature and humidity during the assay. In that case, the empty wells were filled with PBS. Also, bubbles had to be removed with a needle or similar to make sure that they do not block the cells during imaging.

Proliferation: For tracking proliferation, the protocol provided by the manufacturer was followed. On day 0, the cells were seeded in the appropriate well format to reach 30% confluency (10.000 – 15.000 cells/ml seeding stock). The following day, transfection was performed as described earlier. Then, the plate was placed in the Incucyte using a 10x objective. It is crucial to remove any kind of bubbles before this step. Also, the plate was allowed to warm again to 37°C so that all condensation was cleared from the lid of the plate. Images were taken every hour in the phase contrast channel. The experiment was conducted for 48 hours.

Apoptosis: On day 0, cells were seeded to be 30% confluent (10.000 – 15.000 cells/ml seeding stock). On the next day, the cells were transfected. 6 hours after transfection, the medium was changed to a complete growth medium containing 1:1000 Caspase-3/7 Reagent (Essen Bioscience / Sartorius) to reach 5µM concentration while protecting it from light. Then, the plate was transferred to the Incucyte, and after approximately 30min of acclimatization, imaging was started. Proliferation and apoptosis experiments can be run in parallel / in the same well.

Scratch Wound / Migration: For this assay, cells need to be seeded in a way to reach 100% confluency / a monolayer. In case, cells were seeded in a complete growth medium and grown for several days to a monolayer. On the next day, cells were prepared for the scratch wound assay. If needed, 6h before placing the scratch, cells were transfected. Then, the Incucyte WoundMaker (Essen Bioscience/Sartorius) is used according to the manufacturer's instructions to create a reproducible scratch

simultaneously in all wells. Medium is aspirated afterward and cells are washed carefully twice with PBS. Then, the complete growth medium is added to the cells, and the plate is placed into the incubator for imaging using a 10x objective which takes images every 1-3 hours.

Data analysis: Data was analyzed using the included IncuCyze ZOOM Software (Essen Bioscience/Sartorius) by exporting the raw data and normalizing proliferation or apoptosis to the values from the first image. In some cases, the first hour of images was excluded due to the acclimatization of the plate in the IncuCyte.

3.4. Animal Experiments

Study Approval

All murine studies were approved by the local ethics committee (Swedish Board for Agriculture; Ethical permit no. N48/16).

The porcine animal study was approved by the Animal Ethics Committee of the Government of Upper Bavaria (Munich, Germany; protocol no. ROB-55.2-2532.Vet_02-18-53) and was performed following the respective guidelines (EU Directive 2010/62/EU and Animal Welfare Act (2018).

Murine Animal Experiments

Mouse Housekeeping: Mice were housed in the facilities of the Comparative Medicine unit at Karolinska Institutet under standard conditions with *ad libitum* access to water and a standard chow diet. At the end of each experiment, mice were euthanized by CO_2 inhalation and checked for reflexes with a toe pinch before being exsanguinated by heart puncture and 4°C PBS perfusion. Then, organs and plasma were harvested.

Mouse Anesthesia: All procedures were performed under anesthesia using 2% isoflurane-containing oxygenated air. Prior to surgery, complete anesthesia was confirmed by a toe pinch. During surgery, the isoflurane supply was ensured by placing the head of the mouse in an inhalation mask. After the surgery was completed, mice were placed into an enriched cage under an infrared lamp to reduce the drop in body temperature. Once no signs of distress were visible, and full recovery was observed, mice were placed back into their respective cage. In case of complications or signs of lasting pain, mice received additional analgesia or were terminated in accordance with the ethical protocols.

Inducible carotid plaque rupture model and systemic Nudt6 ASO delivery: The inducible carotid plaque rupture model combined with ASO treatment was performed by Dr. Hong Jin from Karolinska Institutet in Stockholm, Sweden.

This model was developed to study plaque rupture and vulnerability using a canonical-shaped cuff and ligation of the carotid bifurcation. By this, shear stress is induced, and eventually, unstable carotid lesions and plaque rupture can occur (Sasaki *et al.* 2006). 10-12 week old *ApoE*$^{-/-}$ mice were anesthetized as described above. An incision was made at the medial neck, and the right common carotid artery was identified and isolated from connective tissue. A 5-0 Vicryl (Ethicon) suture was placed right below the carotid bifurcation resulting in partial ligation of the vessel. Four weeks after the placement of ligation, a cone-shaped plastic cuff (Promolding BV) of 1.7mm length is placed around the common carotid artery proximal to the ligation site. The two halves of the cuff are tied securely with a suture around the vessel. The distal part of the cuff measures 150µm, whereas the proximal end measures 300µm. Before cuff placement, flow through the ligated carotid artery was confirmed by Doppler-enhances ultrasonography (Visualsonics). Four days later, animals were sacrificed, and the right common carotid artery was macroscopically searched for signs of plaque rupture. The arteries were embedded in OCT compound (TissueTek).

10mg/kg fluorescently labeled scramble control or *Nudt6* ASO (both Exiqon, now Qiagen) were injected intraperitoneally on days 1, 11, and 21.

Angiotensin II infusion AAA model and local Nudt6 ASO delivery: Osmotic minipumps (model 2004, Alzet) filled with individual amounts of AngII (Sigma Aldrich) calculated according to Daugherty *et al*. (Daugherty and Cassis 1999) were implanted into the neck area of anesthetized 10-12 week old *ApoE*$^{-/-}$ mice. AngII was delivered at 1000ng/kg/min for four weeks. The abdominal aortic diameter was determined using ultrasound (Visualsonics) on days 0,7,14, and 28. Also, the aortic wall was examined to check for lesions or dilations. Mice were sacrificed on day 28 as described earlier. The abdominal aorta was embedded in OCT compound (TissueTek).

Negative scrambled control or *Nudt6* ASO (Exiqon, now Qiagen) were charge-coupled with cationic microbubbles ($2x10^9$ cMB/ml in H_2O, SonoVue). On days 1, 11, and 21, the mice were injected intraperitoneally with the microbubbles. For local treatment, ultrasound was transmitted at the location of the abdominal aorta and later the aneurysm (which was located prior to the injection using ultrasound and marking the

right location with a pen) with a phased transducer (Sonitron GTS Sonoporation System) for 15min with 1MHz, 2.0 w/cm^2 and 50% duty cycles (Jin *et al.* 2018).

Porcine Pancreatic Elastase perfusion AAA model and systemic Nudt6 ASO delivery: To reduce stress and increase outcomes in mice by reducing surgery time and increasing reproducibility, only experienced surgeons – Dr. Hong Jin (Karolinska Institutet, Stockholm, Sweden) and Dr. Albert Busch (Vascular Surgery Unit, Klinikum Rechts der Isar der TU München) – performed this surgery. C57BL/6J mice were anesthetized, and their aorta was temporarily ligated proximally and distally. An incision was made, an infusion catheter was inserted, and the aorta was flushed for 5min at 100mmHg with saline or saline-containing type I Porcine Pancreatic Elastase (1.5U/ml; Sigma Aldrich). The catheter was removed, and the incision was closed with a suture without aortic lumen constriction. The aortic diameter was measured on days 0, 7, 14, and 28 as described in the previous paragraph. One day after surgery, the mice received one intraperitoneal injection of either negative scrambled control or *Nudt6* ASO (Exiqon, now Qiagen). Organs were harvested as described previously.

Porcine Animal Experiments

LDLR$^{-/-}$ Yucatan mini-Pig Housekeeping: Pigs were housed at the center for preclinical research (ZPF) at Klinikum Rechts der Isar, TU Munich. Prior to surgery, they acclimatized for one week in small groups of 3-4 animals and received water *ad libitum* and a pelleted high-fat diet (Altromin). In this study, eight female and castrated male *LDLR$^{-/-}$* Yucatan mini pigs (Exemplar Genetics) were included. All described procedures were performed by Dr. Albert Busch as well as veterinarians and animal caretakers from the center for preclinical research.

LDLR$^{-/-}$ Yucatan Mini-Pig Anesthesia and Analgesia: The pigs were sedated intramuscularly with 15mg/kg ketamine, 2mg/kg azaperone and 0.1mg/kg atropine. An intravenous catheter was placed, and anesthesia was delivered with 4-8mg/kg propofol. Then, the animal was intubated with a 7-8.5mm cuffed endotracheal tube. During the procedure, anesthesia was changed to 4-8mg/kg propofol. Before the initial skin incision, 750mg of cefuroxime was administered. During the surgery, analgesia was maintained with 50mg/kg metamizole, 4mg/kg carprofen, and 0.001-0.01 mg/kg fentanyl. At the end of the surgery, buprenorphine (0.005-0.01 mg/kg) was administered and continued for at least 2 days after the PPE procedure. For the following five days, 4mg/kg of carprofen was administered orally.

Porcine Pancreatic Elastase Perfusion AAA model with local NUDT6 treatment: On day 0, AAA induction by PPE perfusion and ultrasound (GE) was performed. Two more ultrasound measurements took place on day 8 and day 28 before the respective procedures by two independent examiners using the leading-to-leading-edge technique (Borgbjerg *et al.* 2018). On day 8, an endovascular balloon coated with *NUDT6* was used for local treatment of the abdominal aorta. On day 28, the animals were sacrificed, and organs were harvested.

The procedure was performed via the left lateral flank. The aorta was isolated by surrounding tissue, 3000IU Heparin was administered, and the lumbar arteries were clipped. A 9-11x20mm PTA balloon (Medtronic Admiral Xtreme) was inserted and inflated to 10atm for one minute so that the aorta was pre-dilated. Then, a blunt needle was placed into the aorta, and elastase perfusion at 10IU/ml was performed for 10min with a pressure syringe. After that, the aorta was flushed with saline and closed with a 5-0 suture. All layers were closed, and a spray-on dressing (Aqueos) was applied to the wound to prevent local infection.

On day 8, the intervention was performed. For that, the *NUDT6* ASO was diluted to 33mM (Qiagen) and spray-coated on a 10-12x20mm PTA balloon (Medtronic Admiral Xtreme) and introduced into the abdominal aorta via the femoral artery. The balloon was then inflated to 10atm for 3min. To check for correct placement and to exclude aortic occlusion or dissection, angiography was performed.

After 28 days, >50mg/kg pentobarbital and 40 ml of 1M KCl solution were used to sacrifice the animals. Blood sampling was performed on days 0,8, and 28 under anesthesia.

3.5. Histology

Sample Processing

All patients provided written and informed consent which was approved by the local ethics committee. Carotid atherosclerotic lesions were sampled during carotid endarterectomy surgery. Aneurysmal samples were collected during an open abdominal aortic repair. The control aorta was taken from renal arteries during kidney transplantation surgery.

Samples were handled and embedded by the team of the Munich Vascular Biobank. Tissue specimens were fixed for 48h in 2% zinc-paraformaldehyde and embedded in

paraffin. For immunohistochemistry (IHC), 3-5µm thick sections were cut and mounted on SuperFrost Plus Glass (VWR) slides. Slides dried on a 40°C heating plate.
For *in situ* hybridization (ISH), sections were 5µm thick. To prevent RNase contamination, all equipment was cleaned thoroughly with RNase ZAP (Sigma), and the water bath was filled with RNase-free water. ISH sections were dried at RT for 1-2h and stored at 4°C. On the day of the ISH, paraffin was melted at 60°C for 45min.
For OCT-embedded specimens, OCT was cast into a plastic mold, the abdominal aorta was placed inside, and the mold was stored at -80°C. Hong Jin, PhD from Karolinska Institute, cut sections with a Cryotome (Thermo Fisher).

Immunohistochemistry

For FFPE-sections, IHC was performed with the DAKO REAL Detection Kit (mouse rabbit, Agilent). After cutting, slides were incubated at 56°C overnight in the oven. Then, a descending Ethanol row of Xylol (2x10min), Isopropanol (2x5min), 96% Ethanol (5min), 70% Ethanol (5min), and distilled water (2min) was performed. Slides were cooked for 7min in a pressure cooker filled with freshly prepared citrate buffer (Merck) at pH 6. To wash in between all incubation steps, TRIS buffer (3x2min) was used. Internal peroxidase activity was blocked by applying 0.9% H_2O_2 (Merck) in water for 15min. For carotid artery sections, an additional blocking step of 1h in 5% milk powder (Carl Roth) in the provided antibody diluent (Agilent) was performed to reduce background. After one TRIS washing step, the primary antibody in antibody diluent was applied for 1h followed by incubation with biotinylated secondary antibody for 25min (see section 2.3.7). Streptavidin coupled peroxidase was added for 25min to the slides. DAB and HRP substrate buffers were mixed 1:50 and applied to each section. To observe the development, a light sheet microscope (Leica) was used. The reaction was stopped by placing the slide into the water. A counterstaining with hematoxylin was performed followed by rinsing in lukewarm tap water. Finally, an ascending ethanol row in the same order as written above was performed for 3min each. Lastly, slides were mounted with Pertex (Sigma-Aldrich). Microscopy was done using a brightfield microscope (Leica).
For the murine OCT specimens, sections were thawed for 20min under the hood and fixed in 4%PFA for 10min. After a 5min rinse with PBS, a peroxidase blocker (0.3% H_2O_2 in distilled water) was applied for 30min. Sections were incubated with blocking buffer consisting of 5% goat normal serum and 1% BSA (both from Sigma-Aldrich) in

PBS followed by primary antibody incubation overnight at 4°C in blocking buffer. The next day, sections were washed 3x5min in PBS and incubated with biotinylated secondary antibody in PBS before incubation with ABC reagent (Vector Laboratories) for 30min. Then, an AEC reagent (Nichirei) was used to develop the staining for 5-15min. Sections were rinsed in tap water, and Hematoxylin counterstaining (Vector laboratories) was performed. Excess Hematoxylin was removed by 15min rinse under running lukewarm water. Sections were sealed with CC-mount (Sigma Aldrich).

In situ Hybridization

To gain insight into expression patterns of RNAs in human tissue samples, *in situ* hybridization using the miRCURY LNA™ microRNA ISH Optimization Kit (FFPE) (Qiagen) was performed. Briefly, deparaffinization and Proteinase-K (15µg/ml, provided with the kit) treatment for 15min were performed. A hydrophobic barrier with a Pap-Pen (VWR) was added to prevent the loss or spilling of buffers. Slides were incubated with the respective probes (see section 2.3.9.) in the provided hybridization buffer in a humid hybridization chamber at the recommended temperatures for 120min without adding a coverslip on top. Post-incubation SSC washes in descending concentration were performed at the hybridization temperature. Blocking was performed for 20min and anti-DIG-AP antibody incubation for 70min. The application with AP substrate was made for 90min at 37°C. All other steps – the KTBT stop reaction, counterstaining, rinsing, dehydration, and mounting – were performed according to the provided protocol.

Hematoxylin and Eosin Staining

To obtain an overview of any given FFPE tissue, Hematoxylin & Eosin staining (HE) is performed. After incubating the sections at 56°C overnight, a descending Ethanol row consisting of 2x10min Xylol, 2x5min Isopropanol, 2x5min 96% Ethanol, 2x5min 70% Ethanol and 1min in distilled water is used to re-hydrate the specimen. HTX-Mayer solution is applied for 10min to stain the nuclei. After a brief 2min rinse in tap water, Eosin is applied for 2min to stain the cytoplasm. Specimen dehydration using 96% Ethanol for 30s, 2x Isopropanol for 30s each, and 2x Xylol for 2min each is followed by mounting cover slips with Pertex on top of each slide.

Elastica van Gieson Staining

This staining is used to further gain insight into the composition of FFPE tissue – especially into fiber integrity and muscle tissue appearance.

The slide baking, rehydration, dehydration, and mounting steps are the same as described in the HE staining protocol. After rehydration, slides are incubated in resorcin fuchsin solution (according to Weigert Romeis) for 25min. Two steps of 1.5min in 96% Ethanol follow before slides are put into HTX-Weigert (Weigert-solution 1 and 2 are mixed 1:1) for 15min. The remaining staining solution is removed by a tap water rinse for 2min. Slides incubate for 2min in Picrofuchsin solution before starting the dehydration and mounting steps described above.

3.6. Data analysis

For statistical data analysis, GraphPad Prism 7 or newer was used. Quantitative data are shown as bars representing the mean and dots representing the individual data points. Repetitive data are represented by dots connected by lines which represent the mean. Error bars show the SEM if not indicated otherwise in the figure legend.

Continuous variables of two study populations or experiments were analyzed using a student's t-test. If the population exceeded two groups, 1-way or 2-way ANOVA was used. A time course with repeated measures was analyzed using multiple t-tests. Significance levels are always indicated in the figure legends. Generally, $p<0.05$ was considered statistically significant. Depending on the experimental design and hypothesis, one-tailed and two-tailed t-tests were used. This is also indicated in the respective figure legends.

4. Results

Essential aspects of the experimental procedures and data in this thesis have been published by the author in the following article and might be adopted:

Winter, H., G. Winski, A. Busch, E. Chernogubova, F. Fasolo, Z. Wu, A. Bäcklund, B. B. Khomtchouk, D. J. Van Booven, N. Sachs, H.-H. Eckstein, I. Wittig, R. A. Boon, H. Jin and L. Maegdefessel (2023). "Targeting long non-coding RNA NUDT6 enhances smooth muscle cell survival and limits vascular disease progression." Molecular Therapy. (Winter et al. 2023).

4.1. *NUDT6* and *FGF2* imbalance in human late-stage vascular diseases

To determine disease regulators that may be relevant, laser-capture microdissection on fibrous caps from ten stable and ten unstable/ruptured carotid atherosclerotic plaques was performed by Dr. Uwe Raaz and Dr. Isabell Schellinger (Göttingen University) (Figure 7A). To assess the stability status of the lesions which were sampled during carotid endarterectomy, ≤ 200µm was set as a cutoff. The NAT *NUDT6* was strongly increased, whereas its sense target *FGF2* was decreased in ruptured lesions (Figure 7 B and C).

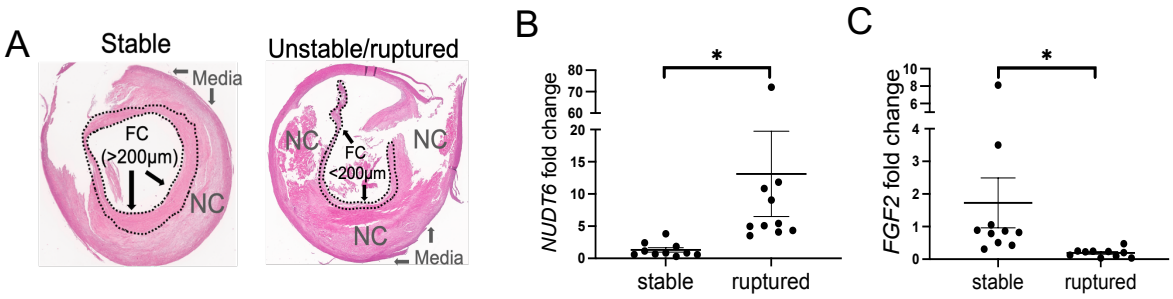

Figure 7 *NUDT6* expression in human ruptured carotid plaques is elevated.
A Haematoxylin and Eosin stained stable and unstable/ruptured atherosclerotic plaques from the Munich Vascular Biobank. The dotted lines mark the Fibrous Cap (FC), shielding the necrotic core (NC) from the lumen. FC>200µm defines stable lesions, and FC<200µl defines unstable lesions. **B** *NUDT6* and **C** *FGF2* expression in micro-dissected carotid fibrous caps of ruptured *versus* stable lesions. P<0.05* in student's t-test, n=10 per group (Winter *et al.* 2023).

In situ hybridization (ISH) and immunohistochemical staining (IHC) gave further insight into the specific *NUDT6* and FGF2 locations within atherosclerotic plaques. Especially *NUDT6* RNA expression was mainly focused on the fibrous cap area with increased signal in ruptured or unstable lesions (Figure 8A). FGF2 IHC showed

expression not only in the fibrous cap area but also in the initial media of the plaques (Figure 8B). The overall FGF2 signal was lower in ruptured or unstable lesions.

Quantitative real-time PCR (qRT-PCR) of fresh frozen whole plaque specimens showed a similar trend for *NUDT6* mRNA, whereas *FGF2* mRNA levels were not as strongly repressed in unstable tissue (Figure 8C and D).

Concomitantly with decreased FGF2 expression, αSMA expression, a marker of SMCs and indicator of a stable fibrous cap, was also reduced (Figure 8E).

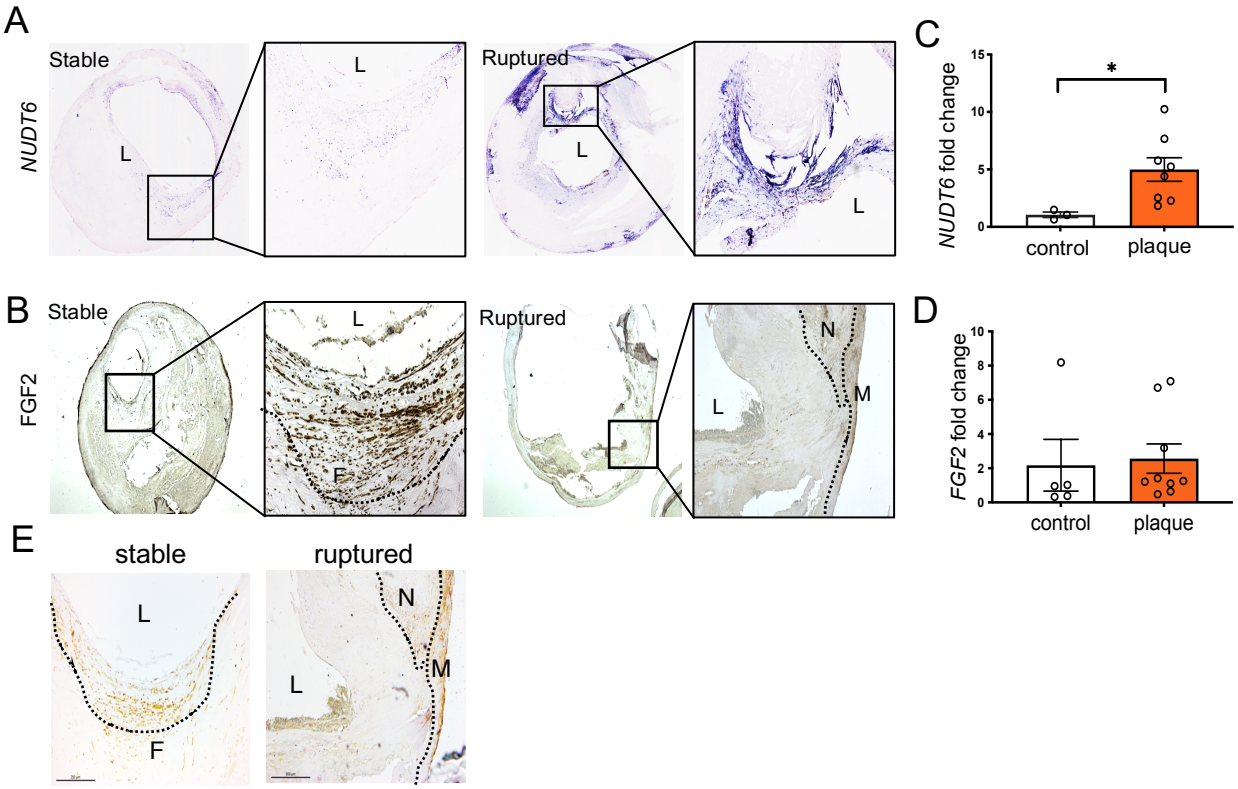

Figure 8 Higher *NUDT6* levels occur in the fibrous cap of human ruptured carotid plaques.
A *In situ* hybridization (ISH) of stable and ruptured atherosclerotic carotid lesions shows a stronger signal in the fibrous caps of ruptured lesions. L= Lumen. N=5. **B** Immunohistochemistry for FGF2 show an opposite expression to *NUDT6* with decreased signal in fibrous cap ruptured lesions. Dashed lines mark the fibrous cap. L= lumen, FC= fibrous cap, M=media, NC=necrotic core. N=3. **C** and **D** qRT-PCR analysis of whole fresh frozen carotid arteries of controls or advanced lesions. Mean+SEM. $p<0.05$* in one-sided student's t-test., N=4-8 per group. **E** Immunohistochemical staining for αSMA of stable and ruptured carotid lesions (Winter *et al.* 2023).

The findings from carotid atherosclerotic plaque samples suggested that *NUDT6* and *FGF2* are involved in SMC dynamics and even survival. Consequently, we were interested, if this deregulation solely exists in fibrous caps of carotid plaques or if it is also important in other vascular diseases where SMCs are crucial. Therefore, we determined both *NUDT6* and *FGF2* expression levels in human fresh frozen and FFPE AAA samples. Interestingly, both ISH and qRT-PCR reflected the same *NUDT6*

pattern observed in carotid atherosclerotic lesions (Figure 9A and C), comparing AAA *versus* non-dilated aortic controls. Also, FGF2 levels were found to be decreased both on protein and RNA levels in human AAA (Figure 9B and D). Downregulation of αSMA, which stains for contractile, healthy SMCs, was also decreased in AAA (Figure 9E).

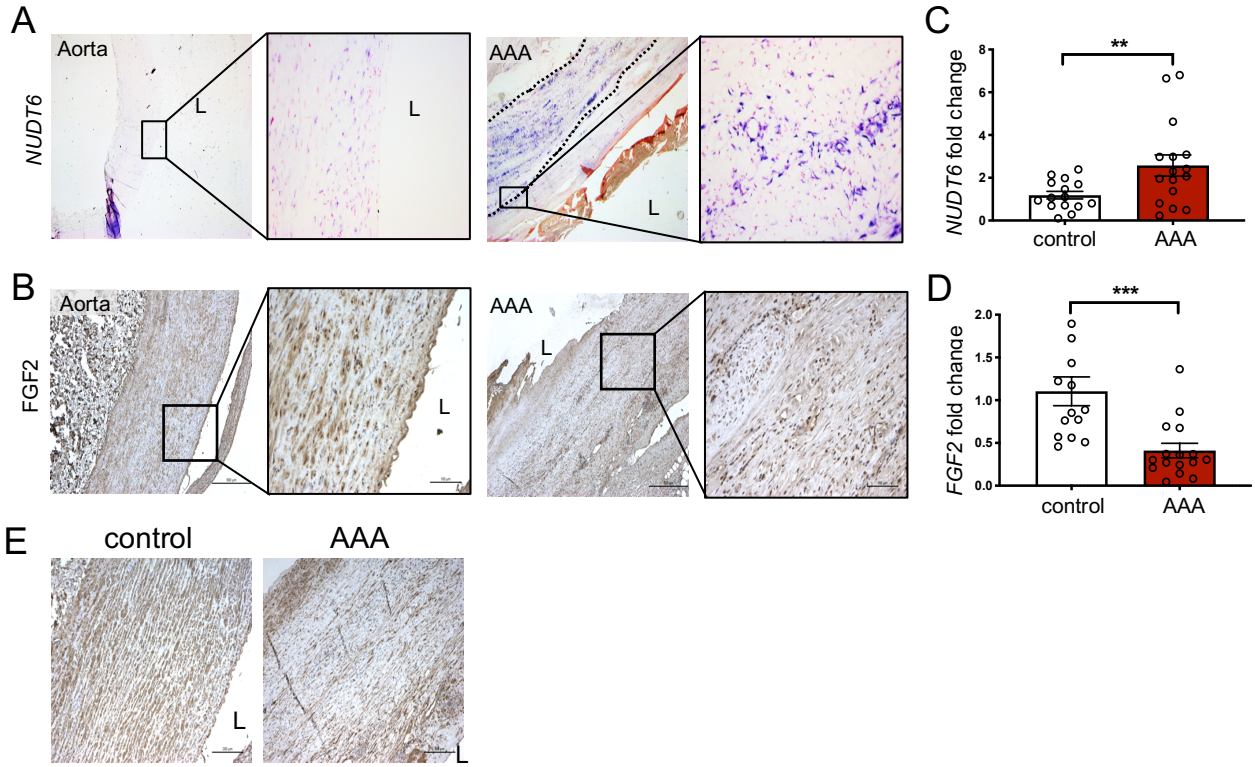

Figure 9 *NUDT6* and FGF2 expression in human AAA mirror the pattern observed in human carotid atherosclerotic lesions.
A *In situ* hybridization of control aorta and abdominal aortic aneurysm (AAA) shows higher expression of *NUDT6* in the smooth muscle cell rich media layer (dashed lines) of the vessel. L=lumen. N=3. **B** Immunohistochemical staining of FGF2 shows decreased expression of both markers in AAA. L=lumen. N=3. **C** and **D** qRT-PCR of whole fresh frozen abdominal aorta (control and AAA). Mean+SEM. p<0,0001****, p<0.01** in one-sided student's t-test, N=13-16. **E** αSMA immunohistochemistry of aortic control tissue and AAA (Winter *et al.* 2023).

4.2. *Nudt6* and *Fgf2* are deregulated in two experimental murine models for vascular diseases

As *NUDT6* is very well conserved within vertebrates (Zhang *et al.* 2008), we sought out expression patterns found in diseased human vessels. Thus, the inducible carotid plaque rupture model (Sasaki *et al.* 2006), which uses incomplete ligation and a cone-shaped cuff, and the AngII model (Daugherty and Cassis 1999), which creates suprarenal aneurysms, were used in *ApoE*-deficient mice. Using ISH and IHC, *Nudt6* RNA and Fgf2 protein localization was visualized. An increase of *Nudt6* in the inducible plaque rupture model and in the AngII AAA model was observed (Figure 10A and C). Fgf2 protein expression, however, was drastically reduced (Figure 10 B and D).

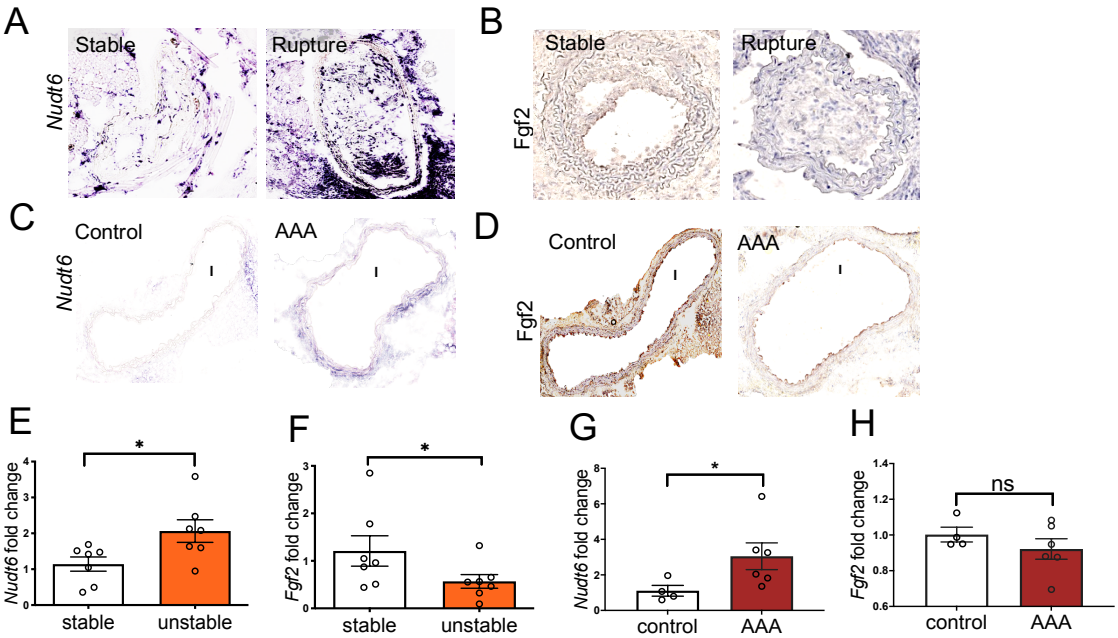

Figure 10 *Nudt6* is elevated while *Fgf2* is lowered on both mRNA and protein levels in two experimental murine vascular disease models.
A and **B** Stable *versus* ruptured carotid plaques derived from the murine inducible plaque rupture model (N=7 per group) were stained for *Nudt6 (in situ* hybridization) and FGF2 (immunohistochemistry) and resemble the phenotype observed in human disease with *Nudt6* gene expression increased and FGF2 protein expression decreased in ruptured lesions compared to stable lesions. N=3 per group. **C** and **D** Saline-infused (control) *versus* AngII-infused (AAA) aorta from the Angiotensin II mouse model (N=6 per group) was stained for *Nudt6* and Fgf2. The observed phenotype was confirmed by qRT-PCR in **E** and **F** murine stable *versus* unstable/ruptured lesions and **G** and **H** murine saline-infused (control) *versus* AngII-infused aorta. Mean+SEM. $p<0.05$* in one-sided student's t-test. N=4-7 per group (Winter *et al.* 2023).

Both observations were, therefore, in line with the distribution in the human vasculature. In addition to the staining, qRT-PCR of laser-captured micro-dissected murine carotid fibrous caps showed the same trend of expression (Figure 10 E and F). Also, AngII-treated murine aorta revealed *Nudt6* to be upregulated and *Fgf2* to be downregulated (Figure 10 G and H). In conclusion, the findings from two different murine vascular disease models were in line with the observations in human vascular tissue.

4.3. *NUDT6* modulation affects SMC proliferation rate, apoptosis events, and migration capacity *in vitro*

After observing specific expression patterns in various tissue specimens, we wanted to test how the cells mainly involved in *NUDT6* – *FGF2* imbalance, carotid and aortic smooth muscle cells, react to *NUDT6* modulation.

4.3.1. Response to pathogenic stimuli and *NUDT6* localization

Since there is a range of potential pathogenic molecules that influence atherosclerosis and AAA, we wanted to observe *NUDT6* expression after a pathogenic stimulus. Such a stimulus was oxidized low-density lipoprotein (oxLDL), which induces foam cell formation in atherosclerosis and derives from macrophages or SMCs (Berliner *et al.* 2009). We used two different doses to treat carotid SMCs, leading to a dose-dependent increase of *NUDT6* while *FGF2* levels decreased (Figure 11A). Another chosen stimulus was AngII which triggers vascular inflammation and AAA formation. Further, it is also used for the AngII mouse model (Li *et al.* 2018). AngII stimulation resulted in a similar effect in aortic SMCs as seen in oxLDL stimulation of carotid SMCs: *NUDT6* expression was increased, whereas *FGF2* mRNA was reduced (Figure 11B).

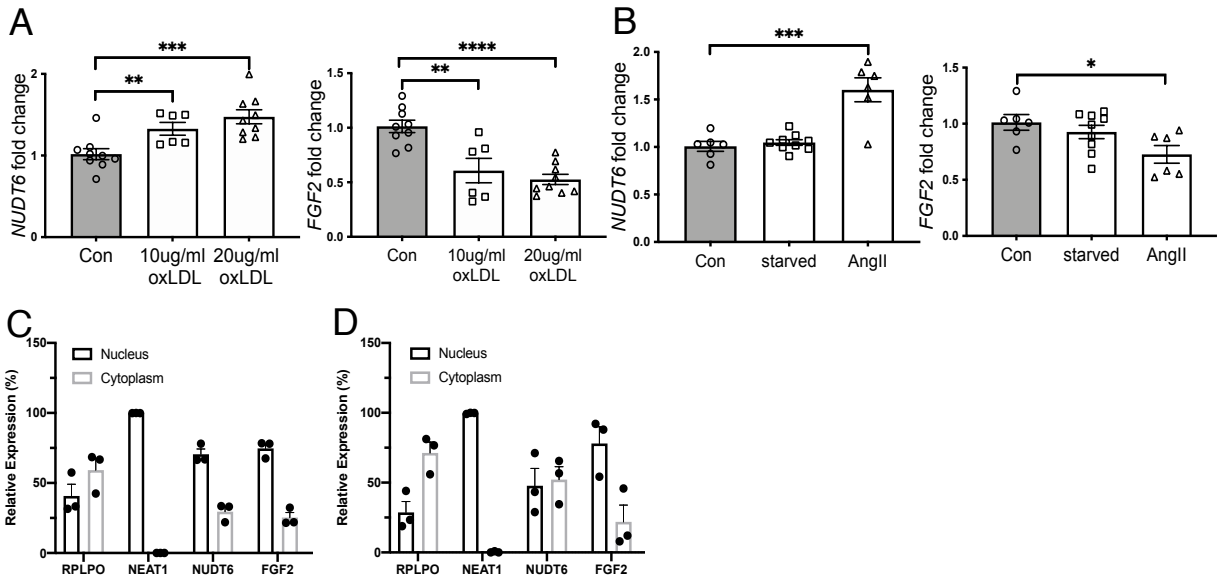

Figure 11 *In vitro* simulation of SMCs with pathogenic stimuli induces *NUDT6* expression. **A** Oxidized LDL treatments results in a dose-dependent increase of *NUDT6* expression whereas *FGF2* expression decreases with increased dosage in human carotid smooth muscle cells (hCtSMCs). Mean+SEM. One-way ANOVA with Sidak. p<0.01**, p<0.001***, N=6 per group. **B** Angiotensin II treatment of human aortic smooth muscle cells (hAoSMCs) results in increased *NUDT6* expression and decreased *FGF2* expression. Mean+SEM. One-way ANOVA with Sidak. p<0.05*, p<0.001***, N=6-9 per group. Nucleocytoplasmic fractionation of **C** hCtSMCs and **D** hAoSMCs show intracellular distribution of *NUDT6* and *FGF2* compared to nuclear expressed *NEAT1* and cytoplasmic expressed *RPLPO* (Winter *et al.* 2023).

In addition to the stimulation experiments, we wanted to receive information about the localization of *NUDT6* within cells. Already in the conducted ISH experiments, it was visible that *NUDT6* expression was not restricted to the nuclei. Nucleocytoplasmic fractionation on both carotid and aortic SMC revealed a 60:40 (carotid) or 50:50 distribution (nucleus:cytoplasm) of *NUDT6* within the cells (Figure 11C and D). *FGF2* seemed to behave similarly in carotid SMCs, whereas, in aortic SMCs, expression was higher in the nucleus (Figure 11C and D).

In summary, *NUDT6* increase is induced both by two pathogenic stimuli that are crucial in the development and progress of carotid artery atherosclerosis and AAA, respectively. With *NUDT6* and *FGF2* expressed primarily in the nucleus, *NUDT6*'s role as a NAT that binds *FGF2* DNA in the nucleus seems to overtop its other potential functions.

4.3.2. Modulation in primary SMCs and Patient-derived SMCs

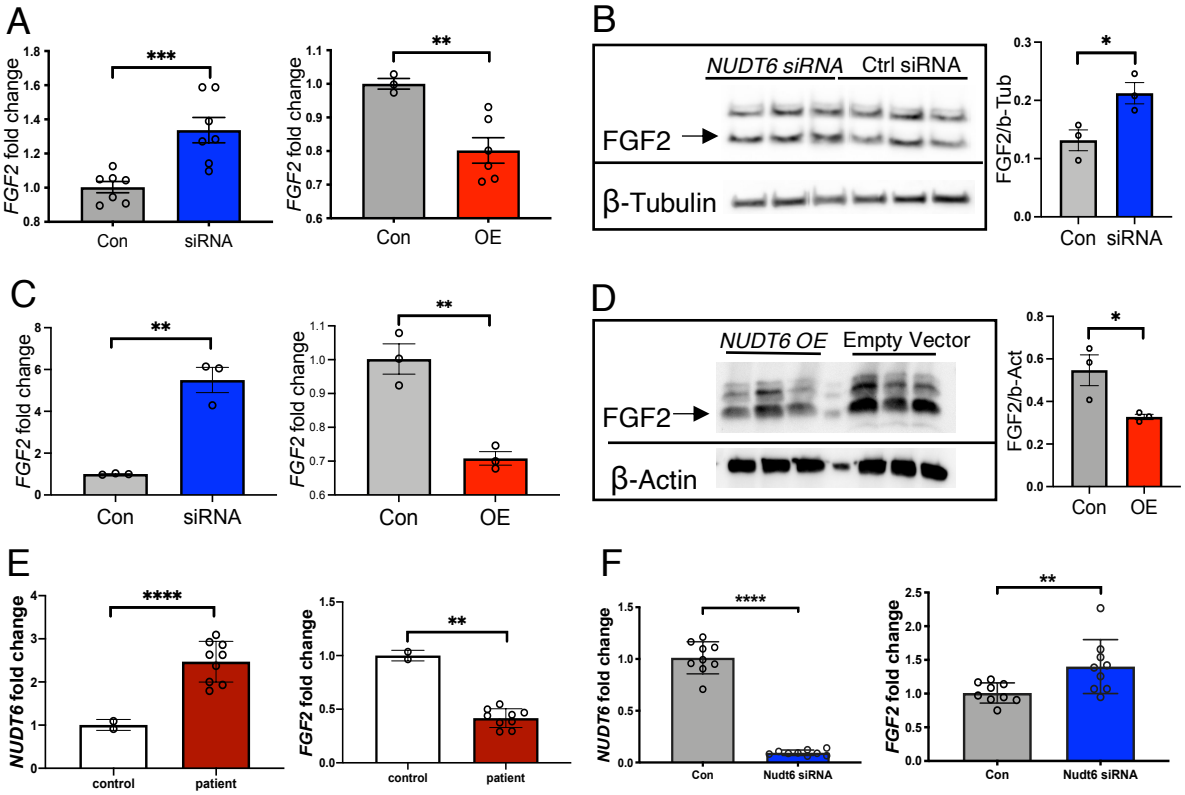

Figure 12 *In vitro* modulation of *NUDT6* has a rescuing effect on FGF2 protein and mRNA in both primary and patient-derived SMCs.
A hCtSMCs and **C** hAoSMCS, siRNA-mediated knockdown of *NUDT6* results in increased *FGF2* expression whereas vector-mediated overexpression of *NUDT6* leads to decreased *FGF2* mRNA levels. Mean+SEM. Student's t-test, p<0,05*, p<0.01**. N=6 per group. Also on protein level, **B, D** NUDT6 silencing can restore FGF2 expression. N=3 per group. **E** *NUDT6* and *FGF2* mRNA expression after qRT-PCR in 3 different patient-derived aortic VSMCs. Mean+SEM. Student's t-test, p<0.01**, p<0.0001****. N=3 per patient. **F** Knocking down *NUDT6* via siRNA in patient-derived aortic VSMCs led to a downregulation of *NUDT6* mRNA but had a rescuing effect on *FGF2* mRNA levels. Mean+SEM. Student's t-test, p<0.01**, p<0.0001****. N=3 per patient (Winter *et al.* 2023).

Since *NUDT6* levels were induced and increased in disease, we were interested in the effect of *NUDT6* silencing and overexpression on *FGF2* levels in human carotid and aortic SMCs. siRNA-mediated silencing of *NUDT6* led to a strong upregulation of *FGF2* levels in both carotid and aortic SMCs (Figure 12A and C), whereas *NUDT6* overexpression reduced *FGF2* levels (Figure 12A and C). The same trend was seen in the FGF2 protein (Figure 12B and D).

Due to the close cooperation with the Department for Vascular and Endovascular Surgery at Klinikum Rechts der Isar, we were able to receive samples taken either during carotid endarterectomy or abdominal aortic repair surgery. SMCs from three patients each were isolated as described previously (Busch *et al.* 2021). *NUDT6* expression in these cells was increased significantly compared to the commercially available primary cells while *FGF2* mRNA expression is strongly decreased in the patient cells (Figure 12E). Modulating the patient-derived SMCs with *NUDT6* targeted siRNA led to a de-repression of *FGF2* levels (Figure 12F).

4.3.3. Dynamic live-cell imaging

To get a deeper insight into how *NUDT6* modulation affects SMCs, we used a dynamic live cell imaging system to track proliferation, apoptotic events visible by fluorescent Caspase 3/7, and migration capacity.

siRNA-mediated *NUDT6* silencing had no effect on proliferation or apoptosis (Figure 13A and B). Contrary to that, *NUDT6* overexpression resulted in decreased proliferation rate and higher apoptotic events (Figure 13A and B) both in hCtSMCs and hAoSMCs. Using a scratch wound model to gain insights into migration capacity after *NUDT6* modulation, we observed a reduction in cells treated with *NUDT6* overexpressing vector in both carotid and aortic SMCs (Figure 13C and D).

Since *NUDT6* can be translated into a micro-peptide, we further assessed the effects of the micro-peptide on SMCs (Li *et al.* 1996, Asa *et al.* 2001). However, treated cells did not show more or less apoptotic events than the control (Figure 13E). We, therefore, could not detect any functional effect for the micro-peptide, which indicates that *NUDT6* NAT in SMCs is exclusively relevant in disease progression and development.

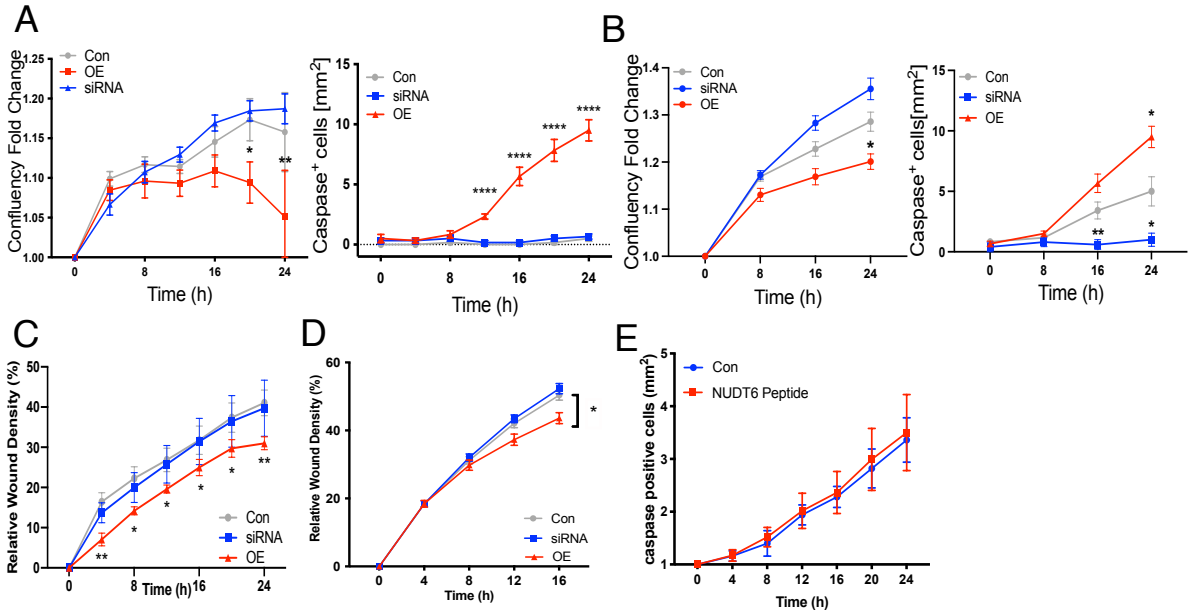

Figure 13 Live cell imaging of *NUDT6*-modulated SMCs reveals effects on proliferation, migration and apoptosis.
A hCtSMCs and **B** hAoSMCs shows impaired proliferation capacity in *NUDT6* overexpressing cells while apoptosis rate is significantly increased. *NUDT6*-siRNA treated cells behave as scramble control treated cells. Mean+SEM. Two-way ANOVA with Tukey. p<0.05*, p<0.01**, p<0.0001****. N>6. Live cell imaging of both **C** hCtSMCs and **D** hAoSMCs show impaired migratory capacity of cells receiving overexpression vector for *NUDT6*. *NUDT6*-siRNA treated cells behave as scramble control. Mean+SEM. Two-way ANOVA with Tukey. P<0.05*, p<0.01**. **E** Dynamic live cell imaging of hCtSMCs treated with NUDT6 peptide do not have an effect on apoptosis. N=5 per group (Winter *et al.* 2023).

4.4. *NUDT6* inhibition in four different animal models leads to a reduction of both rupture rate and AAA growth

4.4.1. Systemic inhibition in the murine inducible plaque rupture model

Custom-designed GapmeR antisense oligonucleotides (ASOs) - which target *Nudt6* at exon 2 – were injected in the inducible plaque rupture model, which led to a decreased rupture rate (Figure 14A). This was further confirmed by ISH and IHC with increased Fgf2 and αSMA signal in ASO-treated *ApoE*$^{-/-}$ mice while the *Nudt6* ISH signal was diminished (Figure 14B). Quantification of the ISH signal also showed a strong reduction in *Nudt6* positive cells (Figure 14C).

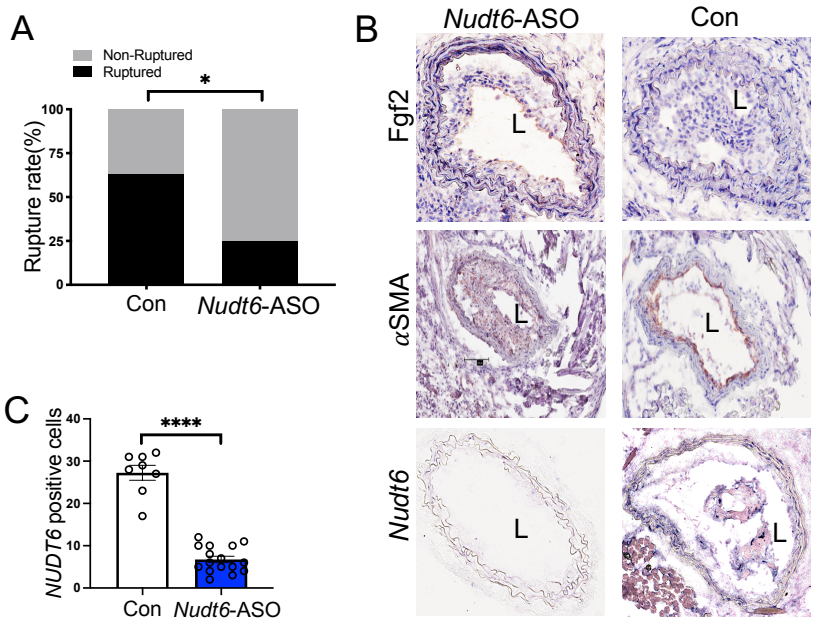

Figure 14 Systemic *Nudt6* inhibition in the inducible plaque rupture model results in reduced rupture rate.
A *Nudt6*-ASO treatment of *ApoE*$^{-/-}$ mice significantly reduced plaque rupture in the inducible plaque rupture model compared to scramble-control treated animals. Difference in rupture rate was calculated with $\chi 2$ test. $p<0.05$*. N=19 (scramble-control) and N=20 (*Nudt6*-ASO) per group. **B** Fgf2 and αSMA immunohistochemistry show restored expression after *Nudt6*-ASO treatment. **C** Signal quantification for *Nudt6* (4 high power fields per image n=8-16 counts). Quantification data kindly provided by Prof. Nick Leeper group, Stanford University, Stanford, USA. *In Vivo* work was performed by Dr. Hong Jin from Karolinska Institute, Stockholm, SE (Winter *et al.* 2023).

4.4.2. Local inhibition in the murine Angiotensin II – aneurysm model

After observing the beneficial effect of *Nudt6* inhibition in the carotid artery, we decided to apply *Nudt6*-ASO locally to the abdominal aorta to rule out eventual off-target effects and to see if the effect intensifies. For that, we chose to deliver *Nudt6*-ASOs *via* ultrasound-targeted microbubble destruction (UTMD) to the abdominal aorta of *ApoE*$^{-/-}$ mice. This resulted in a decrease in abdominal aortic diameter up to 4 weeks after induction (Figure 15A).

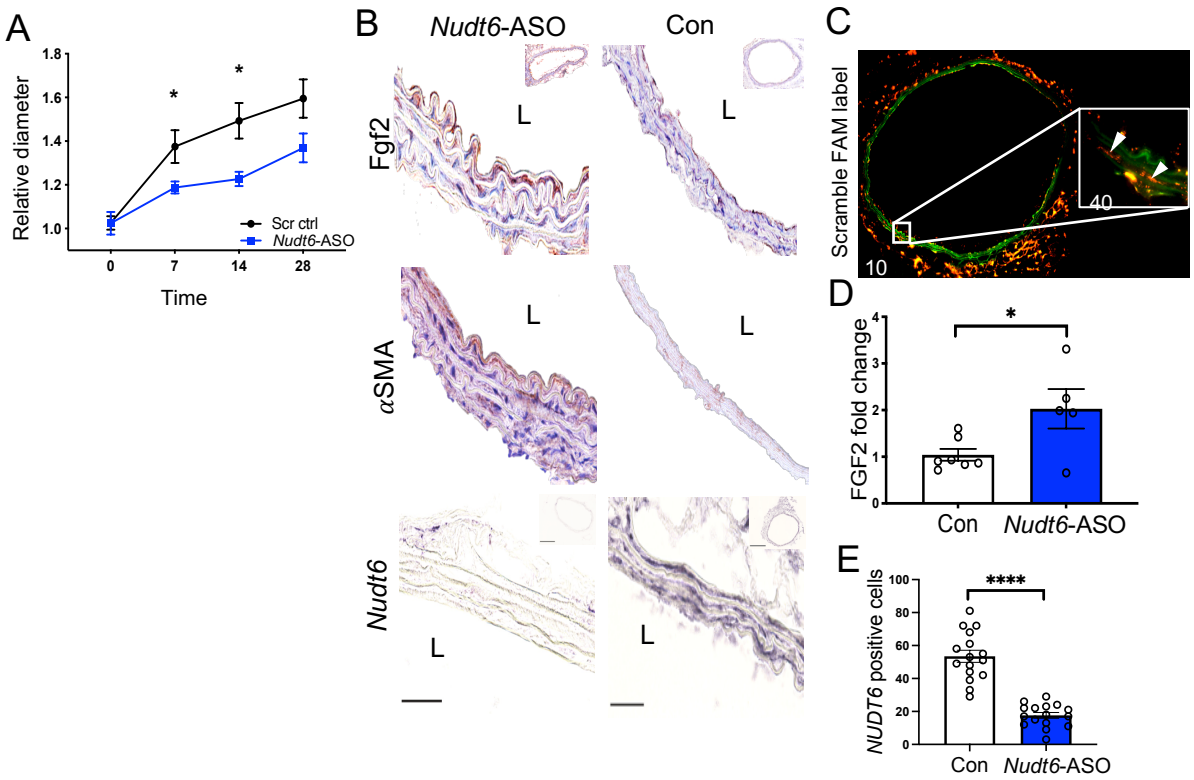

Figure 15 UTMD-mediated local *Nudt6*-ASO delivery to the aorta halts abdominal aortic aneurysm growth.
A In the AngII model, local *Nudt6*-ASO treatment via Ultrasound targeted microbubble destruction (UTMD) led to significantly lower abdominal aortic diameter and reduced growth compared to scramble treatment. Mean+SEM. Data was analysed with multiple t-tests. P<0,05*. **B** Fgf2 and αSMA protein levels are restored in *Nudt6*-ASO treated animals while *Nudt6* signal is diminished. **C** Fluorescent FAM-labelled scramble particles show successful transmission of ASOs to the intima media of the abdominal aorta via Ultrasound targeted microbubble destruction (UTMD). **D** qRT-PCR analysis of abdominal aorta show increased Fgf2 levels in *Nudt6*-ASO treated AngII mice. One-sided student's t-test, p<0.05*. N=5 **E** Signal quantification for *Nudt6* (4 high power fields per image n=8-16 counts). Quantification data kindly provided by Prof. Nick Leeper's group, Stanford University, Stanford, USA. *In Vivo* work was performed by Dr. Hong Jin from Karolinska Institute, Stockholm, SE (Winter *et al.* 2023).

The vessel wall itself was morphologically restored and displayed intact elastic layers, and overall smaller diameters. *Nudt6* ISH signal was not detected (quantified in Figure 15E), whereas Fgf2 and αSMA levels were increased compared to scramble-control treated mice (Figure 15B). Successful tissue absorbance was confirmed by imaging the abdominal aorta of scramble-treated mice, which received a fluorescent FAM-labelled scramble probe (Figure 15C). Also, RNA isolated from the abdominal aorta after the procedure showed a high level of FGF2 in *Nudt6*-ASO-treated animals (Figure 15D).

4.4.3. Systemic inhibition in the murine pancreatic elastase aneurysm model

In addition to the AngII mouse model, we used the PPE mouse model to confirm the findings and to differentiate model-specific observations. The aneurysm was induced in C57BL/6 mice on day 7, followed by a one-time intraperitoneal injection of *Nudt6*-ASO on day 10. After 28 days, we were able to notice a reduction in abdominal aortic diameter (Figure 16A). IHC revealed restored levels of both Fgf2 and αSMA while ISH signal of *Nudt6* was strongly reduced (Figure 16B and C).

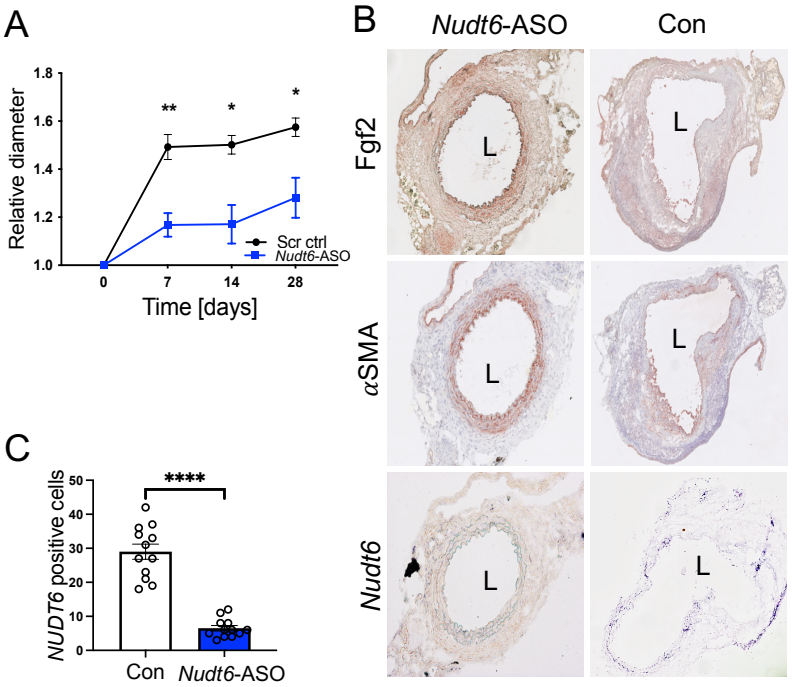

Figure 16 Systemic *Nudt6* inhibition reduces aortic diameter in the PPE mouse model.
A Systemic *Nudt6*-ASO treatment in the porcine pancreatic elastase (PPE) mouse model significantly reduced abdominal aortic diameter and growth rate. Mean+SEM. p<0.001*** in multiple t-tests. N=16 (control), N=4 (*Nudt6*-ASO treatment). **B** Immunohistochemistry of Fgf2 and αSMA shows higher expression in *Nudt6*-ASO group compared to control group while *Nudt6* is strongly reduced. **E** Signal quantification for *Nudt6* (4 high power fields per image n=8-16 counts). Quantification data kindly provided by Prof. Nick Leeper's group, Stanford University, Stanford, USA. *In Vivo* work was performed by Dres. Hong Jin and Alexandra Bäcklund from Karolinska Institute, Stockholm, SE (Winter *et al.* 2023).

In all three mouse models, we were able to show beneficial effects of *Nudt6* inhibition such as reduced rupture rate, halted abdominal aortic growth, and restored vessel wall morphology, respectively.

4.4.4. Local inhibition in the porcine pancreatic elastase aneurysm model

As a proposed attempt to close the translational gap between bench and bedside, we decided to utilize the PPE model in *LDLR*-deficient Yucatan minipigs and treat the abdominal aorta locally with an *NUDT6*-ASO drug-eluting balloon (DEB). The one-year-old male and female pigs received a Western diet for 6 months which is enriched with cholesterol. During that time, atherosclerotic lesions developed in the major vessels like the coronary artery, carotid artery, and abdominal aorta.

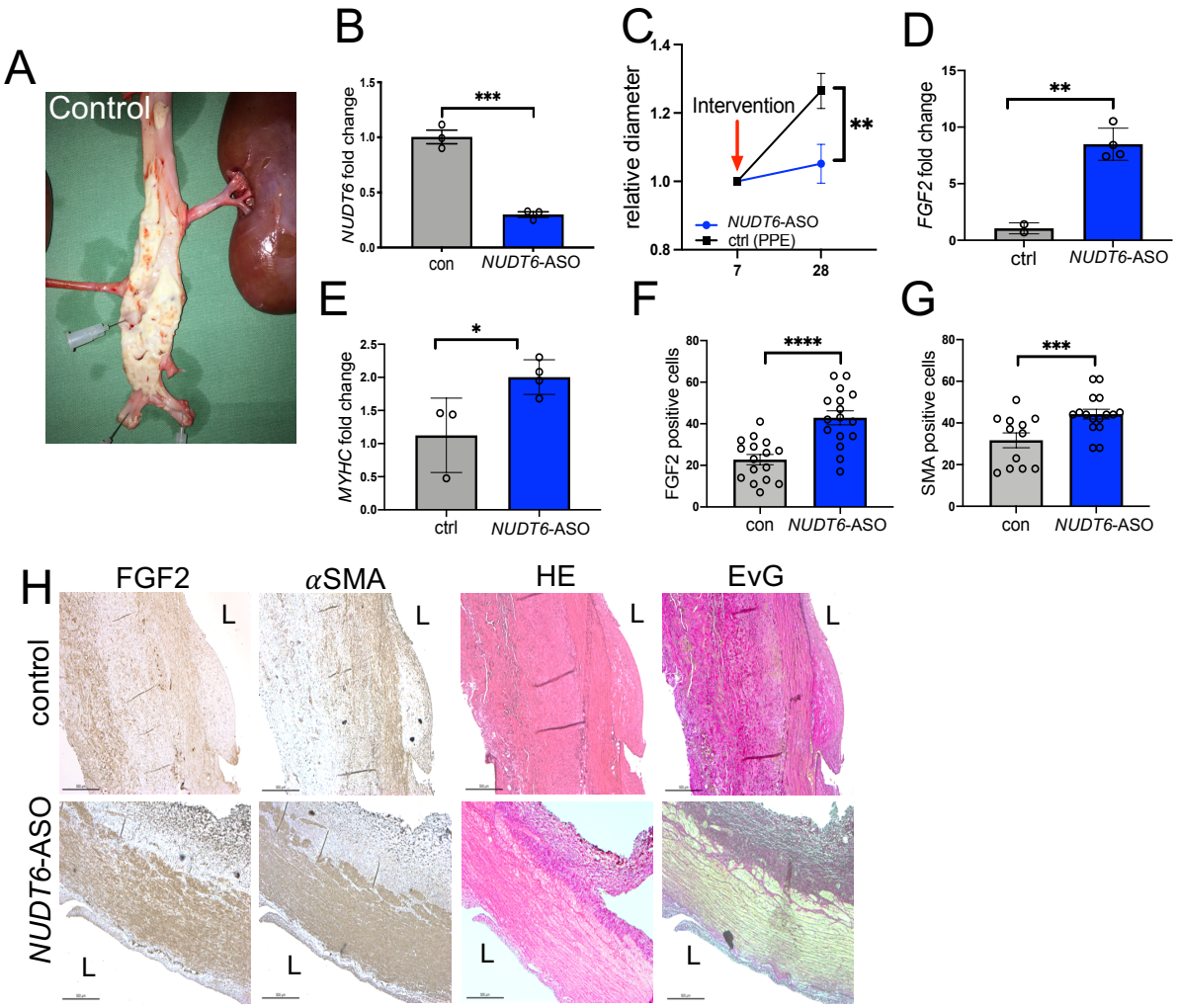

Figure 17 Local *NUDT6* inhibition in a large animal model of AAA.
A Representative image of the abdominal aorta of a control *LDLR*$^{-/-}$ pig. **B** Porcine aortic fibroblasts treated with designed porcine *in vivo* ASOs against *NUDT6* show downregulation of *NUDT6* after treatment. Mean+SEM. p<0.001*** in one-tailed Student's t-test. n= 3. **C** Relative diameter of *NUDT6*-ASO-treated animals shows a decrease compared to PPE only treated animals. Mean+SEM, N= 3(control) *versus* 4(treatment). **D and E** qRT-PCR of whole porcine aortic tissue shows a significant increase of *FGF2* mRNA and also *MYHC* mRNA. Mean+SEM. p<0.01** or p<0.05* in one-sided student's t-test. N=3 (control) or 4 (treatment). Quantification of immunohistochemical staining from **H** for **F** FGF2 and **G** αSMA with Imaris. One-sided student's t-test with n=12-16 locations counted. p<0.001***, p<0.0001****. **H** Immunohistochemical staining of the abdominal aorta of control and *NUDT6*-ASO receiving pigs using antibodies against FGF2 and αSMA as well as HE and EvG staining. "L" indicates lumen. *In vivo* work performed by Dres. Albert Busch (Vascular Surgery Unit, Klinikum rechts der Isar, München), Johannes Fischer (ZPF, Klinikum rechts der Isar, München) and Judith Rauser (ZPF, Klinikum rechts der Isar, München) (Winter *et al.* 2023).

AAA is induced in the pig by infusing PPE *via* a catheter into the infrarenal part of the aorta. One week after the PPE procedure, the abdominal aortic wall was subjected to a one-time treatment with a *NUDT6*-ASO-coated drug-eluting balloon (DEB) (n=4). Control animals received a vehicle control coating (n=3) (Figure 17A). Prior to coating, the *NUDT6*-ASO was tested *in vitro* on Yucatan pig fibroblasts (Figure 17B).

A significant difference in aortic diameter between the two groups was found from the point of intervention to sacrifice on day 28 (Figure 17C). Also, higher *FGF2* and *MYHC* mRNA expression in the *NUDT6*-ASO-treated group were visible (Figure 17D and E). MYHC represents contractile SMCs. Also, IHC of FGF2 and αSMA showed a rescue effect in *NUDT6*-ASO-treated animals, with a great proportion of the cells showing contractile cell features in the EvG staining (Figure 17F-H), where yellow staining indicates elastic and contractile tissue. Also, fewer inflammatory infiltrates and atherosclerotic plaque burden was found in the *NUDT6*-ASO-treated group compared to internal control tissue taken proximally of the aneurysm location (Figure 1711 H).

4.5. *NUDT6* impacts SMC contractility and migration by interacting with CDC42 and CSRP1

We chose to identify protein interactors of *NUDT6* by RNA Pulldown and *in silico* analysis to understand what other roles *NUDT6* may hold in vascular diseases. We performed an RNA pulldown combined with liquid chromatography-mass spectrometry (LC-MS/MS) using aortic SMC lysate with *in vitro* transcribed biotinylated *NUDT6* or a control RNA of similar length. In total, 50 statistically significant proteins were identified to interact with *NUDT6* (Figure 18A). Two proteins, Cysteine and Glycine Rich Protein 1 (CSRP1 *alias* CRP1, 32.6-fold up-regulation) and Cell Division Cycle 42 (CDC42, 6.96-fold up-regulation), were selected for further studies as these two proteins are involved in SMC biology and -physiology (Nobes and Hall 1995, Nobes and Hall 1995, Lilly *et al.* 2001, Chang *et al.* 2003, Tang and Gunst 2004).

To receive further insight into the expression in AAA in between species, we used our single-cell RNA sequencing (scRNAseq) libraries from human AAA and murine as well as porcine PPE-induced AAAs.

Interestingly, we detected *CSRP1* mainly in two SMC clusters, whereas *CDC42* was also expressed in other cell types, mainly ECs (Figure 18B). To be able to distinguish the contractile SMCs, all three scRNAseq datasets also contain the

distribution of Transgelin (*TAGLN*), which is mainly expressed by these cells. Especially in the human dataset (Figure 18C), *TAGLN* and *CSRP1* are co-expressed in the same cell cluster, which is marked as VSMCs and Fibroblasts. *CDC42* expression, however, is visible in many cell types and is not exclusively limited to SMCs. These expression patterns are mirrored both in murine PPE-induced AAAs (Figure 18D) and in porcine PPE-induced AAAs (Figure 18E).

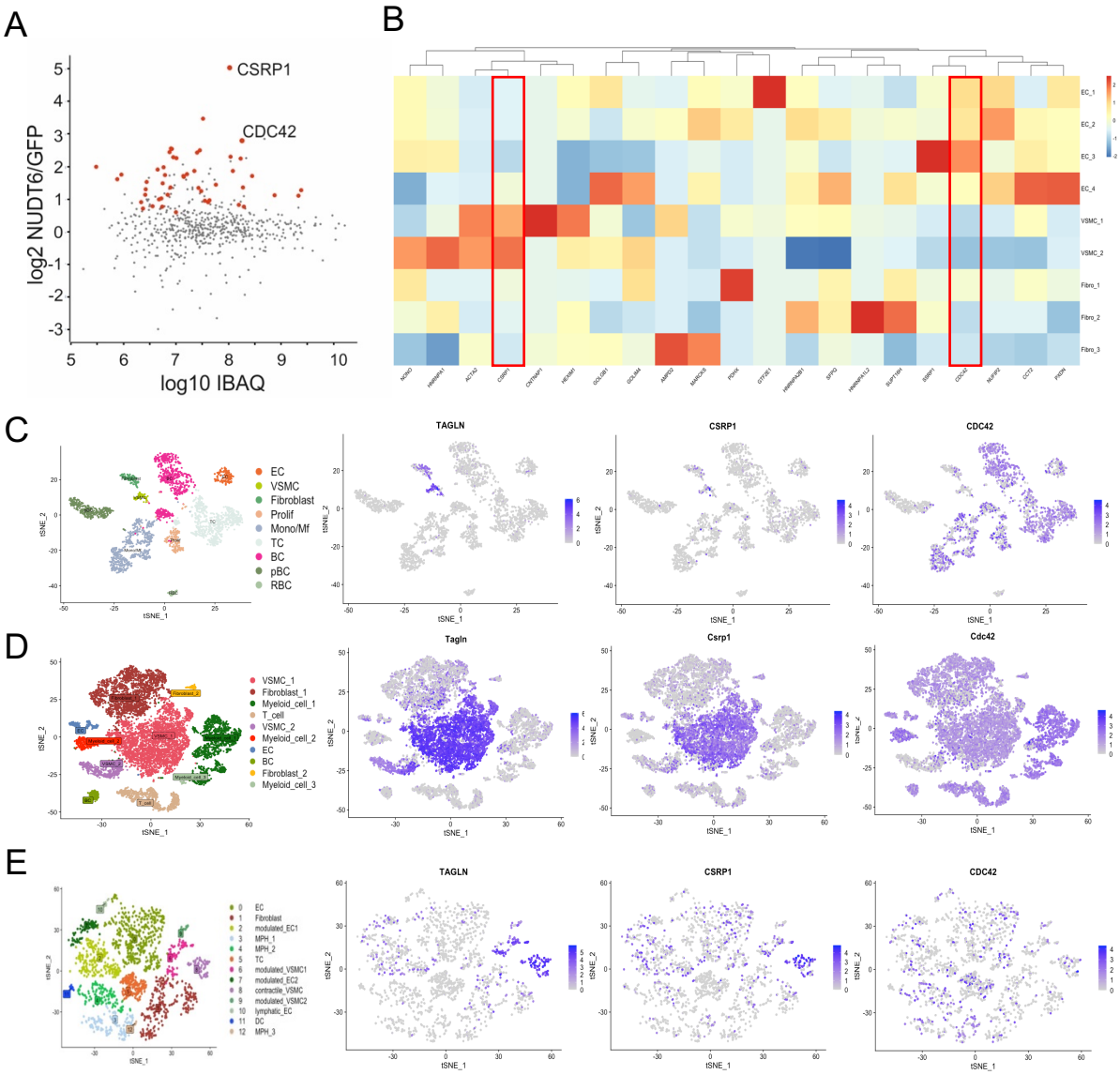

Figure 18 Identification of *NUDT6* interaction partners CSRP1 and CDC42.
A Identified proteins in biotinylated NUDT6 *versus* biotinylated GFP pulldown in hAoSMCs. N=6 per condition. Graph provided by Dr. Ilka Wittig, Goethe University, Frankfurt am Main, Germany. **B** Heat map showing the abundance and expression of *CSRP1* and *CDC42* in VSMCs and ECs from single cell RNA sequencing experiments shown in **C**. tSNE plots of scRNA Sequencing data from **C** human, **D** murine and **E** porcine AAA with expression plots of Transgelin (*TAGLN*) and the two targets. Murine and porcine AAA were induced via PPE (Winter *et al.* 2023).

The scRNAseq data already allowed for an estimated CSRP1 and CDC42 expression *in situ*. However, the distribution could not be compared to normal, healthy aortic tissue. Therefore, IHC of aortic control and AAA with CSRP1 and CDC42 were performed. Interestingly, both CSRP1 and CDC42 staining were strongly reduced in AAA compared to healthy control aorta (Figure 19A and B). Also, qPCR of whole aortic or AAA tissue showed a similar trend for *CSRP1* (Figure 19C and D) but not for *CDC42*. This might be due to the expression of *CDC42* in other cells, which might remain unchanged in disease. In the absence of *NUDT6*, ASO-treated *LDLR*-deficient minipigs show a high level of both CSRP1 and CDC42 in the aorta (Figure 19E and F), which also concomitates with αSMA expression reported in (Figure 17H). This increase in signal is, however, not visible in the control group (Figure 17H).

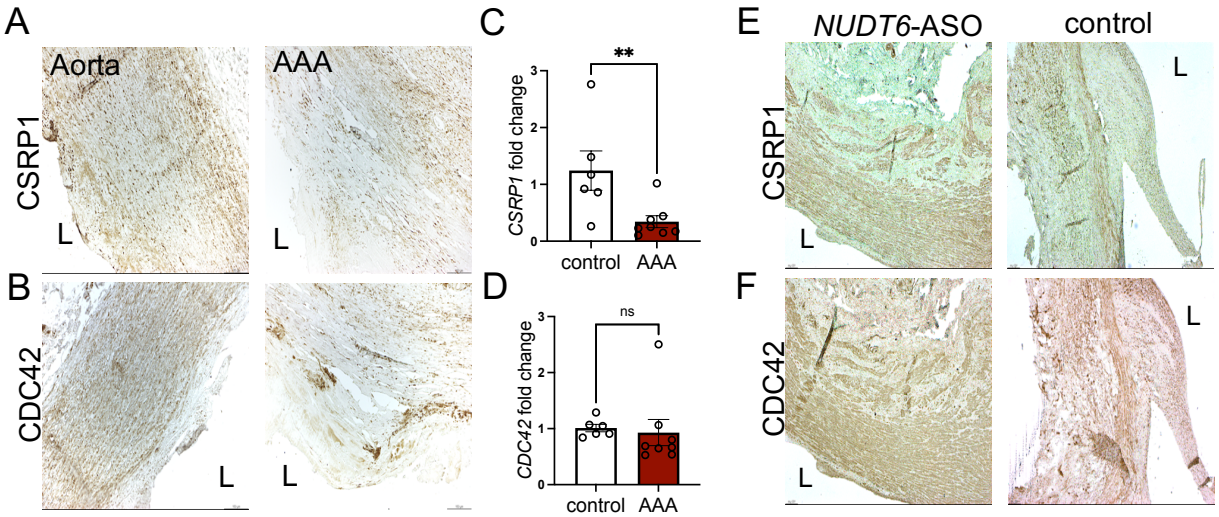

Figure 19 Validation of CSRP1 and CDC42 expression in human and *NUDT6*-ASO-treated porcine AAA.
A CSRP1 and **B** CDC42 in human control aorta and AAA. „L“ indicates lumen. **C** and **D** qRT-PCR of whole fresh frozen abdominal aorta of *CSRP1* and *CDC42* mRNA. Mean+SEM. p<0.01** in one-tailed student's t-test, N=6-8 E CSRP1 and F CDC42 in *NUDT6*-ASO-treated abdominal aorta of *LDLR*$^{-/-}$ Yucatan Minipigs. "L" indicates lumen (Winter *et al.* 2023).

To gain mechanistic insights into the regulation and hierarchy in the interaction between *NUDT6* and CSRP1 or CDC42, modulation studies were performed. Overexpression of *NUDT6* in hAoSMCs led to reduced CSRP1 and CDC42 protein levels (Figure 20A and B). Contrary to that finding, siRNA-mediated *NUDT6* silencing showed an increase in protein expression (Figure 20C and D), pointing towards a repressive role of *NUDT6* in the two proteins. Indeed, we saw that *NUDT6* levels were not affected after the knockdown of the *CSRP1* or *CDC42* (Figure 20E).

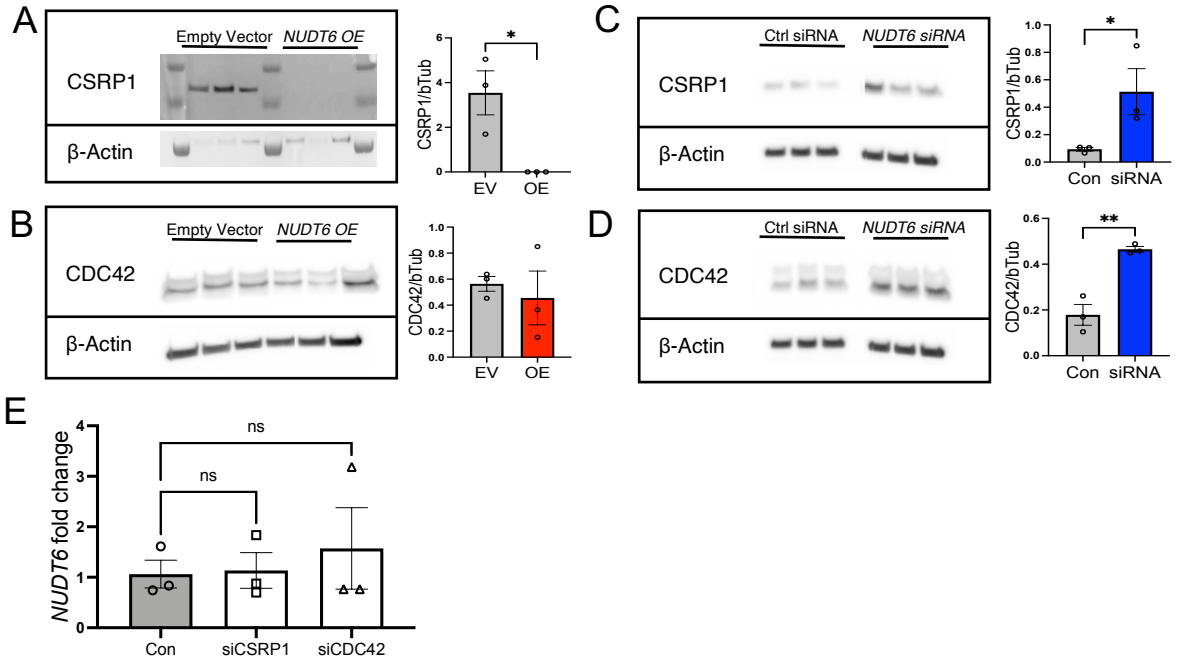

Figure 20 *In vitro* modulation of *NUDT6* reveals mechanistic insights into the interaction between *NUDT6* and CSRP1 or CDC42.
A and B CSRP1 and CDC42 protein levels after *NUDT6* overexpression. **C and D** CSRP1 and CDC42 protein levels after *NUDT6* siRNA-mediated knockdown. **E** *NUDT6* expression after *CSRP1* and *CDC42* knockout. Mean+SEM. P<0.05*, p<0.01** in one-tailed student's t-test, N=3 (Winter *et al.* 2023).

As CSRP1 seemed to be more SMC-specific, we decided to proceed with this protein for a pulldown verification. This was accomplished with RNA Immunoprecipitation (RIP), where an antibody (here CSRP1) is coupled to magnetic beads and added to cellular lysate (**Figure *21***). After incubation and washing steps, RNA was isolated, and finally, its cDNA is used for qRTPCR detection of *NUDT6*. *NUDT6* was enriched in the CSRP-1 eluate compared to the IgG eluate to validate the pulldown.

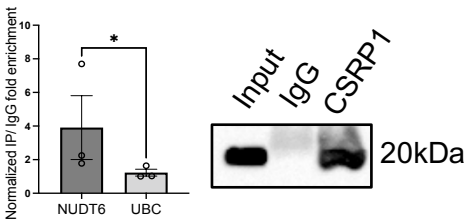

Figure 21 Verification of CSRP1 – *NUDT6* interaction.
Pulldown results, where CSRP1 was found to be enriched in the NUDT6 elution fraction, were confirmed using RNA Immunoprecipitation (RIP) in hAoSMCs. IgG was used as negative control. Enrichment of *NUDT6* was observed in qRT-PCR analysis (left graph) compared to *UBC* Housekeeping and IgG negative control. CSRP1 protein was found only in CSRP1 elution fraction and Input but not in IgG negative control using western blot (right blot). n=3 (Winter *et al.* 2023).

5. Discussion

For a very long time, ncRNAs were considered non-functional junk. However, in recent years, more attention was drawn to the various classes of ncRNAs like microRNAs, circular RNAs, lncRNAs, and others. It seems that even though evolutionary complex organisms have similar numbers of protein-coding genes, they differ from simpler organisms in the size of their non-coding transcriptome (Deveson *et al.* 2017). Nowadays, it is known that ncRNAs indeed are functional – they do not only regulate transcriptional noise, imprint genetic loci, or modulate chromatin architecture, but they also become crucial in maintaining a healthy organism.

In many cases, abnormal ncRNA expression is involved in the initiation, progression, and outcome of several human diseases – even though ncRNAs are usually lower expressed than proteins. In vascular diseases, lncRNAs like *ANRIL, MEG3, HOTAIR, GAS5, H19,* or *MIAT* show their significance in maintaining a healthy balance by regulating disease-specific cells like endothelial cells, smooth muscle cells, or myeloid cells.

NUDT6, the NAT of FGF2, also known as *gfg* or *FGF2-AS*, is one of the first lncRNAs we identified to play important regulatory roles not only in carotid atherosclerosis but also in AAA. We chose to target FGF2 expression *via NUDT6* modulation, using the NAT-activity of *NUDT6* to re-establish FGF2 mRNA and protein levels in late-stage vascular diseases. As mentioned earlier, the reaction between NATs and their sense transcript happens faster compared to interaction with transcription factors (Shimoni *et al.* 2007).

FGF2 is also a well-known protein in cancer, where it is regarded as an oncogene (MacFarlane *et al.* 2010, Sukhthankar *et al.* 2010, Baguma-Nibasheka *et al.* 2012). It is abnormally expressed in cancers like Hodgkin's Lymphoma (Gharbaran *et al.* 2013), breast cancer (Lee *et al.* 2014), or colorectal cancer (Akl *et al.* 2016), where it is associated with metastases, recurrence, or aggressiveness.

Hence, we show that it can be possible to target molecules that were previously thought to be “undruggable” *via* NAT modulation (if available). However, the off-target effects of a global FGF2 de-repression cannot be neglected. FGF2 has been shown to promote cardiac fibrosis and hypertrophy (House *et al.* 2015, Itoh *et al.* 2016). Therefore, a site-specific inhibition must be considered.

5.1. *NUDT6* and FGF2 imbalance in human late-stage vascular diseases

To confirm the laser-capture microdissection performed on human carotid fibrous caps, IHC for protein detection and *in situ* hybridization for RNA detection were combined with whole tissue PCR analysis.

In the human atherosclerotic plaques, *NUDT6* expression was limited to the region of the fibrous cap, while FGF2 expression was found throughout the plaque tissue but not in the fibrous cap. This observation suggests a site-specific inhibition of *FGF2* by its NAT *NUDT6*. Even though the PCR analysis of *FGF2* in whole plaque tissue was not statistically significant, it indicates a remaining robust FGF2 baseline expression in areas apart from the fibrous cap. Therefore, the *in situ* analysis of human specimens need to be taken into account to see the signal's localization.

Consequently, the FGF2 – *NUDT6* imbalance seems to play a more critical role in fibrous cap formation and stability. The formation of a thick fibrous cap in advanced-stage carotid artery stenosis is crucial to prevent plaque rupture (Redgrave *et al.* 2008). Several groups have shown that SMCs lose their ability to migrate into the fibrous cap or undergo apoptosis (Lindner and Reidy 1991, Tsuji-Tamura and Tamura 2022). Autocrine FGF2 expression is crucial for SMC survival (Miyamoto *et al.* 1998), and its inhibition was shown to induce apoptosis in SMCs (Fox and Shanley 1996).

This inhibitory effect in the fibrous cap / smooth muscle cells could also be observed in another vascular disease: AAA. Due to the highly specific expression of *NUDT6* in the fibrous cap, which mainly consists of SMCs, we decided to try to detect *NUDT6* in AAA, where SMCs are also the most affected cell type (Lopez-Candales *et al.* 1997, Rombouts *et al.* 2022). Here, we saw similar patterns as in carotid plaques. *NUDT6* expression was increased in the media in AAA tissue, whereas FGF2 was strongly downregulated. In general, the effect was not specific to a particular site of the aneurysm, which was also mirrored by the robust PCR-derived results.

Interestingly, *NUDT6* ISH-signal in the healthy aorta is restricted to the nucleus, whereas in AAA, it can also be found in the cytoplasm. The nuclear signal might indicate that *NUDT6* is involved in processes like chromatin organization or transcriptional gene expression regulation (Sun *et al.* 2018). Its cytoplasmic expression in the disease context can be a result of differential polyadenylation signals or differential isoform expression patterns (Statello *et al.* 2021). lncRNAs expressed

in the cytoplasm can also influence mRNA stability and turnover (Sebastian-delaCruz *et al.* 2021).

The staining and PCR analyses showed a clear *NUDT6* NAT activity towards FGF2. But what do the genomic organization and complementarity of these two genes look like? The *NUDT6* gene can be transcribed into eight variants; 7 of them include the site of conserved *FGF2* complementarity. The designed human locked nucleic acid (LNA) detection probe targeted exon 1; and 6 variants in total (Figure 22). At the start of this project, the most recent human assembly stemmed from December 2013 (GRCh38/hg38), describing only two variants of *NUDT6*. However, eight variants were annotated in the latest release (January 2022, T2T CHM13v2.0/hs1).

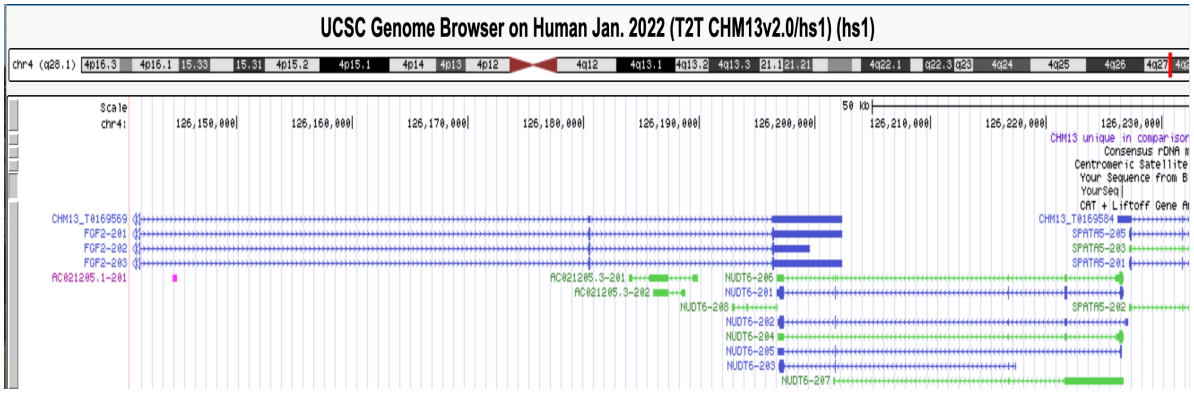

Figure 22 *NUDT6* variant distribution. (screenshot of UCSC Genome Browser release January 2022)

Despite being discovered in oocytes of *Xenopus laevis*, *NUDT6* was also found to be expressed in various fetal and postnatal rat tissues (liver, kidney, heart, intestine; dynamically regulated in early development, (Li *et al.* 1996), adult rat liver (Knee *et al.* 1997)). It is also expressed in various cancer cell lines (HepG2, Seg-1, T98, U87, rat C6 glioma cells) and -tissue (esophageal adenocarcinoma) (Baguma-Nibasheka *et al.* 2007, Zhang *et al.* 2007, McEachern and Murphy 2014). According to the GTEx portal v8, *NUDT6* is mainly expressed in cultured fibroblasts, followed by the testis, thyroid, and adrenal gland, with 5-6 transcripts per million (TPM). At the same time, in the aorta, 2.6 TPM are detected.

5.2. *Nudt6* and Fgf2 are deregulated in two experimental murine models for vascular diseases

We further wanted to see if an effect is visible that resembles the patterns observed in human vascular tissue. Two cardiovascular experimental models were used to

explore *Nudt6* and Fgf2 expression in a murine context and to evaluate if a modulation study would be feasible. An inducible plaque rupture model that functions *via* carotid artery ligation and – later on –placement of a conical cuff to induce turbulent flow conditions was used (Sasaki *et al.* 2006). As a AAA model, the AngII model was chosen, which causes an aneurysm over the time course of 28 days after the initial insertion of an AngII-releasing osmotic minipump (Daugherty and Cassis 1999).

Indeed, the patterns in both mouse models were similar to the staining performed in human carotids and aorta. The initial Fgf2 solid signal in the fibrous cap disappeared in the murine-ruptured carotids, accompanied by increased *Nudt6* levels. Currently, no other groups have attempted to detect *Nudt6* expression *in situ*. Also, there is no availability of a *Nudt6* knockout mouse.

However, as mentioned in chapter 5.1, *NUDT6* is expressed in various cell and tissue types, and it is also highly conserved between species. According to Ensembl, 180 orthologues were detected, ranging from fish, birds, and reptiles to mammals, including rodents and primates (Ensembl Release 69). Even though a lack of conservation does not indicate that the lncRNA is not functional (Johnsson *et al.* 2014), conservation still estimates significant regions and functions of a lncRNA (Diederichs 2014).

5.3. *NUDT6* modulation affects SMC proliferation rate, apoptosis events, and migration capacity in vitro

After we observed the described pattern in human and murine mouse tissue, we aimed to reproduce this state *in vitro*. Therefore, context-relevant primary cells, hCtSMCs, and hAoSMCs were used. These cells have a limited capacity to divide and eventually lose this capacity upon a particular passage and undergo senescence, as observed in our laboratory. However, they are physiologically more relevant; further, there is a lack of a vSMC line, and previous attempts by our group to immortalize primary cells have failed.

To facilitate a disease-like trigger in either aortic or carotid SMCs *in vitro*, oxLDL and AngII were used (Daugherty and Cassis 1999, Berliner *et al.* 2009). The stimulation outcome showed a dose-dependent increase of *NUDT6* and a dose-dependent decrease of *FGF2* in hCtSMCs. In AngII-treated hAoSMCs, a similar effect was observed. These findings suggest that *NUDT6* and *FGF2* are two dynamically

regulated genes influenced by external stimuli. As mentioned in the introduction, oxLDL is a key player in atherogenesis. Also, SMCs can detect and react to oxLDL: It was shown that oxLDL treatment is associated with vSMC apoptosis in human atherosclerosis (Okura *et al.* 2000). Also, as mentioned in the introduction, vSMCs can differentiate into foam cells which can engulf oxLDL (Allahverdian *et al.* 2014, Feil *et al.* 2014). Taken together, these examples show the utility of oxLDL as a disease-relevant stimulus in atherosclerosis research.

AngII mainly functions as a vasoconstrictor and affects the contractility and growth rate of vSMCs *via* the AT_1 receptor (Griendling *et al.* 1997). It was also shown that AngII could alter enhancers but also lncRNAs in vSMCs, which deregulate crucial genes (Das *et al.* 2017). But mainly, its striking effect in the AngII mouse model (Daugherty *et al.* 2000) led to the usage of AngII as a stimulus also for *in vitro* experiments in vSMCs.

As mentioned earlier, lncRNAs can exert various functions depending on their cellular localization. Here, *NUDT6* was found predominantly in the nucleus of hCtSMCs, whereas it was equally spread across the cytoplasm and nucleus in hAoSMCs. The localization of *FGF2* in both cell types was also higher in the nucleus compared to the cytoplasm. This distribution of the two genes suggests a primarily post-transcriptional inhibition of *FGF2* by *NUDT6,* which takes place in the nucleus. The bigger proportion of *NUDT6* in the cytoplasm can be explained by the fact that *NUDT6* mRNA also codes for several micropeptides. Indeed, it was reported that the micropeptides were found both in the nucleus and cytoplasm but also in the mitochondria (Zhang *et al.* 2007). This hints towards the presence of *NUDT6* mRNA in these locations – which then was confirmed *via* PCR (except for mitochondrial presence).

Next, siRNA- and vector-mediated silencing and overexpression, respectively, were performed with a readout on both RNA and protein levels to gain insights into the level of regulation and possible effects of knockdown and overexpression. In both primary cell sources, *NUDT6* downregulation led to restored *FGF2* levels, both RNA and protein. Overexpression of *NUDT6 via* a plasmid led to *FGF2* downregulation in these cells, also on protein levels.

Already in the paper in which *NUDT6* was discovered by Kimelman and colleagues (Kimelman and Kirschner 1989), *NUDT6* cannot entirely repress *FGF2* activity on RNA and protein levels. Therefore, especially the results following *NUDT6*

overexpression are in line with this observation. *NUDT6* was elevated by 80-100 fold (data not shown), but it was still unable to inhibit FGF2 expression fully. Hence, there might be a natural threshold of *NUDT6*'s inhibitory function. The achieved FGF2 de-repression upon siRNA showed more promising effects. This led to the decision to proceed with a *Nudt6* ASO designed for *in vivo* studies. A similar approach with similar observations by Modarresi and colleagues, who inhibited the NAT of Brain-Derived Neurotrophic Factor (BDNF), which suggested the use of NAT inhibitors as a new pharmacological strategy (Modarresi *et al.* 2012).

Since we can access patient-derived aneurysm vSMCs from the vascular surgery unit of our clinics, we measured *NUDT6* and *FGF2* levels in these cells. We could also successfully replicate the situation observed before in the primary cells after AngII stimulation. Interestingly, the baseline expression in these diseased vSMCs depicts the image observed in human vascular tissue samples (comparing Figure 1B and C with Figure 6 E). Again, this shows that the deregulation in vSMCs of the *NUDT6-FGF2* axis in vascular diseases is relevant, especially in AAAs.

Lastly, dynamic live cell imaging was performed on transfected cells to gain more physiological insight into vSMC proliferation, apoptosis, and migration. While siRNA-mediated silenced vSMCs behaved as control cells in terms of proliferation and migration, in hAoSMCs, proliferation was higher, and apoptosis was lesser in siRNA-treated cells, overexpressed vSMCs exerted a worsened phenotype characterized by impaired proliferation, increased apoptosis, and decreased migratory capacity in both, hCtSMCs and hAoSMCs.

Also, we were able to show that the NUDT6 peptide does not interfere with apoptosis in the context of vSMCs. Previously, however, it has been reported that NUDT6 peptide halted cell proliferation (Asa *et al.* 2001) and -when stimulated with cytokines – can increase in expression and translocate to the nucleus (Baguma-Nibasheka *et al.* 2005) where it is believed to exert functions crucial in cell survival and proliferation. However, we could not detect any effects of the NUDT6 peptide on apoptosis, one of the critical events in AAAs. This, again, supports the hypothesis of *NUDT6*'s primary role as the antisense to *FGF2* and regulating FGF2 levels and stability.

5.4. *NUDT6* inhibition in four different animal models leads to a reduction of both rupture rate and AAA growth

We observed a relevant disease-dependent pattern of *Nudt6* and Fgf2 expression in two mouse models and could rescue FGF2 expression *in vitro* substantially by inhibiting *NUDT6* using siRNA. Therefore, we chose to apply *Nudt6* ASOs in four different animal models and two different species which cover both carotid artery disease and AAA.

The ASOs were designed in cooperation with Qiagen (Hilden, Germany). They are equipped with an RNaseH cleavage site which leads to the degradation of the formed ASO-mRNA duplex. Applying the ASO systemically *in vivo* in an inducible plaque rupture model led to a reduced rupture rate and retained αSma and Fgf2 expression within the more stable plaques. We then applied the ASO *via* a local delivery technique in the AngII mouse model to limit potential off-target effects in other organs, such as the liver or heart, and to show translational potential.

UTMD (ultrasound-targeted microbubble destruction) mediated drug delivery has already demonstrated the first positive results in a study with inoperable pancreatic cancer patients (Dimcevski *et al.* 2016). As this system is easily deployable in a vascular context, we used microbubbles to encapsulate the *Nudt6*-specific ASO, which we locally delivered with UTMD. And indeed, the results were striking – compared to the PPE-induced murine model, we saw smaller diameters and overall, a better vessel wall morphology. However, it needs to be taken into account that the *Nudt6* ASO was only applied once in the PPE model due to ethics proposal regulations. But in the PPE model, it seems that aneurysm growth can only be adequately halted when the ASO is given repetitively.

As already mentioned in the introduction, the AngII model and the PPE model differ in various aspects of AAA disease, such as the occurrence of rupture, intramural hemorrhage and dissection, the position of the aneurysm, and the different induction (hormonal *versus* mechanical) (Busch *et al.* 2021). Hence, it is encouraging to see similar effects in the two different mouse models, which hint toward a robust response in aneurysm disease upon *Nudt6* ASO treatment.

Targeting Fgf2 was shown beneficial in previous studies – applying Fgf2-containing hydrogel on the aorta limited aneurysm growth while SMC contractility was retained (Hoshina *et al.* 2004, Kawai *et al.* 2018). Further, lncRNA *Anril* was reported

to induce SMC proliferation by upregulating Fgf2 in intracranial aneurysms (Hu *et al.* 2022). While in an aneurysmatic context, the induction of FGF2 in late-stage disease seems beneficial, little is known about its role in earlier stages or its influence on growth speed and size.

In CAD, FGF2 involvement in atherogenesis has been detrimental. Macrophage infiltration, intimal hyperplasia, and intimal thickening are all associated with increased Fgf levels in the plaques (Liu *et al.* 2013, Parma *et al.* 2020). However, atherosclerosis is a dynamic process. Initially harmful mechanisms or genes can be crucial in late-stage disease to prevent plaque rupture and to strengthen the fibrous cap. Indeed, increased Fgf2 content, combined with PDGF-BB, led to normalized neovessels, which were previously abnormal and thereby contributed to a stable plaque (Mao *et al.* 2020). Our discovery of little to no FGF2 in fibrous caps but in the surrounding, old media parts in human lesions can confirm these findings. Also, in our plaque rupture mouse model, Fgf2 was enriched in the fibrous cap after *Nudt6* inhibition. This hints at a spatially restricted mechanism of action induced by FGF2 limited to the fibrous cap.

Only three years ago, Bianca Nogrady wrote in her Nature article about the challenges of targeted RNA delivery to their destination (Nogrady 2019). The COVID-19 pandemic and the resulting developments in RNA therapeutics and delivery strategies changed that picture entirely within a couple of years. Lipids or lipid-based particles, as well as various polymers, were shown to deliver RNA successfully to their cellular destination (neatly reviewed by (Paunovska *et al.* 2022)). We also demonstrated successful microbubble-mediated delivery of the ASO to the target cells (here: vSMCs).

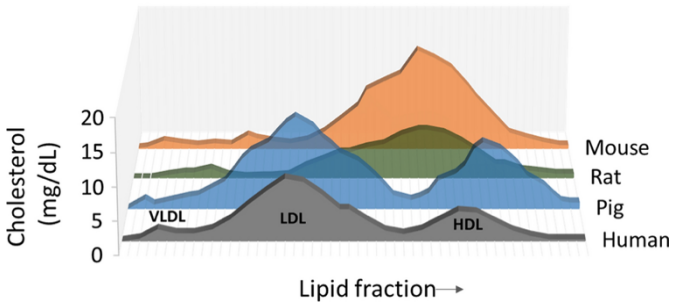

Figure 23 Lipid profiles of different species. From (Golforoush *et al*. 2020) Basic Res Cardiol 115, 73 (2020)

Nevertheless, the differences between humans and mice are still comparably significant, especially regarding circulatory aspects such as flow rate, heart size, and blood volume but also lipid composition (Figure 23). Also, the lack of spontaneous

lesion development or let alone spontaneous plaque rupture, makes it difficult to compare this model organism to humans. This problem, also called the 'translational gap', still prevails in medical research as it is difficult to bridge the gap to human application and clinical studies.

Fortunately, we had the opportunity to deploy *NUDT6* ASO in PPE-induced aneurysms of *LDLR*$^{-/-}$ Yucatan minipigs, thus taking a big leap in translatability. To reduce side effects and the total costs of the inhibitor, we deployed a vascular stent typically used in the everyday practice of vascular surgeons in our clinics. The stent was coated with a custom designed *NUDT6* ASO, whose efficiency was tested before *in vitro*.

Despite the one-time intervention, we saw robust changes in the abdominal aorta – cobblestone-like cells, which in the EvG staining appeared as contractile, less outward remodeling, smaller diameter, and higher FGF2 and αSMA positive cells. This is – to the best of our current knowledge – the first local application of a lncRNA in the vasculature of a large animal model (Huang *et al.* 2020). There have been previous observational efforts made by the team of Kathryn Moore describing the role of lncRNA *CHROME* in non-human primates (Hennessy *et al.* 2019). Also, miR-92a inhibitors were used in the first-in-human trial after showing their efficacy against ischemia-reperfusion injury in pigs (Hinkel *et al.* 2013, Abplanalp *et al.* 2020).

5.5. *NUDT6* impacts SMC contractility and migration by interacting with CDC42 and CSRP1

To elucidate other interaction partners on protein level and respective influence on underlying mechanisms, we performed RNA Pulldown followed by LC-MS/MS. Thus, we could identify proteins that were highly enriched in the *NUDT6* pulldown fraction compared to *GFP* control in hAoSMC lysate: CSRP1 and CDC42.

CSRP1 was higher enriched (32.6-fold) and was chosen for confirmation of interaction using RNA Immunoprecipitation. Indeed, *NUDT6* was significantly enriched in CSRP1 fractions. These results show a verified interaction from both protein and RNA ends.

In disease, we could see that the levels from both proteins were downregulated. To determine the direction of interaction and hierarchy, we analyzed *NUDT6* expression after *CSRP1* or *CDC42* knockdown. Contrary to the two proteins' response to *NUDT6* knockdown, *NUDT6* did not show any significant changes post *CSRP1* or

CDC42 knockdown. This – and the upregulation of the proteins post *NUDT6* knockdown – might hint towards a dominant role of *NUDT6*, which might repress the two proteins.

CDC42 is a small GTPase within the Rho family that regulates actin polymerization, smooth muscle cell migration, and cell cycle progression (Tang and Gunst 2004, Modzelewska *et al.* 2006, Muto *et al.* 2007). We found it to be ubiquitously expressed in many cells within AAA. During migration, CDC42 regulates actomyosin contraction, microtubule stability, direction, and lamelli- and filopodia formation (Figure 24) (Nobes and Hall 1995, Gerthoffer 2007, Afewerki *et al*. 2019).

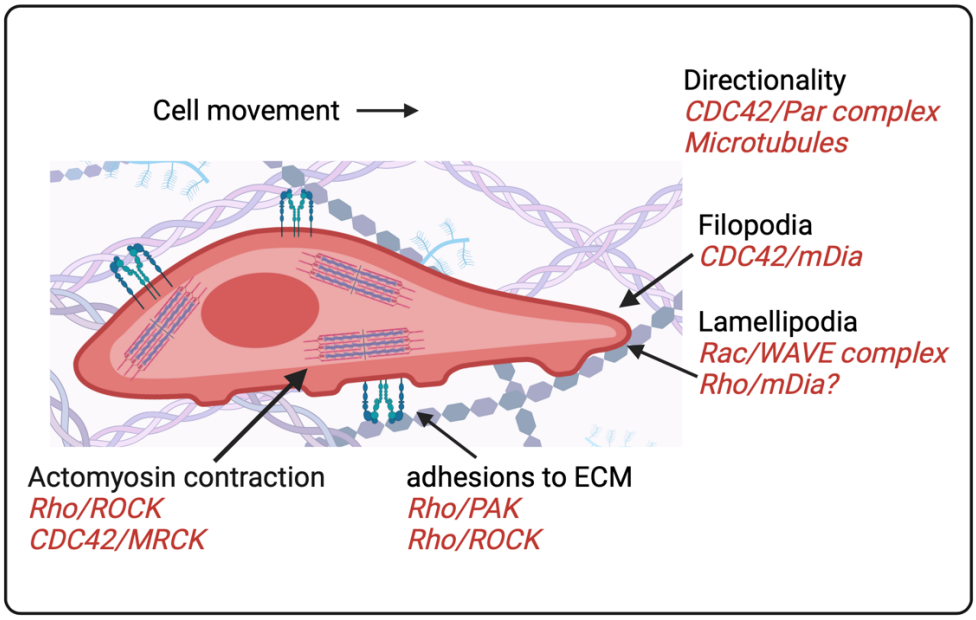

Figure 24 CDC42 in cell migration. Adapted from (Ridley 2015), Curr Opin Cell Biol 36, 103-12

In a vascular context, CDC42 also enables collagen I secretion, which, especially in AAA, is a crucial but lowly expressed molecule needed to maintain vascular bed integrity (Lengfeld *et al.* 2012, Ge *et al.* 2018). Further, CDC42 is involved in SMA promoter activation with Serum Response Factor (SRF) (Sebe *et al.* 2010). Transfecting a constitutively active CDC42 into smooth muscle cells led to an active SMA promoter, while an inactive construct prevented its activation (Sebe *et al.* 2010, Ge *et al.* 2018).

If all these functions are impaired in AAA, which we saw in human specimens, crucial smooth muscle cell genes are prevented from activation, and collagen production is further impaired. Restored CDC42 levels – after *NUDT6*-ASO – might be helpful in late-stage AAA and potentially also CAD to prevent aortic and plaque rupture

by giving the cells a chance to migrate and produce matrix components to strengthen the vessel wall or fibrous cap, respectively.

CRP1 (*alias* CSRP1; in this thesis, it is called CSRP1 while in most literature, CRP1 is more commonly used. That is why in the following part, the name CRP1 is used instead to be consistent with the existing literature) is a member of the CRP family possessing 2 LIM domains (Kadrmas and Beckerle 2004). Their function and regulation could be more well elucidated, but they contribute to actin-related processes. Pomiès *et al.* identified α-actinin as a CRP1 interaction partner (Pomies *et al.* 1997). Further investigation by Tran *et al*. revealed that CRP1 regulates the cross-linking of actin bundles by stabilizing their connection with α-actinin (Tran *et al.* 2005).

One process where this activity is needed is filopodia formation – it was found in the growth cones of neurons. However, if CRP1 is knocked down, filopodia formation in these cells is inhibited (Ma *et al.* 2011). Interestingly, the group also performed a co-transfection of a CRP1 overexpression vector and a constitutively active form of CDC42 with the result of a synergistic increase of filopodia formation (Ma *et al.* 2011). However, it is not known by what means CRP1 regulates CDC42.

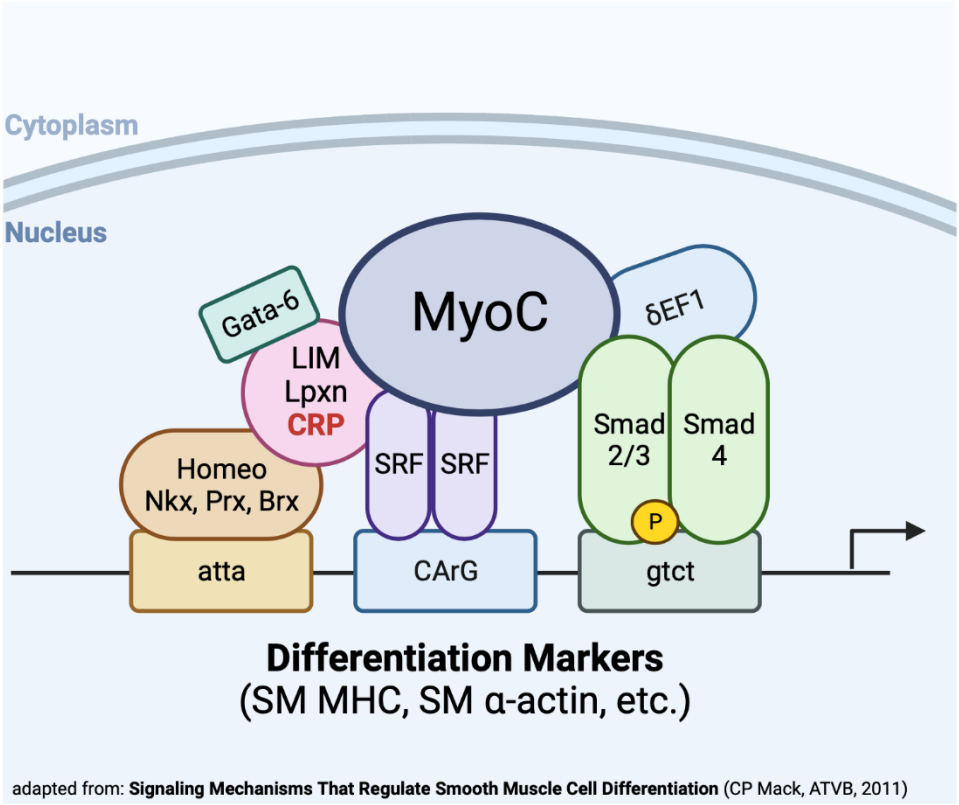

Figure 25 CRP1 regulates SRF1 in Smooth Muscle Cell Differentiation. Adapted from (Mack 2011), ATVB 31, 1495-505

In human vSMCs, where we found CRP1 to be almost exclusively expressed, it is associated with SMC gene differentiation (Lilly *et al.* 2010). Of importance, CRP1 holds an internal enhancer that limits its expression to arterial SMCs (Lilly *et al.* 2001). This enhancer, in turn, includes and is dependent on a CArG box motif that binds SRF (Lilly *et al.* 2001). Chang *et al*. further verified a mechanism in which CRP1 acts as a bridging factor together with GATA6 to facilitate SRF binding to the CArG box on many SMC-related genes (SMA, MHC, CNN, SM22a, etc. (Lilly *et al.* 2001)), thus regulating SMC differentiation (Figure 25) (Chang *et al*. 2003).

Besides its involvement in SMC gene expression regulation, CRP1 expression can be increased by TGF-β1 through Smad and p38 MAPK signaling, leading to improved contractility of SMCs (Jarvinen *et al.* 2012). Especially in AAA, TGFβ is known as a crucial regulator of proliferation, differentiation, and migration (Jarvinen *et al.* 2012). Its malfunction/variation is associated with diseases such as the Loeys-Dietz syndrome (Loeys and Dietz 1993) and the occurrence of AAA (Saratzis and Bown 2014). Also, in CAD, low TGF-β levels associate with a worsened outcome (Ikonomidis *et al.* 2008) as it was ascribed anti-inflammatory functions, which led to a thicker and stronger fibrous cap (Amento *et al.* 1991).

All these functions and associated proteins, such as TGF-β1, imply a crucial role in healthy SMCs. Once this role is lost, cell differentiation is aberrant, migration impaired, and vital factors (like Collagen Type I) are not secreted anymore. Further experiments must be performed to fully confirm the hypothesized dominant and repressive role of *NUDT6* towards CDC42 and CRP1. Also, pulldown experiments in patient-derived SMCs or SMCs under AngII stimulation would provide a better and complementary observation to the IHC images of AAA samples.

5.6. Conclusions

We could show profound deregulation of *NUDT6* and FGF2 in two vascular diseases – AAA and CAD. This deregulation was associated with high *NUDT6* levels in advanced disease stages and poor vSMC survival, proliferation, and migration. Using *NUDT6* ASOs, we were able to restore the balance in four animal models of two different species. On a cellular level, *NUDT6* knockdown induced SMC migration and proliferation – an event beneficial, especially in an advanced disease setting to

reactivate SMCs for their migration into the fibrous cap or proliferation in AAA disease to even out for previous apoptotic events.

We could show two protein interaction partners of *NUDT6*, CDC42, and CRP1. These proteins play crucial roles in SMC differentiation, migration, and actin polymerization. They might provide another insight into the mechanism behind SMC reactivation after *NUDT6* ASO treatment both *in vivo* and *in vitro*.

6. Abstract

Cardiovascular diseases remain the most common cause of death. An underlying pathology of diseases like carotid artery disease (plaque formation) (CAD) or abdominal aortic aneurysm (AAA) is atherosclerosis. Plaque or aortic growth progression and rupture cannot be halted pharmacologically, and therefore, surgery is required. Considering the advanced age of a cardiovascular patient, surgery can pose a high risk. Also, there are no available treatments or biomarkers to predict rupture. Long non-coding RNAs (lncRNAs) orchestrate important functions in the human organism. Their dysfunction (abnormal increase or decrease) can trigger diseases.

Here, we identified the antisense lncRNA *Nudix Hydrolase 6* (*NUDT6)* and its respective sense partner *Fibroblast Growth Factor 2 (FGF2)* to be deregulated in the two vascular diseases mentioned above. In ruptured carotid lesions and advanced AAA lesions, *NUDT6* was strongly upregulated. *NUDT6* inhibition *in vitro* using siRNA led to *FGF2* de-repression. Using dynamic live cell imaging, *NUDT6* inhibition led to reduced apoptosis and increased migration and proliferation. Hence, we designed an antisense oligonucleotide (ASO) inhibitor which targets *NUDT6*. It was then applied in the carotid plaque rupture model as well as locally in the AAA-inducing Angiotensin II and systemically in the Porcine Pancreatic Elastase (PPE) mouse model. *NUDT6* inhibition significantly lowered plaque rupture and abdominal aortic diameter, respectively. FGF2 was increasingly expressed in the vessel wall alongside alpha Smooth Muscle Actin (αSMA). With the pursuit to close the 'translational gap', we locally applied a species-specific ASO in *LDLR*$^{-/-}$ Yucatan minipigs. We saw halted abdominal growth in PPE-induced pigs receiving *NUDT6*-ASO. Further, the vessel wall composition and appearance were greatly improved by the ASO application.

To understand potential other mechanisms and interactions in which *NUDT6* is involved, we used RNA pulldown. We identified two significantly enriched proteins, Cysteine and Glycine Rich Protein 1 (CRP1) and Cell Division Cycle 42 (CDC42). These proteins were also downregulated in late-stage AAA. *NUDT6* inhibition in vascular smooth muscle cells (vSMCs) *in vitro* led to an upregulation of the two proteins. This points towards a dominant role of *NUDT6* in regulation. Both CRP1 and CCD42 were de-repressed in the porcine animal model after *NUDT6*-ASO treatment.

The proteins are involved in migration and cell movement as well as SMC differentiation. The further mechanism and relevance still must be elucidated.

In conclusion, we identified *NUDT6* silencing as a potential novel RNA-based therapeutic approach in advanced vascular diseases. Thus, SMC survival and migration are induced, crucial mechanisms both lacking in late degenerative cardiovascular pathologies.

7. Zusammenfassung

Nach wie vor zählen Herz-Kreislauf-Krankheiten zur häufigsten Todesursache. Oftmals liegt eine Erkrankung der Halsschlagader (Plaquebildung) oder dem abdominellen Aortenaneurysma eine Atherosklerose zugrunde. Eine Plaque-oder Aortenruptur kann nicht medikamentös behandelt oder verhindert werden, sodass ein operativer Eingriff vonnöten ist. In Anbetracht des fortgeschrittenen Alters eines typischen kardiovaskulären Patienten kann eine Operation allerdings ein hohes Risiko darstellen. Außerdem gibt es keine Behandlungsmöglichkeiten oder Biomarker zur Vorhersage einer Ruptur. Lange nicht-kodierende RNAs orchestrieren essentielle Funktionen im menschlichen Organismus. Ihre Fehlfunktion (z.B. durch abnormale Produktion) kann Krankheiten auslösen.

Hier identifizieren und untersuchen wir die Antisense-lncRNA *Nudix Hydrolase 6* (*NUDT6*) und ihren entsprechenden Sense-Partner *Fibroblast Growth Factor 2* (*FGF2*) in den beiden oben genannten Gefäßerkrankungen. In rupturierten Karotisläsionen und fortgeschrittenen AAA-Läsionen war *NUDT6* stark hochreguliert. Die Inhibition von *NUDT6* mittels siRNA in vaskulären glatten Gefäßmuskelzellen (vSMCs) führte zu einer Derepression von *FGF2*. Mit Hilfe eines dynamischen Bildgebungsverfahrens konnten wir feststellen, dass *NUDT6* Inhibition zu einer verringerten Apoptose und erhöhten Migration und Proliferation in vSMCs führte. Daher haben wir einen Antisense-Oligonukleotid (ASO) Inhibitor gegen *NUDT6* entwickelt. Im Karotis-Plaqueruptur Modell sowie lokal appliziert im AAA-induzierten Angiotensin-II- und systemisch im Porcine Pancreatic Elastase (PPE) – Mausmodell wurde er *in vivo* angewendet. Die Hemmung von *NUDT6* führe zu einer signifikanten Verringerung der Plaqueruptur bzw. des Bauchaortendurchmessers. Fgf2 wurde in der Gefäßwand zusammen mit alpha Smooth Muscle Actin (αSma) erhöht exprimiert. Im Bestreben, die ‚translationale Lücke' zu schließen, haben wir ein speziesspezifisches ASO in *LDLR*$^{-/-}$ Yucatan Minischweinen angewendet. Bei den Tieren, die das ASO erhielten, kam das Bauchaortenwachstum, induziert vor Inhibitorgabe mit PPE, zum Stillstand. Außerdem wurden die Zusammensetzung und das Aussehen der Gefäßwände durch die ASO-Anwendung erheblich verbessert.

Um mögliche andere Mechanismen, an denen *NUDT6* beteiligt ist, zu verstehen, verwendeten wir die RNA Pulldown Technik. So konnten wir zwei signifikant angereicherte Proteine, Cysteine and Glycine Rich Protein 1 (CRP1) und

Cell Division Cycle 42 (CDC42), identifizieren. Diese waren auch im späten AAA-Stadium herunterreguliert. Die Inhibition von *NUDT6* mittels siRNA in vSMCs führte zu einer Hochregulierung der beiden Proteine. Dies deutet auf eine dominante Rolle von *NUDT6* bei der Regulierung hin. Sowohl CRP1 als auch CDC42 wurden im Schweinemodell nach der Behandlung mit *NUDT6*-ASO de-reprimiert. Die Proteine sind an der Migration und Zellbewegung sowie SMC-Differenzierung beteiligt. Der weitere Mechanismus und die Bedeutung der Interaktion müssen noch aufgeklärt werden.

Zusammenfassend lässt sich sagen, dass die Inhibition von *NUDT6* ein potentiell neuer therapeutischer Ansatz auf RNA-Basis in fortgeschrittenen Gefäßerkrankungen ist. Auf diese Weise werden das Überleben und die Migration der SMCs gefördert; beides entscheidende Mechanismen, die in späten degenerativen Herz-Kreislauf-Erkrankungen fehlen.

8. Publications

1: **Winter H**, Winski G, Busch A, Chernogubova E, Fasolo F, Wu Z, Bäcklund A, Khomtchouk BB, Van Booven DJ, Sachs N, Eckstein HH, Wittig I, Boon RA, Jin H, Maegdefessel L. Targeting long non-coding RNA *NUDT6* enhances smooth muscle cell survival and limits vascular disease progression. (accepted and in press at Molecular Therapy 2023 Apr 28; doi: 10.1016/j.ymthe.2023.04.020)

2: Cynn E, Li DY, O'Reilly ME, Wang Y, Bashore AC, Jha A, Foulkes AS, Zhang H, Winter H, Maegdefessel L, Yan H, Li M, Ross L, Xue C, Reilly MP. Human Macrophage Long Intergenic Noncoding RNA, SIMALR, Suppresses Inflammatory Macrophage Apoptosis via NTN1 (Netrin-1). Arterioscler Thromb Vasc Biol. 2023 Feb;43(2):286-299. doi: 10.1161/ATVBAHA.122.318353. Epub 2022 Dec 22. PMID: 36546321.

3: Zhou Z, Collado A, SunC, Tratsiakovich Y, Mahdi A, **Winter H**, Chernogubova E, Seime T, Narayanan S, Jiao T, Jin H, Alvarsson M, Zheng X, Yang J, Hedin U, Catrina SB, Maegdefessel L, Pernow J. Downregulation of Erythrocyte miR-210 Induces Endothelial Dysfunction in Type 2 Diabetes. Diabetes. 2022 Feb 1;71(2):285-297. doi: 10.2337/db21-0093. PMID: 34753800.

4: Fasolo F, Jin H, Winski G, Chernogubova E, Pauli J, **Winter H**, Li DY, Glukha N, Bauer S, Metschl S, Wu Z, Koschinsky ML, Reilly M, Pelisek J, Kempf W, Eckstein HH, Soehnlein O, Matic L, Hedin U, Bäcklund A, Bergmark C, Paloschi V,Maegdefessel L. Long Noncoding RNA *MIAT* Controls Advanced Atherosclerotic Lesion Formation and Plaque Destabilization. Circulation. 2021 Nov 9;144(19):1567-1583. doi: 10.1161/CIRCULATIONAHA.120.052023. Epub 2021 Oct 14. PMID: 34647815; PMCID: PMC8570347.

5: Busch A, Pauli J, Winski G, Bleichert S, Chernogubova E, Metschl S, **Winter H**, Trenner M, Wiegering A, Otto C, Fischer J, Reiser J, Werner J, Roy J, Brostjan C, Knappich C, Eckstein HH, Paloschi V, Maegdefessel L. Lenvatinib halts aortic aneurysm growth by restoring smooth muscle cell contractility. JCI Insight. 2021 Aug 9;6(15):e140364. doi: 10.1172/jci.insight.140364. PMID: 34185710; PMCID:

PMC8410098.

6: Winkler MJ, Müller P, Sharifi AM, Wobst J, **Winter H**, Mokry M, Ma L, van der Laan SW, Pang S, Miritsch B, Hinterdobler J, Werner J, Stiller B, Güldener U, Webb TR, Asselbergs FW, Björkegren JLM, Maegdefessel L, Schunkert H, Sager HB, Kessler T. Functional investigation of the coronary artery disease gene SVEP1. Basic Res Cardiol. 2020 Nov 13;115(6):67. doi: 10.1007/s00395-020-00828-6. PMID: 33185739; PMCID: PMC7666586.

7: Paloschi V, **Winter H**, Viola J, Soehnlein O, Maegdefessel L. Mechanistic Links between Non-Coding RNAs and Myeloid Cell Inflammation in Atherosclerosis. Thromb Haemost. 2019 Aug;119(8):1205-1211. doi: 10.1055/s-0039-1687874. Epub 2019 Apr 29. PMID: 31035303.

8: Eken SM, Christersdottir T, Winski G, Sangsuwan T, Jin H, Chernogubova E, Pirault J, Sun C, Simon N, **Winter H**, Backlund A, Haghdoost S, Hansson GK, Halle M, Maegdefessel L. miR-29b Mediates the Chronic Inflammatory Response in Radiotherapy-Induced Vascular Disease. JACC Basic Transl Sci. 2019 Feb 25;4(1):72-82. doi: 10.1016/j.jacbts.2018.10.006. PMID: 30847421; PMCID: PMC6390501.

9: Jin H, Li DY, Chernogubova E, Sun C, Busch A, Eken SM, Saliba-Gustafsson P, **Winter H**, Winski G, Raaz U, Schellinger IN, Simon N, Hegenloh R, Matic LP, Jagodic M, Ehrenborg E, Pelisek J, Eckstein HH, Hedin U, Backlund A, Maegdefessel L. Local Delivery of miR-21 Stabilizes Fibrous Caps in Vulnerable Atherosclerotic Lesions. Mol Ther. 2018 Apr 4;26(4):1040-1055. doi: 10.1016/j.ymthe.2018.01.011. Epub 2018 Jan 31. PMID: 29503197; PMCID: PMC6080193.

<u>In preparation</u>

10: **Winter H**, Maegdefessel L. Targeting non-coding RNAs for novel treatment strategies in vascular diseases (invited short review; accepted at European Heart Journal, 2023 Apr)

11: Fasolo F, Winski G, Li Z, Wu Z, **Winter H**, Glukha N, Roy J, Hultgren R, Pauli J, Busch A, Sachs N, Eckstein HH, Boon RA, Paloschi V, Maegdefessel L. The circular RNA Ataxia-telangiectasia mutated (circATM) regulates oxidative stress in smooth muscle cells in expanding abdominal aortic aneurysms (in revision at Molecular Therapy Nucleic Acids. 2023 Jan)

12: Xie Y, **Winter H**, Rotlan N, et al. LMO7 regulates smooth muscle cell cholesterol esterification to influence plaque stability. Research Square; 2022. DOI: 10.21203/rs.3.rs-1359588/v1

13: Bäcklund A, Strawbridge RJ, Gertow K, Chernogubova E, Jin H, Gonzalez Diez M, Olsson L, **Winter H**, Sabater-Lleal M, Sennblad B, Öhrvik J, Zabaneh D, Veglia F, Folkersen L, Gigante B, Leander K, Vikström M, Ketelhuth DFJ, Silveira A, Colombo GI, Perisic Matic L, Gabrielsen A, Hedin U, Ljungcrantz I, Nilsson J, Savonen K, Giral P, Pirro M, Hansson GK, Eriksson P, Van der Laan SW, Pasterkamp G, Baldassarre D, Tremoli E, De Faire U, Humphries SE, Hamsten A, Holdahl R, Maegdefessel L. Identification of NCF4 as a Novel Regulator in Arterial Remodeling and Advanced Atherosclerosis (in review at BMC Genome Medicine)

14: Pourteymour S, Fan J, Kumar Mahji, R, Guo S-Y, Zhen H, Liu Y, Sun X, **Winter H**, Backlund A, Skenteris N, Chernogubova E, Werngren O, Skogsberg J, Li Y, Matic L, Hedin U, Maegdefessel L, Ehrenborg E, Tian Y, Jin H. Targeting PIEZO1 Refines Macrophage Function in Atherosclerosis. Preprint Available at SSRN: https://ssrn.com/abstract=4154102 or http://dx.doi.org/10.2139/ssrn.4154102

9. References

(1983). "Classics in arteriosclerosis research: On experimental cholesterin steatosis and its significance in the origin of some pathological processes by N. Anitschkow and S. Chalatow, translated by Mary Z. Pelias, 1913." Arteriosclerosis: An Official Journal of the American Heart Association, Inc. **3**(2): 178-182.

(1998). "Mortality results for randomised controlled trial of early elective surgery or ultrasonographic surveillance for small abdominal aortic aneurysms. The UK Small Aneurysm Trial Participants." Lancet **352**(9141): 1649-1655.

Abplanalp, W. T., A. Fischer, D. John, A. M. Zeiher, W. Gosgnach, H. Darville, R. Montgomery, L. Pestano, G. Allee, I. Paty, F. Fougerousse and S. Dimmeler (2020). "Efficiency and Target Derepression of Anti-miR-92a: Results of a First in Human Study." Nucleic Acid Ther **30**(6): 335-345.

Ackers-Johnson, M., A. Talasila, A. P. Sage, X. Long, I. Bot, N. W. Morrell, M. R. Bennett, J. M. Miano and S. Sinha (2015). "Myocardin regulates vascular smooth muscle cell inflammatory activation and disease." Arterioscler Thromb Vasc Biol **35**(4): 817-828.

Afewerki, T., S. Ahmed and D. Warren (2019). "Emerging regulators of vascular smooth muscle cell migration." J Muscle Res Cell Motil **40**(2): 185-196.

Ailawadi, G., J. L. Eliason and G. R. Upchurch, Jr. (2003). "Current concepts in the pathogenesis of abdominal aortic aneurysm." J Vasc Surg **38**(3): 584-588.

Ailawadi, G., C. W. Moehle, H. Pei, S. P. Walton, Z. Yang, I. L. Kron, C. L. Lau and G. K. Owens (2009). "Smooth muscle phenotypic modulation is an early event in aortic aneurysms." J Thorac Cardiovasc Surg **138**(6): 1392-1399.

Akerman, A. W., R. E. Stroud, R. W. Barrs, R. T. Grespin, L. T. McDonald, R. A. C. LaRue, R. Mukherjee, J. S. Ikonomidis, J. A. Jones and J. M. Ruddy (2018). "Elevated Wall Tension Initiates Interleukin-6 Expression and Abdominal Aortic Dilation." Ann Vasc Surg **46**: 193-204.

Akl, M. R., P. Nagpal, N. M. Ayoub, B. Tai, S. A. Prabhu, C. M. Capac, M. Gliksman, A. Goy and K. S. Suh (2016). "Molecular and clinical significance of fibroblast growth factor 2 (FGF2 /bFGF) in malignancies of solid and hematological cancers for personalized therapies." Oncotarget **7**(28): 44735-44762.

Alderman, M. H., S. Madhavan, W. L. Ooi, H. Cohen, J. E. Sealey and J. H. Laragh (1991). "Association of the renin-sodium profile with the risk of myocardial infarction in patients with hypertension." N Engl J Med **324**(16): 1098-1104.

Alencar, G. F., K. M. Owsiany, S. Karnewar, K. Sukhavasi, G. Mocci, A. T. Nguyen, C. M. Williams, S. Shamsuzzaman, M. Mokry, C. A. Henderson, R. Haskins, R. A. Baylis, A. V. Finn, C. A. McNamara, E. R. Zunder, V. Venkata, G. Pasterkamp, J. Bjorkegren, S. Bekiranov and G. K. Owens (2020). "Stem Cell Pluripotency Genes Klf4 and Oct4 Regulate Complex SMC Phenotypic Changes Critical in Late-Stage Atherosclerotic Lesion Pathogenesis." Circulation **142**(21): 2045-2059.

Allahverdian, S., C. Chaabane, K. Boukais, G. A. Francis and M. L. Bochaton-Piallat (2018). "Smooth muscle cell fate and plasticity in atherosclerosis." Cardiovasc Res **114**(4): 540-550.

Allahverdian, S., A. C. Chehroudi, B. M. McManus, T. Abraham and G. A. Francis (2014). "Contribution of intimal smooth muscle cells to cholesterol accumulation and macrophage-like cells in human atherosclerosis." Circulation **129**(15): 1551-1559.

Allaire, E., B. Muscatelli-Groux, C. Mandet, A. M. Guinault, P. Bruneval, P. Desgranges, A. Clowes, D. Melliere and J. P. Becquemin (2002). "Paracrine effect of vascular smooth muscle cells in the prevention of aortic aneurysm formation." J Vasc Surg **36**(5): 1018-1026.

Amento, E. P., N. Ehsani, H. Palmer and P. Libby (1991). "Cytokines and growth factors positively and negatively regulate interstitial collagen gene expression in human vascular smooth muscle cells." Arterioscler Thromb **11**(5): 1223-1230.

Anidjar, S., J. L. Salzmann, D. Gentric, P. Lagneau, J. P. Camilleri and J. B. Michel (1990). "Elastase-induced experimental aneurysms in rats." Circulation **82**(3): 973-981.

Arnett, D. K., R. S. Blumenthal, M. A. Albert, A. B. Buroker, Z. D. Goldberger, E. J. Hahn, C. D. Himmelfarb, A. Khera, D. Lloyd-Jones, J. W. McEvoy, E. D. Michos, M. D. Miedema, D. Munoz, S. C. Smith, Jr., S. S. Virani, K. A. Williams, Sr., J. Yeboah and B. Ziaeian (2019). "2019 ACC/AHA Guideline on the Primary Prevention of Cardiovascular Disease: A Report of the American College of Cardiology/American Heart Association Task Force on Clinical Practice Guidelines." J Am Coll Cardiol **74**(10): e177-e232.

Asa, S. L., L. Ramyar, P. R. Murphy, A. W. Li and S. Ezzat (2001). "The endogenous fibroblast growth factor-2 antisense gene product regulates pituitary cell growth and hormone production." Mol Endocrinol **15**(4): 589-599.

Babij, P., C. Kelly and M. Periasamy (1991). "Characterization of a mammalian smooth muscle myosin heavy-chain gene: complete nucleotide and protein coding sequence and analysis of the 5' end of the gene." Proc Natl Acad Sci U S A **88**(23): 10676-10680.

Back, M., T. C. Gasser, J. B. Michel and G. Caligiuri (2013). "Biomechanical factors in the biology of aortic wall and aortic valve diseases." Cardiovasc Res **99**(2): 232-241.

Baguma-Nibasheka, M., A. W. Li and P. R. Murphy (2007). "The fibroblast growth factor-2 antisense gene inhibits nuclear accumulation of FGF-2 and delays cell cycle progression in C6 glioma cells." Mol Cell Endocrinol **267**(1-2): 127-136.

Baguma-Nibasheka, M., A. W. Li, M. S. Osman, L. Geldenhuys, A. G. Casson, C. K. Too and P. R. Murphy (2005). "Coexpression and regulation of the FGF-2 and FGF antisense genes in leukemic cells." Leuk Res **29**(4): 423-433.

Baguma-Nibasheka, M., L. A. Macfarlane and P. R. Murphy (2012). "Regulation of fibroblast growth factor-2 expression and cell cycle progression by an endogenous antisense RNA." Genes (Basel) **3**(3): 505-520.

Bai, Y., Q. Zhang, Y. Su, Z. Pu and K. Li (2019). "Modulation of the Proliferation/Apoptosis Balance of Vascular Smooth Muscle Cells in Atherosclerosis by lncRNA-MEG3 via Regulation of miR-26a/Smad1 Axis." Int Heart J **60**(2): 444-450.

Balbin, O. A., R. Malik, S. M. Dhanasekaran, J. R. Prensner, X. Cao, Y. M. Wu, D. Robinson, R. Wang, G. Chen, D. G. Beer, A. I. Nesvizhskii and A. M. Chinnaiyan (2015). "The landscape of antisense gene expression in human cancers." Genome Res **25**(7): 1068-1079.

Barlis, P., P. W. Serruys, A. Devries and E. Regar (2008). "Optical coherence tomography assessment of vulnerable plaque rupture: predilection for the plaque 'shoulder'." Eur Heart J **29**(16): 2023.

Barnett, H. J., D. W. Taylor, M. Eliasziw, A. J. Fox, G. G. Ferguson, R. B. Haynes, R. N. Rankin, G. P. Clagett, V. C. Hachinski, D. L. Sackett, K. E. Thorpe, H. E. Meldrum and J. D. Spence (1998). "Benefit of carotid endarterectomy in patients with symptomatic moderate or severe stenosis. North American Symptomatic Carotid Endarterectomy Trial Collaborators." N Engl J Med **339**(20): 1415-1425.

Basatemur, G. L., H. F. Jorgensen, M. C. H. Clarke, M. R. Bennett and Z. Mallat (2019). "Vascular smooth muscle cells in atherosclerosis." Nat Rev Cardiol **16**(12): 727-744.

Beasley, D., M. E. McGuiggin and C. A. Dinarello (1995). "Human vascular smooth muscle cells produce an intracellular form of interleukin-1 receptor antagonist." Am J Physiol **269**(4 Pt 1): C961-968.

Bell, R. D., X. Long, M. Lin, J. H. Bergmann, V. Nanda, S. L. Cowan, Q. Zhou, Y. Han, D. L. Spector, D. Zheng and J. M. Miano (2014). "Identification and initial functional characterization of a human vascular cell-enriched long noncoding RNA." Arterioscler Thromb Vasc Biol **34**(6): 1249-1259.

Bennett, M. R., K. Macdonald, S. W. Chan, J. J. Boyle and P. L. Weissberg (1998). "Cooperative interactions between RB and p53 regulate cell proliferation, cell senescence, and apoptosis in human vascular smooth muscle cells from atherosclerotic plaques." Circ Res **82**(6): 704-712.

Bennett, M. R., S. Sinha and G. K. Owens (2016). "Vascular Smooth Muscle Cells in Atherosclerosis." Circ Res **118**(4): 692-702.

Bentzon, J. F., F. Otsuka, R. Virmani and E. Falk (2014). "Mechanisms of plaque formation and rupture." Circ Res **114**(12): 1852-1866.

Berliner, J. A., N. Leitinger and S. Tsimikas (2009). "The role of oxidized phospholipids in atherosclerosis." J Lipid Res **50 Suppl**: S207-212.

Bhamidipati, C. M., C. A. Whatling, G. S. Mehta, A. K. Meher, V. A. Hajzus, G. Su, M. Salmon, G. R. Upchurch, Jr., G. K. Owens and G. Ailawadi (2014). "5-Lipoxygenase pathway in experimental abdominal aortic aneurysms." Arterioscler Thromb Vasc Biol **34**(12): 2669-2678.

Blanchard, J. F., H. K. Armenian and P. P. Friesen (2000). "Risk factors for abdominal aortic aneurysm: results of a case-control study." Am J Epidemiol **151**(6): 575-583.

Bochaton-Piallat, M. L. and M. Back (2018). "Novel concepts for the role of smooth muscle cells in vascular disease: towards a new smooth muscle cell classification." Cardiovasc Res **114**(4): 477-480.

Boon, R. A., P. Hofmann, K. M. Michalik, N. Lozano-Vidal, D. Berghauser, A. Fischer, A. Knau, N. Jae, C. Schurmann and S. Dimmeler (2016). "Long Noncoding RNA Meg3 Controls Endothelial Cell Aging and Function: Implications for Regenerative Angiogenesis." J Am Coll Cardiol **68**(23): 2589-2591.

Borgbjerg, J., M. Bogsted, J. S. Lindholt, C. Behr-Rasmussen, A. Horlyck and J. B. Frokjaer (2018). "Superior Reproducibility of the Leading to Leading Edge and Inner to Inner Edge Methods in the Ultrasound Assessment of Maximum Abdominal Aortic Diameter." Eur J Vasc Endovasc Surg **55**(2): 206-213.

Boyle, J. J., D. E. Bowyer, P. L. Weissberg and M. R. Bennett (2001). "Human blood-derived macrophages induce apoptosis in human plaque-derived vascular smooth muscle cells by Fas-ligand/Fas interactions." Arterioscler Thromb Vasc Biol **21**(9): 1402-1407.

Brannan, C. I., E. C. Dees, R. S. Ingram and S. M. Tilghman (1990). "The product of the H19 gene may function as an RNA." Mol Cell Biol **10**(1): 28-36.

Britten, R. J. and D. E. Kohne (1968). "Repeated sequences in DNA. Hundreds of thousands of copies of DNA sequences have been incorporated into the genomes of higher organisms." Science **161**(3841): 529-540.

Broadbent, H. M., J. F. Peden, S. Lorkowski, A. Goel, H. Ongen, F. Green, R. Clarke, R. Collins, M. G. Franzosi, G. Tognoni, U. Seedorf, S. Rust, P. Eriksson, A. Hamsten, M. Farrall, H. Watkins and P. consortium (2008). "Susceptibility to coronary artery disease and diabetes is encoded by distinct, tightly linked SNPs in the ANRIL locus on chromosome 9p." Hum Mol Genet **17**(6): 806-814.

Brown, C. J., A. Ballabio, J. L. Rupert, R. G. Lafreniere, M. Grompe, R. Tonlorenzi and H. F. Willard (1991). "A gene from the region of the human X inactivation centre is expressed exclusively from the inactive X chromosome." Nature **349**(6304): 38-44.

Burgess, W. H. and T. Maciag (1989). "The heparin-binding (fibroblast) growth factor family of proteins." Annu Rev Biochem **58**: 575-606.

Busch, A., S. Bleichert, N. Ibrahim, M. Wortmann, H. H. Eckstein, C. Brostjan, M. U. Wagenhauser, C. J. Goergen and L. Maegdefessel (2021). "Translating mouse models of abdominal aortic aneurysm to the translational needs of vascular surgery." JVS Vasc Sci **2**: 219-234.

Busch, A., E. Chernogubova, H. Jin, F. Meurer, H. H. Eckstein, M. Kim and L. Maegdefessel (2018). "Four Surgical Modifications to the Classic Elastase Perfusion Aneurysm Model Enable Haemodynamic Alterations and Extended Elastase Perfusion." Eur J Vasc Endovasc Surg **56**(1): 102-109.

Busch, A., J. Pauli, G. Winski, S. Bleichert, E. Chernogubova, S. Metschl, H. Winter, M. Trenner, A. Wiegering, C. Otto, J. Fischer, J. Reiser, J. Werner, J. Roy, C. Brostjan, C. Knappich, H. H. Eckstein, V. Paloschi and L. Maegdefessel (2021). "Lenvatinib halts aortic aneurysm growth by restoring smooth muscle cell contractility." JCI Insight **6**(15).

Cabili, M. N., C. Trapnell, L. Goff, M. Koziol, B. Tazon-Vega, A. Regev and J. L. Rinn (2011). "Integrative annotation of human large intergenic noncoding RNAs reveals global properties and specific subclasses." Genes Dev **25**(18): 1915-1927.

Cai, B., Z. Li, M. Ma, Z. Wang, P. Han, B. A. Abdalla, Q. Nie and X. Zhang (2017). "LncRNA-Six1 Encodes a Micropeptide to Activate Six1 in Cis and Is Involved in Cell Proliferation and Muscle Growth." Front Physiol **8**: 230.

Carninci, P., T. Kasukawa, S. Katayama, J. Gough, M. C. Frith, N. Maeda, R. Oyama, T. Ravasi, B. Lenhard, C. Wells, R. Kodzius, K. Shimokawa, V. B. Bajic, S. E. Brenner, S. Batalov, A. R. Forrest, M. Zavolan, M. J. Davis, L. G. Wilming, V. Aidinis, J. E. Allen, A. Ambesi-Impiombato, R. Apweiler, R. N. Aturaliya, T. L. Bailey, M. Bansal, L. Baxter, K. W. Beisel, T. Bersano, H. Bono, A. M. Chalk, K. P. Chiu, V. Choudhary, A. Christoffels, D. R. Clutterbuck, M. L. Crowe, E. Dalla, B. P. Dalrymple, B. de Bono, G. Della Gatta, D. di Bernardo, T. Down, P. Engstrom, M. Fagiolini, G. Faulkner, C. F. Fletcher, T. Fukushima, M. Furuno, S. Futaki, M. Gariboldi, P. Georgii-Hemming, T. R. Gingeras, T. Gojobori, R. E. Green, S. Gustincich, M. Harbers, Y. Hayashi, T. K. Hensch, N. Hirokawa, D. Hill, L. Huminiecki, M. Iacono, K. Ikeo, A. Iwama, T. Ishikawa, M. Jakt, A. Kanapin, M. Katoh, Y. Kawasawa, J. Kelso, H. Kitamura, H. Kitano, G. Kollias, S. P. Krishnan, A. Kruger, S. K. Kummerfeld, I. V. Kurochkin, L. F. Lareau, D. Lazarevic, L. Lipovich, J. Liu, S. Liuni, S. McWilliam, M. Madan Babu, M. Madera, L. Marchionni, H. Matsuda, S. Matsuzawa, H. Miki, F. Mignone, S. Miyake, K. Morris, S. Mottagui-Tabar, N. Mulder, N. Nakano, H. Nakauchi, P. Ng, R. Nilsson, S. Nishiguchi, S. Nishikawa, F. Nori, O. Ohara, Y. Okazaki, V. Orlando, K. C. Pang, W. J. Pavan, G. Pavesi, G. Pesole, N. Petrovsky, S. Piazza, J. Reed, J. F. Reid, B. Z. Ring, M. Ringwald, B. Rost, Y. Ruan, S. L. Salzberg, A. Sandelin, C. Schneider, C. Schonbach, K. Sekiguchi, C. A. Semple, S. Seno, L. Sessa, Y. Sheng, Y. Shibata, H. Shimada, K. Shimada, D. Silva, B. Sinclair, S. Sperling, E. Stupka, K. Sugiura, R. Sultana, Y. Takenaka, K. Taki, K. Tammoja, S. L. Tan, S. Tang, M. S. Taylor, J. Tegner, S. A. Teichmann, H. R. Ueda, E. van Nimwegen, R. Verardo, C. L. Wei, K. Yagi, H. Yamanishi, E. Zabarovsky, S. Zhu, A. Zimmer, W. Hide, C. Bult, S. M. Grimmond, R. D. Teasdale, E. T. Liu, V. Brusic, J. Quackenbush, C. Wahlestedt, J. S. Mattick, D. A. Hume, C. Kai, D. Sasaki, Y. Tomaru, S. Fukuda, M. Kanamori-Katayama, M. Suzuki, J. Aoki, T. Arakawa, J. Iida, K. Imamura, M. Itoh, T. Kato, H. Kawaji, N. Kawagashira, T. Kawashima, M. Kojima, S. Kondo, H. Konno, K. Nakano, N. Ninomiya, T. Nishio, M. Okada, C. Plessy, K. Shibata, T. Shiraki, S. Suzuki, M. Tagami, K. Waki, A. Watahiki, Y. Okamura-Oho, H. Suzuki, J. Kawai, Y. Hayashizaki, F. Consortium, R. G. E. R. Group and G. Genome Science (2005).

"The transcriptional landscape of the mammalian genome." Science **309**(5740): 1559-1563.

Carrion, K., J. Dyo, V. Patel, R. Sasik, S. A. Mohamed, G. Hardiman and V. Nigam (2014). "The long non-coding HOTAIR is modulated by cyclic stretch and WNT/beta-CATENIN in human aortic valve cells and is a novel repressor of calcification genes." PLoS One **9**(5): e96577.

Chaikof, E. L., D. C. Brewster, R. L. Dalman, M. S. Makaroun, K. A. Illig, G. A. Sicard, C. H. Timaran, G. R. Upchurch, Jr., F. J. Veith and S. Society for Vascular (2009). "The care of patients with an abdominal aortic aneurysm: the Society for Vascular Surgery practice guidelines." J Vasc Surg **50**(4 Suppl): S2-49.

Chambers, B. R. and G. A. Donnan (2005). "Carotid endarterectomy for asymptomatic carotid stenosis." Cochrane Database Syst Rev(4): CD001923.

Chamley, J. H., U. Groschel-Stewart, G. R. Campbell and G. Burnstock (1977). "Distinction between smooth muscle, fibroblasts and endothelial cells in culture by the use of fluoresceinated antibodies against smooth muscle actin." Cell Tissue Res **177**(4): 445-457.

Chang, D. F., N. S. Belaguli, D. Iyer, W. B. Roberts, S. P. Wu, X. R. Dong, J. G. Marx, M. S. Moore, M. C. Beckerle, M. W. Majesky and R. J. Schwartz (2003). "Cysteine-rich LIM-only proteins CRP1 and CRP2 are potent smooth muscle differentiation cofactors." Dev Cell **4**(1): 107-118.

Chappell, J., J. L. Harman, V. M. Narasimhan, H. Yu, K. Foote, B. D. Simons, M. R. Bennett and H. F. Jorgensen (2016). "Extensive Proliferation of a Subset of Differentiated, yet Plastic, Medial Vascular Smooth Muscle Cells Contributes to Neointimal Formation in Mouse Injury and Atherosclerosis Models." Circ Res **119**(12): 1313-1323.

Chen, L. L. (2016). "Linking Long Noncoding RNA Localization and Function." Trends Biochem Sci **41**(9): 761-772.

Chen, P. Y., L. Qin, G. Li, J. Malagon-Lopez, Z. Wang, S. Bergaya, S. Gujja, A. W. Caulk, S. I. Murtada, X. Zhang, Z. W. Zhuang, D. A. Rao, G. Wang, Z. Tobiasova, B. Jiang, R. R. Montgomery, L. Sun, H. Sun, E. A. Fisher, J. R. Gulcher, C. Fernandez-Hernando, J. D. Humphrey, G. Tellides, T. W. Chittenden and M. Simons (2020). "Smooth Muscle Cell Reprogramming in Aortic Aneurysms." Cell Stem Cell **26**(4): 542-557 e511.

Chen, Y. C., A. V. Bui, J. Diesch, R. Manasseh, C. Hausding, J. Rivera, I. Haviv, A. Agrotis, N. M. Htun, J. Jowett, C. E. Hagemeyer, R. D. Hannan, A. Bobik and K. Peter (2013). "A novel mouse model of atherosclerotic plaque instability for drug testing and mechanistic/therapeutic discoveries using gene and microRNA expression profiling." Circ Res **113**(3): 252-265.

Chen-Plotkin, A. S., G. Sadri-Vakili, G. J. Yohrling, M. W. Braveman, C. L. Benn, K. E. Glajch, D. P. DiRocco, L. A. Farrell, D. Krainc, S. Gines, M. E. MacDonald and J.

H. Cha (2006). "Decreased association of the transcription factor Sp1 with genes downregulated in Huntington's disease." Neurobiol Dis **22**(2): 233-241.

Cherepanova, O. A., D. Gomez, L. S. Shankman, P. Swiatlowska, J. Williams, O. F. Sarmento, G. F. Alencar, D. L. Hess, M. H. Bevard, E. S. Greene, M. Murgai, S. D. Turner, Y. J. Geng, S. Bekiranov, J. J. Connelly, A. Tomilin and G. K. Owens (2016). "Activation of the pluripotency factor OCT4 in smooth muscle cells is atheroprotective." Nat Med **22**(6): 657-665.

Chiou, A. C., B. Chiu and W. H. Pearce (2001). "Murine aortic aneurysm produced by periarterial application of calcium chloride." J Surg Res **99**(2): 371-376.

Clarke, M. C., N. Figg, J. J. Maguire, A. P. Davenport, M. Goddard, T. D. Littlewood and M. R. Bennett (2006). "Apoptosis of vascular smooth muscle cells induces features of plaque vulnerability in atherosclerosis." Nat Med **12**(9): 1075-1080.

Clement, M., J. Chappell, J. Raffort, F. Lareyre, M. Vandestienne, A. L. Taylor, A. Finigan, J. Harrison, M. R. Bennett, P. Bruneval, S. Taleb, H. F. Jorgensen and Z. Mallat (2019). "Vascular Smooth Muscle Cell Plasticity and Autophagy in Dissecting Aortic Aneurysms." Arterioscler Thromb Vasc Biol **39**(6): 1149-1159.

Colin, S., G. Chinetti-Gbaguidi and B. Staels (2014). "Macrophage phenotypes in atherosclerosis." Immunol Rev **262**(1): 153-166.

Consortium, E. P. (2012). "An integrated encyclopedia of DNA elements in the human genome." Nature **489**(7414): 57-74.

Cox, J. and M. Mann (2008). "MaxQuant enables high peptide identification rates, individualized p.p.b.-range mass accuracies and proteome-wide protein quantification." Nat Biotechnol **26**(12): 1367-1372.

Curci, J. A., S. Liao, M. D. Huffman, S. D. Shapiro and R. W. Thompson (1998). "Expression and localization of macrophage elastase (matrix metalloproteinase-12) in abdominal aortic aneurysms." J Clin Invest **102**(11): 1900-1910.

Curci, J. A. and R. W. Thompson (2004). "Adaptive cellular immunity in aortic aneurysms: cause, consequence, or context?" J Clin Invest **114**(2): 168-171.

Das, S., P. Senapati, Z. Chen, M. A. Reddy, R. Ganguly, L. Lanting, V. Mandi, A. Bansal, A. Leung, S. Zhang, Y. Jia, X. Wu, D. E. Schones and R. Natarajan (2017). "Regulation of angiotensin II actions by enhancers and super-enhancers in vascular smooth muscle cells." Nat Commun **8**(1): 1467.

Daugherty, A. and L. Cassis (1999). "Chronic angiotensin II infusion promotes atherogenesis in low density lipoprotein receptor -/- mice." Ann N Y Acad Sci **892**: 108-118.

Daugherty, A. and L. A. Cassis (2002). "Mechanisms of abdominal aortic aneurysm formation." Curr Atheroscler Rep **4**(3): 222-227.

Daugherty, A., L. A. Cassis and H. Lu (2011). "Complex pathologies of angiotensin II-induced abdominal aortic aneurysms." J Zhejiang Univ Sci B **12**(8): 624-628.

Daugherty, A., M. W. Manning and L. A. Cassis (2000). "Angiotensin II promotes atherosclerotic lesions and aneurysms in apolipoprotein E-deficient mice." J Clin Invest **105**(11): 1605-1612.

Davies, J. D., K. L. Carpenter, I. R. Challis, N. L. Figg, R. McNair, D. Proudfoot, P. L. Weissberg and C. M. Shanahan (2005). "Adipocytic differentiation and liver x receptor pathways regulate the accumulation of triacylglycerols in human vascular smooth muscle cells." J Biol Chem **280**(5): 3911-3919.

Davis-Dusenbery, B. N., M. C. Chan, K. E. Reno, A. S. Weisman, M. D. Layne, G. Lagna and A. Hata (2011). "down-regulation of Kruppel-like factor-4 (KLF4) by microRNA-143/145 is critical for modulation of vascular smooth muscle cell phenotype by transforming growth factor-beta and bone morphogenetic protein 4." J Biol Chem **286**(32): 28097-28110.

Depuydt, M. A. C., K. H. M. Prange, L. Slenders, T. Ord, D. Elbersen, A. Boltjes, S. C. A. de Jager, F. W. Asselbergs, G. J. de Borst, E. Aavik, T. Lonnberg, E. Lutgens, C. K. Glass, H. M. den Ruijter, M. U. Kaikkonen, I. Bot, B. Slutter, S. W. van der Laan, S. Yla-Herttuala, M. Mokry, J. Kuiper, M. P. J. de Winther and G. Pasterkamp (2020). "Microanatomy of the Human Atherosclerotic Plaque by Single-Cell Transcriptomics." Circ Res **127**(11): 1437-1455.

Derrien, T., R. Johnson, G. Bussotti, A. Tanzer, S. Djebali, H. Tilgner, G. Guernec, D. Martin, A. Merkel, D. G. Knowles, J. Lagarde, L. Veeravalli, X. Ruan, Y. Ruan, T. Lassmann, P. Carninci, J. B. Brown, L. Lipovich, J. M. Gonzalez, M. Thomas, C. A. Davis, R. Shiekhattar, T. R. Gingeras, T. J. Hubbard, C. Notredame, J. Harrow and R. Guigo (2012). "The GENCODE v7 catalog of human long noncoding RNAs: analysis of their gene structure, evolution, and expression." Genome Res **22**(9): 1775-1789.

Deveson, I. W., S. A. Hardwick, T. R. Mercer and J. S. Mattick (2017). "The Dimensions, Dynamics, and Relevance of the Mammalian Noncoding Transcriptome." Trends Genet **33**(7): 464-478.

Diederichs, S. (2014). "The four dimensions of noncoding RNA conservation." Trends Genet **30**(4): 121-123.

Dimcevski, G., S. Kotopoulis, T. Bjanes, D. Hoem, J. Schjott, B. T. Gjertsen, M. Biermann, A. Molven, H. Sorbye, E. McCormack, M. Postema and O. H. Gilja (2016). "A human clinical trial using ultrasound and microbubbles to enhance gemcitabine treatment of inoperable pancreatic cancer." J Control Release **243**: 172-181.

Djebali, S., C. A. Davis, A. Merkel, A. Dobin, T. Lassmann, A. Mortazavi, A. Tanzer, J. Lagarde, W. Lin, F. Schlesinger, C. Xue, G. K. Marinov, J. Khatun, B. A. Williams, C. Zaleski, J. Rozowsky, M. Roder, F. Kokocinski, R. F. Abdelhamid, T. Alioto, I. Antoshechkin, M. T. Baer, N. S. Bar, P. Batut, K. Bell, I. Bell, S. Chakrabortty, X. Chen, J. Chrast, J. Curado, T. Derrien, J. Drenkow, E. Dumais, J. Dumais, R. Duttagupta, E. Falconnet, M. Fastuca, K. Fejes-Toth, P. Ferreira, S. Foissac, M. J. Fullwood, H. Gao, D. Gonzalez, A. Gordon, H. Gunawardena, C. Howald, S. Jha, R. Johnson, P. Kapranov, B. King, C. Kingswood, O. J. Luo, E. Park, K. Persaud, J. B. Preall, P. Ribeca, B. Risk, D. Robyr, M. Sammeth, L. Schaffer, L. H. See, A. Shahab,

J. Skancke, A. M. Suzuki, H. Takahashi, H. Tilgner, D. Trout, N. Walters, H. Wang, J. Wrobel, Y. Yu, X. Ruan, Y. Hayashizaki, J. Harrow, M. Gerstein, T. Hubbard, A. Reymond, S. E. Antonarakis, G. Hannon, M. C. Giddings, Y. Ruan, B. Wold, P. Carninci, R. Guigo and T. R. Gingeras (2012). "Landscape of transcription in human cells." Nature **489**(7414): 101-108.

Dobnikar, L., A. L. Taylor, J. Chappell, P. Oldach, J. L. Harman, E. Oerton, E. Dzierzak, M. R. Bennett, M. Spivakov and H. F. Jorgensen (2018). "Disease-relevant transcriptional signatures identified in individual smooth muscle cells from healthy mouse vessels." Nat Commun **9**(1): 4567.

Dobrin, P. B., W. H. Baker and W. C. Gley (1984). "Elastolytic and collagenolytic studies of arteries. Implications for the mechanical properties of aneurysms." Arch Surg **119**(4): 405-409.

Duband, J. L., M. Gimona, M. Scatena, S. Sartore and J. V. Small (1993). "Calponin and SM 22 as differentiation markers of smooth muscle: spatiotemporal distribution during avian embryonic development." Differentiation **55**(1): 1-11.

Durham, A. L., M. Y. Speer, M. Scatena, C. M. Giachelli and C. M. Shanahan (2018). "Role of smooth muscle cells in vascular calcification: implications in atherosclerosis and arterial stiffness." Cardiovasc Res **114**(4): 590-600.

Earnshaw, J. J., E. Shaw, M. R. Whyman, K. R. Poskitt and B. P. Heather (2004). "Screening for abdominal aortic aneurysms in men." BMJ **328**(7448): 1122-1124.

Edfeldt, K., J. Swedenborg, G. K. Hansson and Z. Q. Yan (2002). "Expression of toll-like receptors in human atherosclerotic lesions: a possible pathway for plaque activation." Circulation **105**(10): 1158-1161.

Emini Veseli, B., P. Perrotta, G. R. A. De Meyer, L. Roth, C. Van der Donckt, W. Martinet and G. R. Y. De Meyer (2017). "Animal models of atherosclerosis." Eur J Pharmacol **816**: 3-13.

Endemann, G., L. W. Stanton, K. S. Madden, C. M. Bryant, R. T. White and A. A. Protter (1993). "CD36 is a receptor for oxidized low density lipoprotein." J Biol Chem **268**(16): 11811-11816.

Falk, E., P. K. Shah and V. Fuster (1995). "Coronary plaque disruption." Circulation **92**(3): 657-671.

Fang, S., L. Zhang, J. Guo, Y. Niu, Y. Wu, H. Li, L. Zhao, X. Li, X. Teng, X. Sun, L. Sun, M. Q. Zhang, R. Chen and Y. Zhao (2018). "NONCODEV5: a comprehensive annotation database for long non-coding RNAs." Nucleic Acids Res **46**(D1): D308-D314.

Farb, A., A. P. Burke, A. L. Tang, T. Y. Liang, P. Mannan, J. Smialek and R. Virmani (1996). "Coronary plaque erosion without rupture into a lipid core. A frequent cause of coronary thrombosis in sudden coronary death." Circulation **93**(7): 1354-1363.

Fasolo, F., K. Di Gregoli, L. Maegdefessel and J. L. Johnson (2019). "Non-coding RNAs in cardiovascular cell biology and atherosclerosis." Cardiovasc Res **115**(12): 1732-1756.

Fasolo, F., H. Jin, G. Winski, E. Chernogubova, J. Pauli, H. Winter, D. Y. Li, N. Glukha, S. Bauer, S. Metschl, Z. Wu, M. L. Koschinsky, M. Reilly, J. Pelisek, W. Kempf, H. H. Eckstein, O. Soehnlein, L. Matic, U. Hedin, A. Backlund, C. Bergmark, V. Paloschi and L. Maegdefessel (2021). "Long Noncoding RNA MIAT Controls Advanced Atherosclerotic Lesion Formation and Plaque Destabilization." Circulation **144**(19): 1567-1583.

Feil, S., B. Fehrenbacher, R. Lukowski, F. Essmann, K. Schulze-Osthoff, M. Schaller and R. Feil (2014). "Transdifferentiation of vascular smooth muscle cells to macrophage-like cells during atherogenesis." Circ Res **115**(7): 662-667.

Finkel, T. and N. J. Holbrook (2000). "Oxidants, oxidative stress and the biology of ageing." Nature **408**(6809): 239-247.

Forsdahl, S. H., K. Singh, S. Solberg and B. K. Jacobsen (2009). "Risk factors for abdominal aortic aneurysms: a 7-year prospective study: the Tromso Study, 1994-2001." Circulation **119**(16): 2202-2208.

Fox, J. C. and J. R. Shanley (1996). "Antisense inhibition of basic fibroblast growth factor induces apoptosis in vascular smooth muscle cells." J Biol Chem **271**(21): 12578-12584.

Freestone, T., R. J. Turner, A. Coady, D. J. Higman, R. M. Greenhalgh and J. T. Powell (1995). "Inflammation and matrix metalloproteinases in the enlarging abdominal aortic aneurysm." Arterioscler Thromb Vasc Biol **15**(8): 1145-1151.

Gabbiani, G., E. Schmid, S. Winter, C. Chaponnier, C. de Ckhastonay, J. Vandekerckhove, K. Weber and W. W. Franke (1981). "Vascular smooth muscle cells differ from other smooth muscle cells: predominance of vimentin filaments and a specific alpha-type actin." Proc Natl Acad Sci U S A **78**(1): 298-302.

Galindo, M. I., J. I. Pueyo, S. Fouix, S. A. Bishop and J. P. Couso (2007). "Peptides encoded by short ORFs control development and define a new eukaryotic gene family." PLoS Biol **5**(5): e106.

Gardner, S. E., M. Humphry, M. R. Bennett and M. C. Clarke (2015). "Senescent Vascular Smooth Muscle Cells Drive Inflammation Through an Interleukin-1alpha-Dependent Senescence-Associated Secretory Phenotype." Arterioscler Thromb Vasc Biol **35**(9): 1963-1974.

Ge, J., L. Burnier, M. Adamopoulou, M. Q. Kwa, M. Schaks, K. Rottner and C. Brakebusch (2018). "RhoA, Rac1, and Cdc42 differentially regulate alphaSMA and collagen I expression in mesenchymal stem cells." J Biol Chem **293**(24): 9358-9369.

Geisler, S. and J. Coller (2013). "RNA in unexpected places: long non-coding RNA functions in diverse cellular contexts." Nat Rev Mol Cell Biol **14**(11): 699-712.

Gerthoffer, W. T. (2007). "Mechanisms of vascular smooth muscle cell migration." Circ Res **100**(5): 607-621.

Gharbaran, R., A. Goy, T. Tanaka, J. Park, C. Kim, N. Hasan, S. Vemulapalli, S. Sarojini, M. Tuluc, K. Nalley, P. Bhattacharyya, A. Pecora and K. S. Suh (2013). "Fibroblast growth factor-2 (FGF2) and syndecan-1 (SDC1) are potential biomarkers for putative circulating CD15+/CD30+ cells in poor outcome Hodgkin lymphoma patients." J Hematol Oncol **6**: 62.

Gistera, A., D. F. J. Ketelhuth, S. G. Malin and G. K. Hansson (2022). "Animal Models of Atherosclerosis-Supportive Notes and Tricks of the Trade." Circ Res **130**(12): 1869-1887.

Golforoush, P., D. M. Yellon and S. M. Davidson (2020). "Mouse models of atherosclerosis and their suitability for the study of myocardial infarction." Basic Res Cardiol **115**(6): 73.

Golledge, J. (2019). "Abdominal aortic aneurysm: update on pathogenesis and medical treatments." Nat Rev Cardiol **16**(4): 225-242.

Golledge, J., S. M. Krishna and Y. Wang (2022). "Mouse models for abdominal aortic aneurysm." Br J Pharmacol **179**(5): 792-810.

Golledge, J., J. Muller, A. Daugherty and P. Norman (2006). "Abdominal aortic aneurysm: pathogenesis and implications for management." Arterioscler Thromb Vasc Biol **26**(12): 2605-2613.

Golledge, J., P. E. Norman, M. P. Murphy and R. L. Dalman (2017). "Challenges and opportunities in limiting abdominal aortic aneurysm growth." J Vasc Surg **65**(1): 225-233.

Gomez, D., R. A. Baylis, B. G. Durgin, A. A. C. Newman, G. F. Alencar, S. Mahan, C. St Hilaire, W. Muller, A. Waisman, S. E. Francis, E. Pinteaux, G. J. Randolph, H. Gram and G. K. Owens (2018). "Interleukin-1beta has atheroprotective effects in advanced atherosclerotic lesions of mice." Nat Med **24**(9): 1418-1429.

Gomez, D. and G. K. Owens (2012). "Smooth muscle cell phenotypic switching in atherosclerosis." Cardiovasc Res **95**(2): 156-164.

Gomez, D., L. S. Shankman, A. T. Nguyen and G. K. Owens (2013). "Detection of histone modifications at specific gene loci in single cells in histological sections." Nat Methods **10**(2): 171-177.

Gong, C. and L. E. Maquat (2011). "lncRNAs transactivate STAU1-mediated mRNA decay by duplexing with 3' UTRs via Alu elements." Nature **470**(7333): 284-288.

Griendling, K. K., M. Ushio-Fukai, B. Lassegue and R. W. Alexander (1997). "Angiotensin II signaling in vascular smooth muscle. New concepts." Hypertension **29**(1 Pt 2): 366-373.

Grootaert, M. O. J. and M. R. Bennett (2021). "Vascular smooth muscle cells in atherosclerosis: time for a re-assessment." Cardiovasc Res **117**(11): 2326-2339.

Grootaert, M. O. J., M. Moulis, L. Roth, W. Martinet, C. Vindis, M. R. Bennett and G. R. Y. De Meyer (2018). "Vascular smooth muscle cell death, autophagy and senescence in atherosclerosis." Cardiovasc Res **114**(4): 622-634.

Grote, P. and B. G. Herrmann (2013). "The long non-coding RNA Fendrr links epigenetic control mechanisms to gene regulatory networks in mammalian embryogenesis." RNA Biol **10**(10): 1579-1585.

Gschwendtner, A., S. Bevan, J. W. Cole, A. Plourde, M. Matarin, H. Ross-Adams, T. Meitinger, E. Wichmann, B. D. Mitchell, K. Furie, A. Slowik, S. S. Rich, P. D. Syme, M. J. MacLeod, J. F. Meschia, J. Rosand, S. J. Kittner, H. S. Markus, B. Muller-Myhsok, M. Dichgans and C. International Stroke Genetics (2009). "Sequence variants on chromosome 9p21.3 confer risk for atherosclerotic stroke." Ann Neurol **65**(5): 531-539.

Gui, Y., H. Zheng and R. Y. Cao (2022). "Foam Cells in Atherosclerosis: Novel Insights Into Its Origins, Consequences, and Molecular Mechanisms." Front Cardiovasc Med **9**: 845942.

Guttman, M. and J. L. Rinn (2012). "Modular regulatory principles of large non-coding RNAs." Nature **482**(7385): 339-346.

Hadji, F., M. C. Boulanger, S. P. Guay, N. Gaudreault, S. Amellah, G. Mkannez, R. Bouchareb, J. T. Marchand, M. J. Nsaibia, S. Guauque-Olarte, P. Pibarot, L. Bouchard, Y. Bosse and P. Mathieu (2016). "Altered DNA Methylation of Long Noncoding RNA H19 in Calcific Aortic Valve Disease Promotes Mineralization by Silencing NOTCH1." Circulation **134**(23): 1848-1862.

Halvorsen, B., K. Otterdal, T. B. Dahl, M. Skjelland, L. Gullestad, E. Oie and P. Aukrust (2008). "Atherosclerotic plaque stability--what determines the fate of a plaque?" Prog Cardiovasc Dis **51**(3): 183-194.

Hansson, G. K. and A. Hermansson (2011). "The immune system in atherosclerosis." Nat Immunol **12**(3): 204-212.

Harismendy, O., D. Notani, X. Song, N. G. Rahim, B. Tanasa, N. Heintzman, B. Ren, X. D. Fu, E. J. Topol, M. G. Rosenfeld and K. A. Frazer (2011). "9p21 DNA variants associated with coronary artery disease impair interferon-gamma signalling response." Nature **470**(7333): 264-268.

Hartford, C. C. R. and A. Lal (2020). "When Long Noncoding Becomes Protein Coding." Mol Cell Biol **40**(6).

Hartvigsen, K., M. Y. Chou, L. F. Hansen, P. X. Shaw, S. Tsimikas, C. J. Binder and J. L. Witztum (2009). "The role of innate immunity in atherogenesis." J Lipid Res **50 Suppl**: S388-393.

Hatsukami, T. S., R. Ross, N. L. Polissar and C. Yuan (2000). "Visualization of fibrous cap thickness and rupture in human atherosclerotic carotid plaque in vivo with high-resolution magnetic resonance imaging." Circulation **102**(9): 959-964.

Helgadottir, A., G. Thorleifsson, K. P. Magnusson, S. Gretarsdottir, V. Steinthorsdottir, A. Manolescu, G. T. Jones, G. J. Rinkel, J. D. Blankensteijn, A. Ronkainen, J. E. Jaaskelainen, Y. Kyo, G. M. Lenk, N. Sakalihasan, K. Kostulas, A. Gottsater, A. Flex, H. Stefansson, T. Hansen, G. Andersen, S. Weinsheimer, K. Borch-Johnsen, T. Jorgensen, S. H. Shah, A. A. Quyyumi, C. B. Granger, M. P. Reilly, H. Austin, A. I. Levey, V. Vaccarino, E. Palsdottir, G. B. Walters, T. Jonsdottir, S. Snorradottir, D. Magnusdottir, G. Gudmundsson, R. E. Ferrell, S. Sveinbjornsdottir, J. Hernesniemi, M. Niemela, R. Limet, K. Andersen, G. Sigurdsson, R. Benediktsson, E. L. Verhoeven, J. A. Teijink, D. E. Grobbee, D. J. Rader, D. A. Collier, O. Pedersen, R. Pola, J. Hillert, B. Lindblad, E. M. Valdimarsson, H. B. Magnadottir, C. Wijmenga, G. Tromp, A. F. Baas, Y. M. Ruigrok, A. M. van Rij, H. Kuivaniemi, J. T. Powell, S. E. Matthiasson, J. R. Gulcher, G. Thorgeirsson, A. Kong, U. Thorsteinsdottir and K. Stefansson (2008). "The same sequence variant on 9p21 associates with myocardial infarction, abdominal aortic aneurysm and intracranial aneurysm." Nat Genet **40**(2): 217-224.

Hennessy, E. J., C. van Solingen, K. R. Scacalossi, M. Ouimet, M. S. Afonso, J. Prins, G. J. Koelwyn, M. Sharma, B. Ramkhelawon, S. Carpenter, A. Busch, E. Chernogubova, L. P. Matic, U. Hedin, L. Maegdefessel, B. E. Caffrey, M. A. Hussein, E. P. Ricci, R. E. Temel, M. J. Garabedian, J. S. Berger, K. C. Vickers, M. Kanke, P. Sethupathy, D. Teupser, L. M. Holdt and K. J. Moore (2019). "The long noncoding RNA CHROME regulates cholesterol homeostasis in primate." Nat Metab **1**(1): 98-110.

Herbin, O., H. Ait-Oufella, W. Yu, G. N. Fredrikson, B. Aubier, N. Perez, V. Barateau, J. Nilsson, A. Tedgui and Z. Mallat (2012). "Regulatory T-cell response to apolipoprotein B100-derived peptides reduces the development and progression of atherosclerosis in mice." Arterioscler Thromb Vasc Biol **32**(3): 605-612.

Hinkel, R., D. Penzkofer, S. Zuhlke, A. Fischer, W. Husada, Q. F. Xu, E. Baloch, E. van Rooij, A. M. Zeiher, C. Kupatt and S. Dimmeler (2013). "Inhibition of microRNA-92a protects against ischemia/reperfusion injury in a large-animal model." Circulation **128**(10): 1066-1075.

Hofmann, P., J. Sommer, K. Theodorou, L. Kirchhof, A. Fischer, Y. Li, L. Perisic, U. Hedin, L. Maegdefessel, S. Dimmeler and R. A. Boon (2019). "Long non-coding RNA H19 regulates endothelial cell aging via inhibition of STAT3 signalling." Cardiovasc Res **115**(1): 230-242.

Holdt, L. M., S. Hoffmann, K. Sass, D. Langenberger, M. Scholz, K. Krohn, K. Finstermeier, A. Stahringer, W. Wilfert, F. Beutner, S. Gielen, G. Schuler, G. Gabel, H. Bergert, I. Bechmann, P. F. Stadler, J. Thiery and D. Teupser (2013). "Alu elements in ANRIL non-coding RNA at chromosome 9p21 modulate atherogenic cell functions through trans-regulation of gene networks." PLoS Genet **9**(7): e1003588.

Hong, K. N., V. Fuster, R. S. Rosenson, C. Rosendorff and D. L. Bhatt (2017). "How Low to Go With Glucose, Cholesterol, and Blood Pressure in Primary Prevention of CVD." J Am Coll Cardiol **70**(17): 2171-2185.

Hoshina, K., H. Koyama, T. Miyata, H. Shigematsu, T. Takato, R. L. Dalman and H. Nagawa (2004). "Aortic wall cell proliferation via basic fibroblast growth factor gene

transfer limits progression of experimental abdominal aortic aneurysm." J Vasc Surg **40**(3): 512-518.

House, S. L., J. Wang, A. M. Castro, C. Weinheimer, A. Kovacs and D. M. Ornitz (2015). "Fibroblast growth factor 2 is an essential cardioprotective factor in a closed-chest model of cardiac ischemia-reperfusion injury." Physiol Rep **3**(1).

Howard, D. P. J., L. Gaziano, P. M. Rothwell and S. Oxford Vascular (2021). "Risk of stroke in relation to degree of asymptomatic carotid stenosis: a population-based cohort study, systematic review, and meta-analysis." Lancet Neurol **20**(3): 193-202.

Hsieh, C. C., M. H. Yen, C. H. Yen and Y. T. Lau (2001). "Oxidized low density lipoprotein induces apoptosis via generation of reactive oxygen species in vascular smooth muscle cells." Cardiovasc Res **49**(1): 135-145.

Hu, Y., W. Chen, C. Li, X. Wang, J. Luo and B. Cheng (2022). "LncRNA ANRIL Facilitates Vascular Smooth Muscle Cell Proliferation and Suppresses Apoptosis via Modulation of miR-7/FGF2 Pathway in Intracranial Aneurysms." Neurocrit Care **36**(1): 106-115.

Huang, C. K., S. Kafert-Kasting and T. Thum (2020). "Preclinical and Clinical Development of Noncoding RNA Therapeutics for Cardiovascular Disease." Circ Res **126**(5): 663-678.

Ignatowski, A. (1909). "Über die Wirkung des tierischen Eiweißes auf die Aorta und die parenchymatösen Organe der Kaninchen." Virchows Archiv für pathologische Anatomie und Physiologie und für klinische Medizin **198**(2): 248-270.

Ikonomidis, I., K. Stamatelopoulos, J. Lekakis, G. D. Vamvakou and D. T. Kremastinos (2008). "Inflammatory and non-invasive vascular markers: the multimarker approach for risk stratification in coronary artery disease." Atherosclerosis **199**(1): 3-11.

Ingolia, N. T., G. A. Brar, N. Stern-Ginossar, M. S. Harris, G. J. Talhouarne, S. E. Jackson, M. R. Wills and J. S. Weissman (2014). "Ribosome profiling reveals pervasive translation outside of annotated protein-coding genes." Cell Rep **8**(5): 1365-1379.

Investigators, I. T. (2017). "Comparative clinical effectiveness and cost effectiveness of endovascular strategy v open repair for ruptured abdominal aortic aneurysm: three year results of the IMPROVE randomised trial." BMJ **359**: j4859.

Itoh, N., H. Ohta, Y. Nakayama and M. Konishi (2016). "Roles of FGF Signals in Heart Development, Health, and Disease." Front Cell Dev Biol **4**: 110.

Jarinova, O., A. F. Stewart, R. Roberts, G. Wells, P. Lau, T. Naing, C. Buerki, B. W. McLean, R. C. Cook, J. S. Parker and R. McPherson (2009). "Functional analysis of the chromosome 9p21.3 coronary artery disease risk locus." Arterioscler Thromb Vasc Biol **29**(10): 1671-1677.

Jarvinen, P. M., M. Myllarniemi, H. Liu, H. M. Moore, O. Lepparanta, K. Salmenkivi, K. Koli, L. Latonen, A. M. Band and M. Laiho (2012). "Cysteine-rich protein 1 is

regulated by transforming growth factor-beta1 and expressed in lung fibrosis." J Cell Physiol **227**(6): 2605-2612.

Ji, Z., R. Song, A. Regev and K. Struhl (2015). "Many lncRNAs, 5'UTRs, and pseudogenes are translated and some are likely to express functional proteins." Elife **4**: e08890.

Jin, H., D. Y. Li, E. Chernogubova, C. Sun, A. Busch, S. M. Eken, P. Saliba-Gustafsson, H. Winter, G. Winski, U. Raaz, I. N. Schellinger, N. Simon, R. Hegenloh, L. P. Matic, M. Jagodic, E. Ehrenborg, J. Pelisek, H. H. Eckstein, U. Hedin, A. Backlund and L. Maegdefessel (2018). "Local Delivery of miR-21 Stabilizes Fibrous Caps in Vulnerable Atherosclerotic Lesions." Mol Ther **26**(4): 1040-1055.

Johnson, J. L. (2007). "Matrix metalloproteinases: influence on smooth muscle cells and atherosclerotic plaque stability." Expert Rev Cardiovasc Ther **5**(2): 265-282.

Johnsson, P., L. Lipovich, D. Grander and K. V. Morris (2014). "Evolutionary conservation of long non-coding RNAs; sequence, structure, function." Biochim Biophys Acta **1840**(3): 1063-1071.

Johnston, K. W., R. B. Rutherford, M. D. Tilson, D. M. Shah, L. Hollier and J. C. Stanley (1991). "Suggested standards for reporting on arterial aneurysms. Subcommittee on Reporting Standards for Arterial Aneurysms, Ad Hoc Committee on Reporting Standards, Society for Vascular Surgery and North American Chapter, International Society for Cardiovascular Surgery." J Vasc Surg **13**(3): 452-458.

Jonasson, L., J. Holm and G. K. Hansson (1988). "Cyclosporin A inhibits smooth muscle proliferation in the vascular response to injury." Proc Natl Acad Sci U S A **85**(7): 2303-2306.

Jovinge, S., A. Hultgardh-Nilsson, J. Regnstrom and J. Nilsson (1997). "Tumor necrosis factor-alpha activates smooth muscle cell migration in culture and is expressed in the balloon-injured rat aorta." Arterioscler Thromb Vasc Biol **17**(3): 490-497.

Kadrmas, J. L. and M. C. Beckerle (2004). "The LIM domain: from the cytoskeleton to the nucleus." Nat Rev Mol Cell Biol **5**(11): 920-931.

Kapranov, P., J. Cheng, S. Dike, D. A. Nix, R. Duttagupta, A. T. Willingham, P. F. Stadler, J. Hertel, J. Hackermuller, I. L. Hofacker, I. Bell, E. Cheung, J. Drenkow, E. Dumais, S. Patel, G. Helt, M. Ganesh, S. Ghosh, A. Piccolboni, V. Sementchenko, H. Tammana and T. R. Gingeras (2007). "RNA maps reveal new RNA classes and a possible function for pervasive transcription." Science **316**(5830): 1484-1488.

Kato, S., A. Muraishi, T. Miyamoto and J. C. Fox (1998). "Basic fibroblast growth factor regulates extracellular matrix and contractile protein expression independent of proliferation in vascular smooth muscle cells." In Vitro Cell Dev Biol Anim **34**(4): 341-346.

Kawai, N., H. Iwata, K. Shimabukuro, N. Ishida, H. Ogura, E. Umeda and K. Doi (2018). "Suppression of aortic expansion and contractile recovery in a rat abdominal

aortic aneurysm model by biodegradable gelatin hydrogel sheet incorporating basic fibroblast growth factor." Heart Vessels **33**(7): 793-801.

Kent, K. C., R. M. Zwolak, N. N. Egorova, T. S. Riles, A. Manganaro, A. J. Moskowitz, A. C. Gelijns and G. Greco (2010). "Analysis of risk factors for abdominal aortic aneurysm in a cohort of more than 3 million individuals." J Vasc Surg **52**(3): 539-548.

Khatana, C., N. K. Saini, S. Chakrabarti, V. Saini, A. Sharma, R. V. Saini and A. K. Saini (2020). "Mechanistic Insights into the Oxidized Low-Density Lipoprotein-Induced Atherosclerosis." Oxid Med Cell Longev **2020**: 5245308.

Kim, Y. K., L. Furic, L. Desgroseillers and L. E. Maquat (2005). "Mammalian Staufen1 recruits Upf1 to specific mRNA 3'UTRs so as to elicit mRNA decay." Cell **120**(2): 195-208.

Kimelman, D. and M. W. Kirschner (1989). "An antisense mRNA directs the covalent modification of the transcript encoding fibroblast growth factor in Xenopus oocytes." Cell **59**(4): 687-696.

Kita, T., N. Kume, M. Minami, K. Hayashida, T. Murayama, H. Sano, H. Moriwaki, H. Kataoka, E. Nishi, H. Horiuchi, H. Arai and M. Yokode (2001). "Role of oxidized LDL in atherosclerosis." Ann N Y Acad Sci **947**: 199-205; discussion 205-196.

Klingenberg, R., M. Lebens, A. Hermansson, G. N. Fredrikson, D. Strodthoff, M. Rudling, D. F. Ketelhuth, N. Gerdes, J. Holmgren, J. Nilsson and G. K. Hansson (2010). "Intranasal immunization with an apolipoprotein B-100 fusion protein induces antigen-specific regulatory T cells and reduces atherosclerosis." Arterioscler Thromb Vasc Biol **30**(5): 946-952.

Kloster, B. O., L. Lund and J. S. Lindholt (2015). "Induction of continuous expanding infrarenal aortic aneurysms in a large porcine animal model." Ann Med Surg (Lond) **4**(1): 30-35.

Knee, R., A. W. Li and P. R. Murphy (1997). "Characterization and tissue-specific expression of the rat basic fibroblast growth factor antisense mRNA and protein." Proc Natl Acad Sci U S A **94**(10): 4943-4947.

Koch, A. E., G. K. Haines, R. J. Rizzo, J. A. Radosevich, R. M. Pope, P. G. Robinson and W. H. Pearce (1990). "Human abdominal aortic aneurysms. Immunophenotypic analysis suggesting an immune-mediated response." Am J Pathol **137**(5): 1199-1213.

Kolodgie, F. D., A. P. Burke, A. Farb, H. K. Gold, J. Yuan, J. Narula, A. V. Finn and R. Virmani (2001). "The thin-cap fibroatheroma: a type of vulnerable plaque: the major precursor lesion to acute coronary syndromes." Curr Opin Cardiol **16**(5): 285-292.

Koshland, D. E., Jr., A. Goldbeter and J. B. Stock (1982). "Amplification and adaptation in regulatory and sensory systems." Science **217**(4556): 220-225.

Krishna, S. M., S. K. Morton, J. Li and J. Golledge (2020). "Risk Factors and Mouse Models of Abdominal Aortic Aneurysm Rupture." Int J Mol Sci **21**(19).

Kuhnl, A., A. Erk, M. Trenner, M. Salvermoser, V. Schmid and H. H. Eckstein (2017). "Incidence, Treatment and Mortality in Patients with Abdominal Aortic Aneurysms." Dtsch Arztebl Int **114**(22-23): 391-398.

Lederle, F. A. (2012). "The strange relationship between diabetes and abdominal aortic aneurysm." Eur J Vasc Endovasc Surg **43**(3): 254-256.

Lederle, F. A., S. E. Wilson, G. R. Johnson, D. B. Reinke, F. N. Littooy, C. W. Acher, D. J. Ballard, L. M. Messina, I. L. Gordon, E. P. Chute, W. C. Krupski, S. J. Busuttil, G. W. Barone, S. Sparks, L. M. Graham, J. H. Rapp, M. S. Makaroun, G. L. Moneta, R. A. Cambria, R. G. Makhoul, D. Eton, H. J. Ansel, J. A. Freischlag, D. Bandyk, D. Aneurysm and G. Management Veterans Affairs Cooperative Study (2002). "Immediate repair compared with surveillance of small abdominal aortic aneurysms." N Engl J Med **346**(19): 1437-1444.

Lee, H. J., A. N. Seo, S. Y. Park, J. Y. Kim, J. Y. Park, J. H. Yu, J. H. Ahn and G. Gong (2014). "Low prognostic implication of fibroblast growth factor family activation in triple-negative breast cancer subsets." Ann Surg Oncol **21**(5): 1561-1568.

Lee, S., B. Liu, S. Lee, S. X. Huang, B. Shen and S. B. Qian (2012). "Global mapping of translation initiation sites in mammalian cells at single-nucleotide resolution." Proc Natl Acad Sci U S A **109**(37): E2424-2432.

Lee, Y. T., H. Y. Lin, Y. W. Chan, K. H. Li, O. T. To, B. P. Yan, T. Liu, G. Li, W. T. Wong, W. Keung and G. Tse (2017). "Mouse models of atherosclerosis: a historical perspective and recent advances." Lipids Health Dis **16**(1): 12.

Lengfeld, J., Q. Wang, A. Zohlman, S. Salvarezza, S. Morgan, J. Ren, K. Kato, E. Rodriguez-Boulan and B. Liu (2012). "Protein kinase C delta regulates the release of collagen type I from vascular smooth muscle cells via regulation of Cdc42." Mol Biol Cell **23**(10): 1955-1963.

Li, A. W., G. Seyoum, R. P. Shiu and P. R. Murphy (1996). "Expression of the rat BFGF antisense RNA transcript is tissue-specific and developmentally regulated." Mol Cell Endocrinol **118**(1-2): 113-123.

Li, A. W., C. K. Too and P. R. Murphy (1996). "The basic fibroblast growth factor (FGF-2) antisense RNA (GFG) is translated into a MutT-related protein in vivo." Biochem Biophys Res Commun **223**(1): 19-23.

Li, D. Y., A. Busch, H. Jin, E. Chernogubova, J. Pelisek, J. Karlsson, B. Sennblad, S. Liu, S. Lao, P. Hofmann, A. Backlund, S. M. Eken, J. Roy, P. Eriksson, B. Dacken, D. Ramanujam, A. Dueck, S. Engelhardt, R. A. Boon, H. H. Eckstein, J. M. Spin, P. S. Tsao and L. Maegdefessel (2018). "H19 Induces Abdominal Aortic Aneurysm Development and Progression." Circulation **138**(15): 1551-1568.

Li, P. F., R. Dietz and R. von Harsdorf (1997). "Reactive oxygen species induce apoptosis of vascular smooth muscle cell." FEBS Lett **404**(2-3): 249-252.

Li, S., D. Z. Wang, Z. Wang, J. A. Richardson and E. N. Olson (2003). "The serum response factor coactivator myocardin is required for vascular smooth muscle development." Proc Natl Acad Sci U S A **100**(16): 9366-9370.

Libby, P. (2008). "The molecular mechanisms of the thrombotic complications of atherosclerosis." J Intern Med **263**(5): 517-527.

Libby, P. (2021). "The changing landscape of atherosclerosis." Nature **592**(7855): 524-533.

Libby, P., P. M. Ridker and G. K. Hansson (2011). "Progress and challenges in translating the biology of atherosclerosis." Nature **473**(7347): 317-325.

Lilly, B., K. A. Clark, M. Yoshigi, S. Pronovost, M. L. Wu, M. Periasamy, M. Chi, R. J. Paul, S. F. Yet and M. C. Beckerle (2010). "Loss of the serum response factor cofactor, cysteine-rich protein 1, attenuates neointima formation in the mouse." Arterioscler Thromb Vasc Biol **30**(4): 694-701.

Lilly, B., E. N. Olson and M. C. Beckerle (2001). "Identification of a CArG box-dependent enhancer within the cysteine-rich protein 1 gene that directs expression in arterial but not venous or visceral smooth muscle cells." Dev Biol **240**(2): 531-547.

Lindholt, J. S., R. Sogaard and J. Laustsen (2012). "Prognosis of ruptured abdominal aortic aneurysms in Denmark from 1994-2008." Clin Epidemiol **4**: 111-113.

Lindner, V. and M. A. Reidy (1991). "Proliferation of smooth muscle cells after vascular injury is inhibited by an antibody against basic fibroblast growth factor." Proc Natl Acad Sci U S A **88**(9): 3739-3743.

Liu, M. and D. Gomez (2019). "Smooth Muscle Cell Phenotypic Diversity." Arterioscler Thromb Vasc Biol **39**(9): 1715-1723.

Liu, M. H., Z. H. Tang, G. H. Li, S. L. Qu, Y. Zhang, Z. Ren, L. S. Liu and Z. S. Jiang (2013). "Janus-like role of fibroblast growth factor 2 in arteriosclerotic coronary artery disease: atherogenesis and angiogenesis." Atherosclerosis **229**(1): 10-17.

Liu, Y., S. Sinha, O. G. McDonald, Y. Shang, M. H. Hoofnagle and G. K. Owens (2005). "Kruppel-like factor 4 abrogates myocardin-induced activation of smooth muscle gene expression." J Biol Chem **280**(10): 9719-9727.

Loeys, B. L. and H. C. Dietz (1993). Loeys-Dietz Syndrome. GeneReviews((R)). M. P. Adam, D. B. Everman, G. M. Mirzaa et al. Seattle (WA).

Long, J. Z., K. J. Svensson, L. Tsai, X. Zeng, H. C. Roh, X. Kong, R. R. Rao, J. Lou, I. Lokurkar, W. Baur, J. J. Castellot, Jr., E. D. Rosen and B. M. Spiegelman (2014). "A smooth muscle-like origin for beige adipocytes." Cell Metab **19**(5): 810-820.

Longo, G. M., W. Xiong, T. C. Greiner, Y. Zhao, N. Fiotti and B. T. Baxter (2002). "Matrix metalloproteinases 2 and 9 work in concert to produce aortic aneurysms." J Clin Invest **110**(5): 625-632.

Lopez-Candales, A., D. R. Holmes, S. Liao, M. J. Scott, S. A. Wickline and R. W. Thompson (1997). "Decreased vascular smooth muscle cell density in medial degeneration of human abdominal aortic aneurysms." Am J Pathol **150**(3): 993-1007.

Lu, H., W. Du, L. Ren, M. H. Hamblin, R. C. Becker, Y. E. Chen and Y. Fan (2021). "Vascular Smooth Muscle Cells in Aortic Aneurysm: From Genetics to Mechanisms." J Am Heart Assoc **10**(24): e023601.

Lusis, A. J., R. Mar and P. Pajukanta (2004). "Genetics of atherosclerosis." Annu Rev Genomics Hum Genet **5**: 189-218.

Lv, J., L. Wang, J. Zhang, R. Lin, L. Wang, W. Sun, H. Wu and S. Xin (2018). "Long noncoding RNA H19-derived miR-675 aggravates restenosis by targeting PTEN." Biochem Biophys Res Commun **497**(4): 1154-1161.

Lysgaard Poulsen, J., J. Stubbe and J. S. Lindholt (2016). "Animal Models Used to Explore Abdominal Aortic Aneurysms: A Systematic Review." Eur J Vasc Endovasc Surg **52**(4): 487-499.

Ma, L., J. A. Greenwood and M. Schachner (2011). "CRP1, a protein localized in filopodia of growth cones, is involved in dendritic growth." J Neurosci **31**(46): 16781-16791.

MacFarlane, L. A., Y. Gu, A. G. Casson and P. R. Murphy (2010). "Regulation of fibroblast growth factor-2 by an endogenous antisense RNA and by argonaute-2." Mol Endocrinol **24**(4): 800-812.

Mack, C. P. (2011). "Signaling mechanisms that regulate smooth muscle cell differentiation." Arterioscler Thromb Vasc Biol **31**(7): 1495-1505.

Mahmood, S. S., D. Levy, R. S. Vasan and T. J. Wang (2014). "The Framingham Heart Study and the epidemiology of cardiovascular disease: a historical perspective." Lancet **383**(9921): 999-1008.

Majesky, M. W., H. Horita, A. Ostriker, S. Lu, J. N. Regan, A. Bagchi, X. R. Dong, J. Poczobutt, R. A. Nemenoff and M. C. Weiser-Evans (2017). "Differentiated Smooth Muscle Cells Generate a Subpopulation of Resident Vascular Progenitor Cells in the Adventitia Regulated by Klf4." Circ Res **120**(2): 296-311.

Mao, Y., X. Q. Liu, Y. Song, C. G. Zhai, X. L. Xu, L. Zhang and Y. Zhang (2020). "Fibroblast growth factor-2/platelet-derived growth factor enhances atherosclerotic plaque stability." J Cell Mol Med **24**(1): 1128-1140.

Marini, C., S. Morbelli, R. Armonino, G. Spinella, M. Riondato, M. Massollo, F. Sarocchi, B. Pane, C. Augeri, L. Abete, G. Ghigliotti, D. Palmieri, F. Fiz, G. Cittadini, E. Fulcheri, D. Palombo and G. Sambuceti (2012). "Direct relationship between cell density and FDG uptake in asymptomatic aortic aneurysm close to surgical threshold: an in vivo and in vitro study." Eur J Nucl Med Mol Imaging **39**(1): 91-101.

Marx, S. O. and A. R. Marks (2001). "Bench to bedside: the development of rapamycin and its application to stent restenosis." Circulation **104**(8): 852-855.

Matthews, C., I. Gorenne, S. Scott, N. Figg, P. Kirkpatrick, A. Ritchie, M. Goddard and M. Bennett (2006). "Vascular smooth muscle cells undergo telomere-based senescence in human atherosclerosis: effects of telomerase and oxidative stress." Circ Res **99**(2): 156-164.

McEachern, L. A. and P. R. Murphy (2014). "Chromatin-remodeling factors mediate the balance of sense-antisense transcription at the FGF2 locus." Mol Endocrinol **28**(4): 477-489.

McMillan, W. D., N. A. Tamarina, M. Cipollone, D. A. Johnson, M. A. Parker and W. H. Pearce (1997). "Size matters: the relationship between MMP-9 expression and aortic diameter." Circulation **96**(7): 2228-2232.

Meijer, C. A., T. Stijnen, M. N. Wasser, J. F. Hamming, J. H. van Bockel, J. H. Lindeman and G. Pharmaceutical Aneurysm Stabilisation Trial Study (2013). "Doxycycline for stabilization of abdominal aortic aneurysms: a randomized trial." Ann Intern Med **159**(12): 815-823.

Meng, X. D., H. H. Yao, L. M. Wang, M. Yu, S. Shi, Z. X. Yuan and J. Liu (2020). "Knockdown of GAS5 Inhibits Atherosclerosis Progression via Reducing EZH2-Mediated ABCA1 Transcription in ApoE(-/-) Mice." Mol Ther Nucleic Acids **19**: 84-96.

Meschia, J. F., J. P. Klaas, R. D. Brown, Jr. and T. G. Brott (2017). "Evaluation and Management of Atherosclerotic Carotid Stenosis." Mayo Clin Proc **92**(7): 1144-1157.

Michel, J. B., Z. Li and P. Lacolley (2012). "Smooth muscle cells and vascular diseases." Cardiovasc Res **95**(2): 135-137.

Michel, J. B., J. L. Martin-Ventura, J. Egido, N. Sakalihasan, V. Treska, J. Lindholt, E. Allaire, U. Thorsteinsdottir, G. Cockerill, J. Swedenborg and F. E. consortium (2011). "Novel aspects of the pathogenesis of aneurysms of the abdominal aorta in humans." Cardiovasc Res **90**(1): 18-27.

Middleton, R. K., G. M. Lloyd, M. J. Bown, N. J. Cooper, N. J. London and R. D. Sayers (2007). "The pro-inflammatory and chemotactic cytokine microenvironment of the abdominal aortic aneurysm wall: a protein array study." J Vasc Surg **45**(3): 574-580.

Miller, F. J., Jr. (2002). "Aortic aneurysms: It's all about the stress." Arterioscler Thromb Vasc Biol **22**(12): 1948-1949.

Miller, F. J., Jr., W. J. Sharp, X. Fang, L. W. Oberley, T. D. Oberley and N. L. Weintraub (2002). "Oxidative stress in human abdominal aortic aneurysms: a potential mediator of aneurysmal remodeling." Arterioscler Thromb Vasc Biol **22**(4): 560-565.

Misra, A., Z. Feng, R. R. Chandran, I. Kabir, N. Rotllan, B. Aryal, A. Q. Sheikh, L. Ding, L. Qin, C. Fernandez-Hernando, G. Tellides and D. M. Greif (2018). "Integrin beta3 regulates clonality and fate of smooth muscle-derived atherosclerotic plaque cells." Nat Commun **9**(1): 2073.

Miyamoto, T., I. Leconte, J. L. Swain and J. C. Fox (1998). "Autocrine FGF signaling is required for vascular smooth muscle cell survival in vitro." J Cell Physiol **177**(1): 58-67.

Modarresi, F., M. A. Faghihi, M. A. Lopez-Toledano, R. P. Fatemi, M. Magistri, S. P. Brothers, M. P. van der Brug and C. Wahlestedt (2012). "Inhibition of natural antisense transcripts in vivo results in gene-specific transcriptional upregulation." Nat Biotechnol **30**(5): 453-459.

Modzelewska, K., L. P. Newman, R. Desai and P. J. Keely (2006). "Ack1 mediates Cdc42-dependent cell migration and signaling to p130Cas." J Biol Chem **281**(49): 37527-37535.

Moore, J. E., Jr., D. N. Ku, C. K. Zarins and S. Glagov (1992). "Pulsatile flow visualization in the abdominal aorta under differing physiologic conditions: implications for increased susceptibility to atherosclerosis." J Biomech Eng **114**(3): 391-397.

Murphy, P. R. and R. S. Knee (1994). "Identification and characterization of an antisense RNA transcript (gfg) from the human basic fibroblast growth factor gene." Mol Endocrinol **8**(7): 852-859.

Muto, A., T. N. Fitzgerald, J. M. Pimiento, S. P. Maloney, D. Teso, J. J. Paszkowiak, T. S. Westvik, F. A. Kudo, T. Nishibe and A. Dardik (2007). "Smooth muscle cell signal transduction: implications of vascular biology for vascular surgeons." J Vasc Surg **45 Suppl A**(6S): A15-24.

Naik, V., E. M. Leaf, J. H. Hu, H. Y. Yang, N. B. Nguyen, C. M. Giachelli and M. Y. Speer (2012). "Sources of cells that contribute to atherosclerotic intimal calcification: an in vivo genetic fate mapping study." Cardiovasc Res **94**(3): 545-554.

Nakashima, Y., A. S. Plump, E. W. Raines, J. L. Breslow and R. Ross (1994). "ApoE-deficient mice develop lesions of all phases of atherosclerosis throughout the arterial tree." Arterioscler Thromb **14**(1): 133-140.

Naylor, A. R. (2017). "Medical treatment strategies to reduce perioperative morbidity and mortality after carotid surgery." Semin Vasc Surg **30**(1): 17-24.

Newman, K. M., J. Jean-Claude, H. Li, J. V. Scholes, Y. Ogata, H. Nagase and M. D. Tilson (1994). "Cellular localization of matrix metalloproteinases in the abdominal aortic aneurysm wall." J Vasc Surg **20**(5): 814-820.

Nicholls, S. J., R. Puri, T. Anderson, C. M. Ballantyne, L. Cho, J. J. Kastelein, W. Koenig, R. Somaratne, H. Kassahun, J. Yang, S. M. Wasserman, R. Scott, I. Ungi, J. Podolec, A. O. Ophuis, J. H. Cornel, M. Borgman, D. M. Brennan and S. E. Nissen (2016). "Effect of Evolocumab on Progression of Coronary Disease in Statin-Treated Patients: The GLAGOV Randomized Clinical Trial." JAMA **316**(22): 2373-2384.

Nicholls, S. J., E. M. Tuzcu, I. Sipahi, A. W. Grasso, P. Schoenhagen, T. Hu, K. Wolski, T. Crowe, M. Y. Desai, S. L. Hazen, S. R. Kapadia and S. E. Nissen (2007). "Statins, high-density lipoprotein cholesterol, and regression of coronary atherosclerosis." JAMA **297**(5): 499-508.

Nobes, C. D. and A. Hall (1995). "Rho, rac and cdc42 GTPases: regulators of actin structures, cell adhesion and motility." Biochem Soc Trans **23**(3): 456-459.

Nobes, C. D. and A. Hall (1995). "Rho, rac, and cdc42 GTPases regulate the assembly of multimolecular focal complexes associated with actin stress fibers, lamellipodia, and filopodia." Cell **81**(1): 53-62.

Nogrady, B. (2019). "The challenge of delivering RNA-interference therapeutics to their target cells." Nature **574**(7778): S8-S9.

Nordon, I. M., R. J. Hinchliffe, I. M. Loftus and M. M. Thompson (2011). "Pathophysiology and epidemiology of abdominal aortic aneurysms." Nat Rev Cardiol **8**(2): 92-102.

Okura, Y., M. Brink, H. Itabe, K. J. Scheidegger, A. Kalangos and P. Delafontaine (2000). "Oxidized low-density lipoprotein is associated with apoptosis of vascular smooth muscle cells in human atherosclerotic plaques." Circulation **102**(22): 2680-2686.

Oliver-Williams, C., M. J. Sweeting, G. Turton, D. Parkin, D. Cooper, C. Rodd, S. G. Thompson, J. J. Earnshaw, Gloucestershire and P. Swindon Abdominal Aortic Aneurysm Screening (2018). "Lessons learned about prevalence and growth rates of abdominal aortic aneurysms from a 25-year ultrasound population screening programme." Br J Surg **105**(1): 68-74.

Oppi, S., T. F. Luscher and S. Stein (2019). "Mouse Models for Atherosclerosis Research-Which Is My Line?" Front Cardiovasc Med **6**: 46.

Ouimet, M., V. Franklin, E. Mak, X. Liao, I. Tabas and Y. L. Marcel (2011). "Autophagy regulates cholesterol efflux from macrophage foam cells via lysosomal acid lipase." Cell Metab **13**(6): 655-667.

Owens, G. K., M. S. Kumar and B. R. Wamhoff (2004). "Molecular regulation of vascular smooth muscle cell differentiation in development and disease." Physiol Rev **84**(3): 767-801.

Ozsolak, F., P. Kapranov, S. Foissac, S. W. Kim, E. Fishilevich, A. P. Monaghan, B. John and P. M. Milos (2010). "Comprehensive polyadenylation site maps in yeast and human reveal pervasive alternative polyadenylation." Cell **143**(6): 1018-1029.

Pan, H., C. Xue, B. J. Auerbach, J. Fan, A. C. Bashore, J. Cui, D. Y. Yang, S. B. Trignano, W. Liu, J. Shi, C. O. Ihuegbu, E. C. Bush, J. Worley, L. Vlahos, P. Laise, R. A. Solomon, E. S. Connolly, A. Califano, P. A. Sims, H. Zhang, M. Li and M. P. Reilly (2020). "Single-Cell Genomics Reveals a Novel Cell State During Smooth Muscle Cell Phenotypic Switching and Potential Therapeutic Targets for Atherosclerosis in Mouse and Human." Circulation **142**(21): 2060-2075.

Parma, L., H. A. B. Peters, T. J. Sluiter, K. H. Simons, P. Lazzari, M. R. de Vries and P. H. A. Quax (2020). "bFGF blockade reduces intraplaque angiogenesis and macrophage infiltration in atherosclerotic vein graft lesions in ApoE3*Leiden mice." Sci Rep **10**(1): 15968.

Parodi, J. C., J. C. Palmaz and H. D. Barone (1991). "Transfemoral intraluminal graft implantation for abdominal aortic aneurysms." Ann Vasc Surg **5**(6): 491-499.

Paunovska, K., D. Loughrey and J. E. Dahlman (2022). "Drug delivery systems for RNA therapeutics." Nat Rev Genet **23**(5): 265-280.

Pelechano, V. and L. M. Steinmetz (2013). "Gene regulation by antisense transcription." Nat Rev Genet **14**(12): 880-893.

Pfeffer, M. A., E. Braunwald, L. A. Moye, L. Basta, E. J. Brown, Jr., T. E. Cuddy, B. R. Davis, E. M. Geltman, S. Goldman, G. C. Flaker and et al. (1992). "Effect of captopril on mortality and morbidity in patients with left ventricular dysfunction after myocardial infarction. Results of the survival and ventricular enlargement trial. The SAVE Investigators." N Engl J Med **327**(10): 669-677.

Plump, A. S. and J. L. Breslow (1995). "Apolipoprotein E and the apolipoprotein E-deficient mouse." Annu Rev Nutr **15**: 495-518.

Pomies, P., H. A. Louis and M. C. Beckerle (1997). "CRP1, a LIM domain protein implicated in muscle differentiation, interacts with alpha-actinin." J Cell Biol **139**(1): 157-168.

Potter, D. D., C. G. Sobey, P. K. Tompkins, J. D. Rossen and D. D. Heistad (1998). "Evidence that macrophages in atherosclerotic lesions contain angiotensin II." Circulation **98**(8): 800-807.

Prinssen, M., E. L. Verhoeven, J. Buth, P. W. Cuypers, M. R. van Sambeek, R. Balm, E. Buskens, D. E. Grobbee, J. D. Blankensteijn and G. Dutch Randomized Endovascular Aneurysm Management Trial (2004). "A randomized trial comparing conventional and endovascular repair of abdominal aortic aneurysms." N Engl J Med **351**(16): 1607-1618.

Pyo, R., J. K. Lee, J. M. Shipley, J. A. Curci, D. Mao, S. J. Ziporin, T. L. Ennis, S. D. Shapiro, R. M. Senior and R. W. Thompson (2000). "Targeted gene disruption of matrix metalloproteinase-9 (gelatinase B) suppresses development of experimental abdominal aortic aneurysms." J Clin Invest **105**(11): 1641-1649.

Qian, G., O. Adeyanju, A. Olajuyin and X. Guo (2022). "Abdominal Aortic Aneurysm Formation with a Focus on Vascular Smooth Muscle Cells." Life (Basel) **12**(2).

Quintana, R. A. and W. R. Taylor (2019). "Cellular Mechanisms of Aortic Aneurysm Formation." Circ Res **124**(4): 607-618.

Raffetto, J. D. and R. A. Khalil (2008). "Matrix metalloproteinases and their inhibitors in vascular remodeling and vascular disease." Biochem Pharmacol **75**(2): 346-359.

Raffort, J., F. Lareyre, M. Clement, R. Hassen-Khodja, G. Chinetti and Z. Mallat (2017). "Monocytes and macrophages in abdominal aortic aneurysm." Nat Rev Cardiol **14**(8): 457-471.

Rastogi, V., S. J. M. Stefens, J. Houwaart, H. J. M. Verhagen, J. L. de Bruin, I. van der Pluijm and J. Essers (2022). "Molecular Imaging of Aortic Aneurysm and Its Translational Power for Clinical Risk Assessment." Front Med (Lausanne) **9**: 814123.

Raveh, E., I. J. Matouk, M. Gilon and A. Hochberg (2015). "The H19 Long non-coding RNA in cancer initiation, progression and metastasis - a proposed unifying theory." Mol Cancer **14**: 184.

Redgrave, J. N., P. Gallagher, J. K. Lovett and P. M. Rothwell (2008). "Critical cap thickness and rupture in symptomatic carotid plaques: the oxford plaque study." Stroke **39**(6): 1722-1729.

Regan, C. P., P. J. Adam, C. S. Madsen and G. K. Owens (2000). "Molecular mechanisms of decreased smooth muscle differentiation marker expression after vascular injury." J Clin Invest **106**(9): 1139-1147.

Rerkasem, A., S. Orrapin, D. P. Howard and K. Rerkasem (2020). "Carotid endarterectomy for symptomatic carotid stenosis." Cochrane Database Syst Rev **9**: CD001081.

Ridker, P. M. (1999). "Evaluating novel cardiovascular risk factors: can we better predict heart attacks?" Ann Intern Med **130**(11): 933-937.

Ridker, P. M., B. M. Everett, T. Thuren, J. G. MacFadyen, W. H. Chang, C. Ballantyne, F. Fonseca, J. Nicolau, W. Koenig, S. D. Anker, J. J. P. Kastelein, J. H. Cornel, P. Pais, D. Pella, J. Genest, R. Cifkova, A. Lorenzatti, T. Forster, Z. Kobalava, L. Vida-Simiti, M. Flather, H. Shimokawa, H. Ogawa, M. Dellborg, P. R. F. Rossi, R. P. T. Troquay, P. Libby, R. J. Glynn and C. T. Group (2017). "Antiinflammatory Therapy with Canakinumab for Atherosclerotic Disease." N Engl J Med **377**(12): 1119-1131.

Ridley, A. J. (2015). "Rho GTPase signalling in cell migration." Curr Opin Cell Biol **36**: 103-112.

Rinn, J. L. and H. Y. Chang (2012). "Genome regulation by long noncoding RNAs." Annu Rev Biochem **81**: 145-166.

Rombouts, K. B., T. A. R. van Merrienboer, J. C. F. Ket, N. Bogunovic, J. van der Velden and K. K. Yeung (2022). "The role of vascular smooth muscle cells in the development of aortic aneurysms and dissections." Eur J Clin Invest **52**(4): e13697.

Ross, R. (1993). "The pathogenesis of atherosclerosis: a perspective for the 1990s." Nature **362**(6423): 801-809.

Ross, R. (1999). "Atherosclerosis is an inflammatory disease." Am Heart J **138**(5 Pt 2): S419-420.

Ruddy, J. M., J. A. Jones, F. G. Spinale and J. S. Ikonomidis (2008). "Regional heterogeneity within the aorta: relevance to aneurysm disease." J Thorac Cardiovasc Surg **136**(5): 1123-1130.

Saba, L., F. Potters, A. van der Lugt and G. Mallarini (2010). "Imaging of the fibrous cap in atherosclerotic carotid plaque." Cardiovasc Intervent Radiol **33**(4): 681-689.

Sacco, R. L., S. E. Kasner, J. P. Broderick, L. R. Caplan, J. J. Connors, A. Culebras, M. S. Elkind, M. G. George, A. D. Hamdan, R. T. Higashida, B. L. Hoh, L. S. Janis, C. S. Kase, D. O. Kleindorfer, J. M. Lee, M. E. Moseley, E. D. Peterson, T. N. Turan, A. L. Valderrama, H. V. Vinters, C. o. C. S. American Heart Association Stroke Council, Anesthesia, R. Council on Cardiovascular, Intervention, C. Council on, N. Stroke, E. Council on, Prevention, D. Council on Peripheral Vascular, P. A. Council on Nutrition and Metabolism (2013). "An updated definition of stroke for the 21st century: a statement for healthcare professionals from the American Heart Association/American Stroke Association." Stroke **44**(7): 2064-2089.

Sakalihasan, N., R. Limet and O. D. Defawe (2005). "Abdominal aortic aneurysm." Lancet **365**(9470): 1577-1589.

Sakalihasan, N., J. B. Michel, A. Katsargyris, H. Kuivaniemi, J. O. Defraigne, A. Nchimi, J. T. Powell, K. Yoshimura and R. Hultgren (2018). "Abdominal aortic aneurysms." Nat Rev Dis Primers **4**(1): 34.

Salmena, L., L. Poliseno, Y. Tay, L. Kats and P. P. Pandolfi (2011). "A ceRNA hypothesis: the Rosetta Stone of a hidden RNA language?" Cell **146**(3): 353-358.

Samani, N. J., J. Erdmann, A. S. Hall, C. Hengstenberg, M. Mangino, B. Mayer, R. J. Dixon, T. Meitinger, P. Braund, H. E. Wichmann, J. H. Barrett, I. R. Konig, S. E. Stevens, S. Szymczak, D. A. Tregouet, M. M. Iles, F. Pahlke, H. Pollard, W. Lieb, F. Cambien, M. Fischer, W. Ouwehand, S. Blankenberg, A. J. Balmforth, A. Baessler, S. G. Ball, T. M. Strom, I. Braenne, C. Gieger, P. Deloukas, M. D. Tobin, A. Ziegler, J. R. Thompson, H. Schunkert, Wtccc and C. the Cardiogenics (2007). "Genomewide association analysis of coronary artery disease." N Engl J Med **357**(5): 443-453.

Sampson, U. K., P. E. Norman, F. G. Fowkes, V. Aboyans, Y. Song, F. E. Harrell, Jr., M. H. Forouzanfar, M. Naghavi, J. O. Denenberg, M. M. McDermott, M. H. Criqui, G. A. Mensah, M. Ezzati and C. Murray (2014). "Estimation of global and regional incidence and prevalence of abdominal aortic aneurysms 1990 to 2010." Glob Heart **9**(1): 159-170.

Saraff, K., F. Babamusta, L. A. Cassis and A. Daugherty (2003). "Aortic dissection precedes formation of aneurysms and atherosclerosis in angiotensin II-infused, apolipoprotein E-deficient mice." Arterioscler Thromb Vasc Biol **23**(9): 1621-1626.

Saratzis, A. and M. J. Bown (2014). "The genetic basis for aortic aneurysmal disease." Heart **100**(12): 916-922.

Sasaki, T., M. Kuzuya, K. Nakamura, X. W. Cheng, T. Shibata, K. Sato and A. Iguchi (2006). "A simple method of plaque rupture induction in apolipoprotein E-deficient mice." Arterioscler Thromb Vasc Biol **26**(6): 1304-1309.

Sato, Y., T. Shimada and R. Takaki (1991). "Autocrinological role of basic fibroblast growth factor on tube formation of vascular endothelial cells in vitro." Biochem Biophys Res Commun **180**(2): 1098-1102.

Satta, J., T. Juvonen, K. Haukipuro, M. Juvonen and M. I. Kairaluoma (1995). "Increased turnover of collagen in abdominal aortic aneurysms, demonstrated by measuring the concentration of the aminoterminal propeptide of type III procollagen in peripheral and aortal blood samples." J Vasc Surg **22**(2): 155-160.

Schmitz, K. M., C. Mayer, A. Postepska and I. Grummt (2010). "Interaction of noncoding RNA with the rDNA promoter mediates recruitment of DNMT3b and silencing of rRNA genes." Genes Dev **24**(20): 2264-2269.

Schmitz, S. U., P. Grote and B. G. Herrmann (2016). "Mechanisms of long noncoding RNA function in development and disease." Cell Mol Life Sci **73**(13): 2491-2509.

Sebastian-delaCruz, M., I. Gonzalez-Moro, A. Olazagoitia-Garmendia, A. Castellanos-Rubio and I. Santin (2021). "The Role of lncRNAs in Gene Expression Regulation through mRNA Stabilization." Noncoding RNA **7**(1).

Sebe, A., Z. Erdei, K. Varga, C. Bodor, I. Mucsi and L. Rosivall (2010). "Cdc42 regulates myocardin-related transcription factor nuclear shuttling and alpha-smooth muscle actin promoter activity during renal tubular epithelial-mesenchymal transition." Nephron Exp Nephrol **114**(3): e117-125.

Senemaud, J., G. Caligiuri, H. Etienne, S. Delbosc, J. B. Michel and R. Coscas (2017). "Translational Relevance and Recent Advances of Animal Models of Abdominal Aortic Aneurysm." Arterioscler Thromb Vasc Biol **37**(3): 401-410.

Seneviratne, A., M. Hulsmans, P. Holvoet and C. Monaco (2013). "Biomechanical factors and macrophages in plaque stability." Cardiovasc Res **99**(2): 284-293.

Shah, A. D., C. Langenberg, E. Rapsomaniki, S. Denaxas, M. Pujades-Rodriguez, C. P. Gale, J. Deanfield, L. Smeeth, A. Timmis and H. Hemingway (2015). "Type 2 diabetes and incidence of cardiovascular diseases: a cohort study in 1.9 million people." Lancet Diabetes Endocrinol **3**(2): 105-113.

Shah, P. K. (2003). "Mechanisms of plaque vulnerability and rupture." J Am Coll Cardiol **41**(4 Suppl S): 15S-22S.

Shankman, L. S., D. Gomez, O. A. Cherepanova, M. Salmon, G. F. Alencar, R. M. Haskins, P. Swiatlowska, A. A. Newman, E. S. Greene, A. C. Straub, B. Isakson, G. J. Randolph and G. K. Owens (2015). "KLF4-dependent phenotypic modulation of smooth muscle cells has a key role in atherosclerotic plaque pathogenesis." Nat Med **21**(6): 628-637.

Shibamura, H., J. M. Olson, C. van Vlijmen-Van Keulen, S. G. Buxbaum, D. M. Dudek, G. Tromp, T. Ogata, M. Skunca, N. Sakalihasan, G. Pals, R. Limet, G. L. MacKean, O. Defawe, A. Verloes, C. Arthur, A. G. Lossing, M. Burnett, T. Sueda and H. Kuivaniemi (2004). "Genome scan for familial abdominal aortic aneurysm using

sex and family history as covariates suggests genetic heterogeneity and identifies linkage to chromosome 19q13." Circulation **109**(17): 2103-2108.

Shimoni, Y., G. Friedlander, G. Hetzroni, G. Niv, S. Altuvia, O. Biham and H. Margalit (2007). "Regulation of gene expression by small non-coding RNAs: a quantitative view." Mol Syst Biol **3**: 138.

Sillesen, H., N. Eldrup, R. Hultgren, J. Lindeman, K. Bredahl, M. Thompson, A. Wanhainen, U. Wingren, J. Swedenborg and A. T. Investigators (2015). "Randomized clinical trial of mast cell inhibition in patients with a medium-sized abdominal aortic aneurysm." Br J Surg **102**(10): 1295.

Skalen, K., M. Gustafsson, E. K. Rydberg, L. M. Hulten, O. Wiklund, T. L. Innerarity and J. Boren (2002). "Subendothelial retention of atherogenic lipoproteins in early atherosclerosis." Nature **417**(6890): 750-754.

Song, P., Z. Fang, H. Wang, Y. Cai, K. Rahimi, Y. Zhu, F. G. R. Fowkes, F. J. I. Fowkes and I. Rudan (2020). "Global and regional prevalence, burden, and risk factors for carotid atherosclerosis: a systematic review, meta-analysis, and modelling study." Lancet Glob Health **8**(5): e721-e729.

Speakman, J. R. (2019). "Use of high-fat diets to study rodent obesity as a model of human obesity." Int J Obes (Lond) **43**(8): 1491-1492.

Stary, H. C., A. B. Chandler, R. E. Dinsmore, V. Fuster, S. Glagov, W. Insull, Jr., M. E. Rosenfeld, C. J. Schwartz, W. D. Wagner and R. W. Wissler (1995). "A definition of advanced types of atherosclerotic lesions and a histological classification of atherosclerosis. A report from the Committee on Vascular Lesions of the Council on Arteriosclerosis, American Heart Association." Arterioscler Thromb Vasc Biol **15**(9): 1512-1531.

Stary, H. C., A. B. Chandler, S. Glagov, J. R. Guyton, W. Insull, Jr., M. E. Rosenfeld, S. A. Schaffer, C. J. Schwartz, W. D. Wagner and R. W. Wissler (1994). "A definition of initial, fatty streak, and intermediate lesions of atherosclerosis. A report from the Committee on Vascular Lesions of the Council on Arteriosclerosis, American Heart Association." Circulation **89**(5): 2462-2478.

Statello, L., C. J. Guo, L. L. Chen and M. Huarte (2021). "Gene regulation by long non-coding RNAs and its biological functions." Nat Rev Mol Cell Biol **22**(2): 96-118.

Steinberg, D. and J. L. Witztum (2010). "Oxidized low-density lipoprotein and atherosclerosis." Arterioscler Thromb Vasc Biol **30**(12): 2311-2316.

Sukhthankar, M., C. K. Choi, A. English, J. S. Kim and S. J. Baek (2010). "A potential proliferative gene, NUDT6, is down-regulated by green tea catechins at the posttranscriptional level." J Nutr Biochem **21**(2): 98-106.

Sun, Q., Q. Hao and K. V. Prasanth (2018). "Nuclear Long Noncoding RNAs: Key Regulators of Gene Expression." Trends Genet **34**(2): 142-157.

Sun, Z., X. Nie, S. Sun, S. Dong, C. Yuan, Y. Li, B. Xiao, D. Jie and Y. Liu (2017). "Long Non-Coding RNA MEG3 Downregulation Triggers Human Pulmonary Artery

Smooth Muscle Cell Proliferation and Migration via the p53 Signaling Pathway." Cell Physiol Biochem **42**(6): 2569-2581.

Tang, D. D. and S. J. Gunst (2004). "The small GTPase Cdc42 regulates actin polymerization and tension development during contractile stimulation of smooth muscle." J Biol Chem **279**(50): 51722-51728.

Tang, J., H. Wang, X. Huang, F. Li, H. Zhu, Y. Li, L. He, H. Zhang, W. Pu, K. Liu, H. Zhao, J. F. Bentzon, Y. Yu, Y. Ji, Y. Nie, X. Tian, L. Zhang, D. Gao and B. Zhou (2020). "Arterial Sca1(+) Vascular Stem Cells Generate De Novo Smooth Muscle for Artery Repair and Regeneration." Cell Stem Cell **26**(1): 81-96 e84.

Thomas, H., J. Diamond, A. Vieco, S. Chaudhuri, E. Shinnar, S. Cromer, P. Perel, G. A. Mensah, J. Narula, C. O. Johnson, G. A. Roth and A. E. Moran (2018). "Global Atlas of Cardiovascular Disease 2000-2016: The Path to Prevention and Control." Glob Heart **13**(3): 143-163.

Thompson, R. W., J. A. Curci, T. L. Ennis, D. Mao, M. B. Pagano and C. T. Pham (2006). "Pathophysiology of abdominal aortic aneurysms: insights from the elastase-induced model in mice with different genetic backgrounds." Ann N Y Acad Sci **1085**: 59-73.

Thompson, R. W., D. R. Holmes, R. A. Mertens, S. Liao, M. D. Botney, R. P. Mecham, H. G. Welgus and W. C. Parks (1995). "Production and localization of 92-kilodalton gelatinase in abdominal aortic aneurysms. An elastolytic metalloproteinase expressed by aneurysm-infiltrating macrophages." J Clin Invest **96**(1): 318-326.

Timmis, A., P. Vardas, N. Townsend, A. Torbica, H. Katus, D. De Smedt, C. P. Gale, A. P. Maggioni, S. E. Petersen, R. Huculeci, D. Kazakiewicz, V. B. Rubio, B. Ignatiuk, Z. Raisi-Estabragh, A. Pawlak, E. Karagiannidis, R. Treskes, D. Gaita, J. F. Beltrame, A. McConnachie, I. Bardinet, I. Graham, M. Flather, P. Elliott, E. A. Mossialos, F. Weidinger and S. Achenbach (2022). "European Society of Cardiology: cardiovascular disease statistics 2021: Executive Summary." Eur Heart J Qual Care Clin Outcomes **8**(4): 377-382.

Tran, T. C., C. Singleton, T. S. Fraley and J. A. Greenwood (2005). "Cysteine-rich protein 1 (CRP1) regulates actin filament bundling." BMC Cell Biol **6**: 45.

Tromp, G., H. Kuivaniemi, I. Hinterseher and D. J. Carey (2010). "Novel genetic mechanisms for aortic aneurysms." Curr Atheroscler Rep **12**(4): 259-266.

Tsuji-Tamura, K. and M. Tamura (2022). "Basic fibroblast growth factor uniquely stimulates quiescent vascular smooth muscle cells and induces proliferation and dedifferentiation." FEBS Lett **596**(13): 1686-1699.

Tyanova, S., T. Temu, P. Sinitcyn, A. Carlson, M. Y. Hein, T. Geiger, M. Mann and J. Cox (2016). "The Perseus computational platform for comprehensive analysis of (prote)omics data." Nat Methods **13**(9): 731-740.

Vacante, F., L. Denby, J. C. Sluimer and A. H. Baker (2019). "The function of miR-143, miR-145 and the MiR-143 host gene in cardiovascular development and disease." Vascul Pharmacol **112**: 24-30.

van der Loop, F. T., G. Schaart, E. D. Timmer, F. C. Ramaekers and G. J. van Eys (1996). "Smoothelin, a novel cytoskeletal protein specific for smooth muscle cells." J Cell Biol **134**(2): 401-411.

van Tits, L. J., R. Stienstra, P. L. van Lent, M. G. Netea, L. A. Joosten and A. F. Stalenhoef (2011). "Oxidized LDL enhances pro-inflammatory responses of alternatively activated M2 macrophages: a crucial role for Kruppel-like factor 2." Atherosclerosis **214**(2): 345-349.

Vesselinovitch, D., R. W. Wissler and J. Doull (1968). "Experimental production of atherosclerosis in mice. 1. Effect of various synthetic diets and radiation on survival time, food consumption and body weight in mice." J Atheroscler Res **8**(3): 483-495.

Virani, S. S., A. Alonso, H. J. Aparicio, E. J. Benjamin, M. S. Bittencourt, C. W. Callaway, A. P. Carson, A. M. Chamberlain, S. Cheng, F. N. Delling, M. S. V. Elkind, K. R. Evenson, J. F. Ferguson, D. K. Gupta, S. S. Khan, B. M. Kissela, K. L. Knutson, C. D. Lee, T. T. Lewis, J. Liu, M. S. Loop, P. L. Lutsey, J. Ma, J. Mackey, S. S. Martin, D. B. Matchar, M. E. Mussolino, S. D. Navaneethan, A. M. Perak, G. A. Roth, Z. Samad, G. M. Satou, E. B. Schroeder, S. H. Shah, C. M. Shay, A. Stokes, L. B. VanWagner, N. Y. Wang, C. W. Tsao, E. American Heart Association Council on, C. Prevention Statistics and S. Stroke Statistics (2021). "Heart Disease and Stroke Statistics-2021 Update: A Report From the American Heart Association." Circulation **143**(8): e254-e743.

Virchow, R. (1989). "Cellular pathology. As based upon physiological and pathological histology. Lecture XVI--Atheromatous affection of arteries. 1858." Nutr Rev **47**(1): 23-25.

Virmani, R., A. P. Burke and A. Farb (1999). "Plaque rupture and plaque erosion." Thromb Haemost **82 Suppl 1**: 1-3.

Virmani, R., F. D. Kolodgie, A. P. Burke, A. Farb and S. M. Schwartz (2000). "Lessons from sudden coronary death: a comprehensive morphological classification scheme for atherosclerotic lesions." Arterioscler Thromb Vasc Biol **20**(5): 1262-1275.

Vollmar, J. F., E. Paes, P. Pauschinger, E. Henze and A. Friesch (1989). "Aortic aneurysms as late sequelae of above-knee amputation." Lancet **2**(8667): 834-835.

Wang, D., P. S. Chang, Z. Wang, L. Sutherland, J. A. Richardson, E. Small, P. A. Krieg and E. N. Olson (2001). "Activation of cardiac gene expression by myocardin, a transcriptional cofactor for serum response factor." Cell **105**(7): 851-862.

Wang, X. and R. A. Khalil (2018). "Matrix Metalloproteinases, Vascular Remodeling, and Vascular Disease." Adv Pharmacol **81**: 241-330.

Wang, Y., H. Ait-Oufella, O. Herbin, P. Bonnin, B. Ramkhelawon, S. Taleb, J. Huang, G. Offenstadt, C. Combadiere, L. Renia, J. L. Johnson, P. L. Tharaux, A. Tedgui and Z. Mallat (2010). "TGF-beta activity protects against inflammatory aortic aneurysm progression and complications in angiotensin II-infused mice." J Clin Invest **120**(2): 422-432.

Wang, Z., M. R. Castresana and W. H. Newman (2001). "NF-kappaB is required for TNF-alpha-directed smooth muscle cell migration." FEBS Lett **508**(3): 360-364.

Wanhainen, A., F. Verzini, I. Van Herzeele, E. Allaire, M. Bown, T. Cohnert, F. Dick, J. van Herwaarden, C. Karkos, M. Koelemay, T. Kolbel, I. Loftus, K. Mani, G. Melissano, J. Powell, Z. Szeberin, C. Esvs Guidelines, G. J. de Borst, N. Chakfe, S. Debus, R. Hinchliffe, S. Kakkos, I. Koncar, P. Kolh, J. S. Lindholt, M. Vega de Ceniga, F. Vermassen, R. Document, M. Bjorck, S. Cheng, R. Dalman, L. Davidovic, K. Donas, J. Earnshaw, H. H. Eckstein, J. Golledge, S. Haulon, T. Mastracci, R. Naylor, J. B. Ricco and H. Verhagen (2020). "Corrigendum to 'European Society for Vascular Surgery (ESVS) 2019 Clinical Practice Guidelines on the Management of Abdominal Aorto-iliac Artery Aneurysms' [European Journal of Vascular & Endovascular Surgery 57/1 (2019) 8-93]." Eur J Vasc Endovasc Surg **59**(3): 494.

Werner, A. (2013). "Biological functions of natural antisense transcripts." BMC Biol **11**: 31.

Winter, H., G. Winski, A. Busch, E. Chernogubova, F. Fasolo, Z. Wu, A. Bäcklund, B. B. Khomtchouk, D. J. Van Booven, N. Sachs, H.-H. Eckstein, I. Wittig, R. A. Boon, H. Jin and L. Maegdefessel (2023). "Targeting long non-coding RNA NUDT6 enhances smooth muscle cell survival and limits vascular disease progression." Molecular Therapy.

Wirka, R. C., D. Wagh, D. T. Paik, M. Pjanic, T. Nguyen, C. L. Miller, R. Kundu, M. Nagao, J. Coller, T. K. Koyano, R. Fong, Y. J. Woo, B. Liu, S. B. Montgomery, J. C. Wu, K. Zhu, R. Chang, M. Alamprese, M. D. Tallquist, J. B. Kim and T. Quertermous (2019). "Atheroprotective roles of smooth muscle cell phenotypic modulation and the TCF21 disease gene as revealed by single-cell analysis." Nat Med **25**(8): 1280-1289.

Wolf, M. P. and P. Hunziker (2020). "Atherosclerosis: Insights into Vascular Pathobiology and Outlook to Novel Treatments." J Cardiovasc Transl Res **13**(5): 744-757.

Wu, G., J. Cai, Y. Han, J. Chen, Z. P. Huang, C. Chen, Y. Cai, H. Huang, Y. Yang, Y. Liu, Z. Xu, D. He, X. Zhang, X. Hu, L. Pinello, D. Zhong, F. He, G. C. Yuan, D. Z. Wang and C. Zeng (2014). "LincRNA-p21 regulates neointima formation, vascular smooth muscle cell proliferation, apoptosis, and atherosclerosis by enhancing p53 activity." Circulation **130**(17): 1452-1465.

Xu, N., T. Papagiannakopoulos, G. Pan, J. A. Thomson and K. S. Kosik (2009). "MicroRNA-145 regulates OCT4, SOX2, and KLF4 and represses pluripotency in human embryonic stem cells." Cell **137**(4): 647-658.

Xu, Z., W. Wei, J. Gagneur, S. Clauder-Munster, M. Smolik, W. Huber and L. M. Steinmetz (2011). "Antisense expression increases gene expression variability and locus interdependency." Mol Syst Biol **7**: 468.

Yamanouchi, D., S. Morgan, C. Stair, S. Seedial, J. Lengfeld, K. C. Kent and B. Liu (2012). "Accelerated aneurysmal dilation associated with apoptosis and inflammation

in a newly developed calcium phosphate rodent abdominal aortic aneurysm model." J Vasc Surg **56**(2): 455-461.

Ye, Z. M., S. Yang, Y. P. Xia, R. T. Hu, S. Chen, B. W. Li, S. L. Chen, X. Y. Luo, L. Mao, Y. Li, H. Jin, C. Qin and B. Hu (2019). "LncRNA MIAT sponges miR-149-5p to inhibit efferocytosis in advanced atherosclerosis through CD47 upregulation." Cell Death Dis **10**(2): 138.

Yoshida, T., S. Sinha, F. Dandre, B. R. Wamhoff, M. H. Hoofnagle, B. E. Kremer, D. Z. Wang, E. N. Olson and G. K. Owens (2003). "Myocardin is a key regulator of CArG-dependent transcription of multiple smooth muscle marker genes." Circ Res **92**(8): 856-864.

Yoshida, T., M. Yamashita and M. Hayashi (2012). "Kruppel-like factor 4 contributes to high phosphate-induced phenotypic switching of vascular smooth muscle cells into osteogenic cells." J Biol Chem **287**(31): 25706-25714.

Yu, S. Y. and H. T. Blumenthal (1965). "The Calcification of Elastic Fiber. 4. Epinephrine and Beta-Aminopropionitrile-Induced Calcification in Animal Aortas." J Atheroscler Res **5**(2): 159-173.

Zhang, L., H. Cheng, Y. Yue, S. Li, D. Zhang and R. He (2018). "H19 knockdown suppresses proliferation and induces apoptosis by regulating miR-148b/WNT/beta-catenin in ox-LDL -stimulated vascular smooth muscle cells." J Biomed Sci **25**(1): 11.

Zhang, S. C., C. Barclay, L. A. Alexander, L. Geldenhuys, G. A. Porter, A. G. Casson and P. R. Murphy (2007). "Alternative splicing of the FGF antisense gene: differential subcellular localization in human tissues and esophageal adenocarcinoma." J Mol Med (Berl) **85**(11): 1215-1228.

Zhang, S. C., K. A. MacDonald, M. Baguma-Nibasheka, L. Geldenhuys, A. G. Casson and P. R. Murphy (2008). "Alternative splicing and differential subcellular localization of the rat FGF antisense gene product." BMC Mol Biol **9**: 10.

Zhao, G., H. Lu, Z. Chang, Y. Zhao, T. Zhu, L. Chang, Y. Guo, M. T. Garcia-Barrio, Y. E. Chen and J. Zhang (2021). "Single-cell RNA sequencing reveals the cellular heterogeneity of aneurysmal infrarenal abdominal aorta." Cardiovasc Res **117**(5): 1402-1416.

Zhao, J., W. Zhang, M. Lin, W. Wu, P. Jiang, E. Tou, M. Xue, A. Richards, D. Jourd'heuil, A. Asif, D. Zheng, H. A. Singer, J. M. Miano and X. Long (2016). "MYOSLID Is a Novel Serum Response Factor-Dependent Long Noncoding RNA That Amplifies the Vascular Smooth Muscle Differentiation Program." Arterioscler Thromb Vasc Biol **36**(10): 2088-2099.

Zhao, Y., G. Feng, Y. Wang, Y. Yue and W. Zhao (2014). "Regulation of apoptosis by long non-coding RNA HIF1A-AS1 in VSMCs: implications for TAA pathogenesis." Int J Clin Exp Pathol **7**(11): 7643-7652.

10. Acknowledgements

To my principal supervisor – Thank you, Lars for your trust and guidance. Little did I know I would write my doctoral thesis in your lab after applying for a research stay during my Bachelor times. You are a great mentor and inspiration; you gave me the freedom to grow and to make mistakes. Your door was always open for questions and discussions, which I highly appreciate. The atmosphere and environment you created in the lab are truly beneficial and I feel really privileged to work in a group that practices this open question and discussion culture as we do.

To my supervisors and mentors - A big thank you to Prof. Aphrodite Kapurniotu and my mentor Prof. Jaroslav Pelisek. I always enjoyed the meetings and discussions and valued all your feedback and guidance.

Till mitt labb i Stockholm - tack så mycket för all tid vi tillbringat tillsammans i labbet, djurhuset men också för de trevliga aktiviteterna utanför labbet eller på konferenser. Stockholm och KI kommer alltid att förbli ett hem långt hemifrån.

Katja – you taught me everything I needed to know in the field of RNA research. We had so many good discussions and inspirational conversations that I truly miss. I could ask you anything – you always know the answer or find a concentration, dilution or datasheet that I missed. Thank you so much for all of that and so much more!

Hong – you are a genius when it comes to animal work. Such precision and skill combined with a huge amount of care for each and every mouse. Thank you so much for letting me join you in the animal house and for teaching me the AngII model. But also sharing the *NUDT6* project with you and finally getting it published – these were truly exciting times! Thanks for everything.

Greg – you were my fellow PhD student and – unfortunately – most of our PhD, we spent in different countries. I always value your input, suggestions, and critical questions you had for the project. After seeing you graduate last year while I was still writing up, it already gave me a taste that all of this will be worth going through. I hope we'll have an equally great party as we had after your defense!

Alex – Thank you so much for helping me out and giving input in so many situations. Also, your advice for writing was always super helpful! Unfortunately, we did not work together for as long, but I value the time we spent together in the lab!

To my lab in Munich – I enjoyed every minute with you- not only in the lab but especially outside of it..in a beer garden, on top of a mountain, or wherever! Nadiya, Julia and Renate – vielen lieben Dank für eure Assistenz und Hilfe und die schöne Atmosphäre im Labor! Albert, I especially thank you for the several in vivo studies you led for the project. Your important work gave me a truly unique insight into a wide range of animal models. Even though you are no longer in Munich, I am always happy when you drop by the lab unexpectedly and we meet again and can catch up a little! I would also like to thank Susanne very much for her great insights into the large animal model. Your remarkable and dedicated work with the animals is really something that many scientists can take a leaf out of their book! I would also like to thank Li and Wu for their assistance with anything sequencing-related. Unfortunately, I never had the time (but more than that) the courage to self-teach me this as you did. I also thank

Nadja, who really brought out the best site of the biobank! Everything has become so much easier since you are here and I would not want to miss the times we spent so far at conferences, retreats, or in the lab over a cup of coffee!
Special thanks goes to Vale and Fra – your input and experimental assistance and experience were a great help to me. I remember how Fra and I sat over the protocol for the pulldown for hours trying to figure out the purpose of each and every step. Not to forget the ISH-Core Facility of course..! Vale, thank you for sharing your experience with cells and also fluorescent stains from which I benefitted a lot!
Jessi, my partner in crime – I truly value having you as a fellow PhD! It has been a lot of fun with you and it was nice to have someone else with me on this – sometimes – aggravating journey. Retreats, conferences, R-courses, playing samba drums at our kick-off seminar…we did it all. Thank you for all of this and of course also for always being open to discussing results and giving feedback.
To my family – Mama, Papa und Lisa. Ihr habt meine Reise von Anfang an begleitet. In schweren Momenten wart ihr immer für mich da. Aber auch in den guten, wo wir die Erfolge gefeiert haben. Auch, wenn ihr manchmal nicht genau wusstet, wieso ich mich gerade geärgert oder gefreut habe; ihr habt immer mitgefiebert und mitgefühlt. Ich danke euch für eure jahrelange Unterstützung! Oma, mein vermutlich ältester “Fan”. Du hast für den „Support von ganz oben“ gesorgt und mich mit Gebeten und dem Anzünden verschiedenster Kerzen (mittlerweile sind es bestimmt einige, die auf mein Konto gehen) versorgt und abgesichert. Ich danke dir dafür! Ich habe dich sehr lieb!
To Anand – you, who always supports me and is always there for me. You kept me sane in countless situations. You showed so much interest in my work, read articles, and watched videos to understand what I do and to discuss with me. You make me feel proud of my accomplishments, celebrating them together (very much looking forward to this one upcoming now!). I know I can always count on you. Finally, we both are Dres!